http://researchcommons.waikato.ac.nz/

Research Commons at the University of Waikato

Copyright Statement:

The digital copy of this thesis is protected by the Copyright Act 1994 (New Zealand).

The thesis may be consulted by you, provided you comply with the provisions of the Act and the following conditions of use:

- Any use you make of these documents or images must be for research or private study purposes only, and you may not make them available to any other person.
- Authors control the copyright of their thesis. You will recognise the author's right to be identified as the author of the thesis, and due acknowledgement will be made to the author where appropriate.
- You will obtain the author's permission before publishing any material from the thesis.

Evaporation at Kopuatai bog: an investigation of dry and wet canopy evaporation regimes

A thesis submitted in partial fulfilment

of the requirements for the degree

of

Master of Science in Environmental Sciences

at

The University of Waikato

by

Leeza Speranskaya

THE UNIVERSITY OF
WAIKATO
Te Whare Wānanga o Waikato

2023

Abstract

Peatlands store disproportionately large amounts of carbon (C) per unit area compared to other ecosystems, a function that depends on maintaining a high and stable water table. Water table levels are in turn influenced by evaporation (E), which consists of surface E, transpiration, and interception loss (E_{int}) components. In boreal peatlands, E rates have been predicted to increase due to climate change-induced increases in vapour pressure deficit (VPD), potentially causing water table drawdown and threatening the ability of peatlands to store C. However, the response of E to VPD has not yet been quantified for Aotearoa New Zealand peatlands dominated by a very water-conservative vegetation species, *Empodisma robustum*. In addition, the E_{int} component of E has not been extensively investigated in these peatlands. Therefore, to gain a better understanding of the E regimes of this peatland type, this thesis firstly investigated the extent of E restrictions by *E. robustum* and the response of E to increasing VPD at Kopuatai bog, using an 11-year eddy covariance (EC) dataset. This analysis was replicated on a 20-year dataset from Mer Bleue bog, a 'typical' shrub and moss-dominated Northern Hemisphere peatland. Mean annual E was 45% lower than mean annual equilibrium E (E_{eq}) at Kopuatai but only 16% lower at Mer Bleue, demonstrating much greater limitations on E at the former. The mean midday (10:00–14:30) dry canopy Bowen ratio (β) at Kopuatai was 1.96, compared to 0.77 at Mer Bleue, as the sensible heat flux (H) dominated over the latent heat flux (LE) at Kopuatai, and vice versa at Mer Bleue. In addition, the response of E to VPD at Kopuatai indicated that more water was conserved at high VPD than at Mer Bleue. This likely occurred due to stronger stomatal limitation of transpiration at Kopuatai, while at Mer Bleue the effect of stomatal limitation by shrubs may have been offset by a high moss E.

The second component of this thesis determined the magnitude of E_{int} at Kopuatai using two E_{int} modelling approaches and a canopy water balance field experiment. The field data overestimated E_{int}, while modelling produced much lower and more realistic estimates. Therefore, the models likely provided the best estimates of E_{int} as a proportion of gross rainfall (E_{int}/P_g) and total E (E_{int}/E), with annual-scale values of 15.5–18.3% and 31.3–36.6%,

respectively, and a canopy storage capacity of 1.5 mm. Controls on E_{int}/P_g were rain event size, net radiation, and canopy height/density.

This research has shown that, during dry canopy conditions, *E. robustum* enables a much more conservative *E* regime at Kopuatai compared to Mer Bleue, potentially enabling greater "hydrological resistance" to increased VPD under future climate warming compared to Northern Hemisphere peatlands. This may be a crucial factor in ensuring resilience of the C sink function at Kopuatai under a warming and drying climate. During wet canopy conditions, however, E_{int} enables much greater water loss from Kopuatai than when the canopy is dry.

Acknowledgements

First and foremost, I am very grateful to Dave, my wonderful supervisor! Thank you for being so supportive, patient, and kind throughout the years. You are super inspiring to work with and have so much motivation and passion that it's infectious - in fact, your influence has turned me into a true "peaty type"! I've really enjoyed our time working together, and I've learnt and grown a lot, so thank you for being such a great supervisor!

I am grateful to the University of Waikato and Manaaki Whenua Landcare Research for providing scholarships and funding for our research, to the mana whenua Te Kupenga O Ngāti Hako and the Department of Conservation for permitting us to access and undertake research at Kopuatai bog, and to the Brewster family for access across their farmland. Your support has enabled us to obtain very useful insights into the functioning of this unique and special ecosystem! Our hope is that this research will help future peatland restoration efforts across Aotearoa, so all of you have helped take another step towards better outcomes for these ecosystems.

To our Canadian co-authors, Peter and Elyn - thank you so much for sharing your Mer Bleue data with us and helping us prepare the paper for submission! I'm very happy to have had the opportunity to work with such passionate people in our field, and I'm proud of the awesome paper that we've crafted together as a result.

I would also like to thank Louis and Aaron for your advice and help with my MSc, whether it was to do with MATLAB or understanding the big picture of my project. Your help has been invaluable! I also really appreciate your support and encouragement throughout my MSc - both of you have helped me build confidence in myself and my work, so thank you!

Thank you to all of the graduate students in Hamilton and Tauranga for your positivity and encouragement - you are such wonderful people and I'm so grateful to have met you all! I would also like to thank the students at the Tauranga campus - Natalie, Claire, Lizzie, Aku,

Tim, Caleb, Megan, and many others - for giving me such a warm welcome when I moved to Tauranga.

Thank you to the people that helped with my fieldwork, including Kat, Ben, Robert, and even a number of visitors from elsewhere in NZ and other countries. It was great to have people around who wanted to join us in the field and get stuck (sometimes literally) into something new and exciting!

To my friends and family – thank you for giving me plenty of encouragement throughout the years! A special thank you to my Mum, Dad and my sister, Anna, for helping me through all the study-related stress - I'm grateful to have such an awesome support network and I love you all so much!

Finally, I would like to thank my partner, Ryan, for being so supportive throughout the roller coaster that was my MSc - you helped me stay motivated and I really appreciate you being there for me!

Table of Contents

List of Figures

List of Tables

Chapter 1

Introduction

Peatlands provide important ecosystem services, including carbon (C) sequestration, flood attenuation, habitat provision for rare species, and water quality improvement through denitrification (Bonn et al., 2016). The C sequestration function of peatlands is particularly important, as global peatlands are estimated to contain over a third of global soil C, but only cover ~3% of Earth's land surface area (Yu et al., 2010; Scharlemann et al., 2014; Xu et al., 2018). The ability of peatlands to sequester C is closely linked to their hydrological conditions - these ecosystems typically have a high water table, which reduces the rate of organic matter decomposition below that of plant litter production, enabling net C accumulation as peat (Joosten & Clarke, 2002). Conversely, when water table drawdown occurs due to environmental or anthropogenic factors, C can be lost from peatland ecosystems (Kwon et al., 2022).

One important process indirectly affecting the water table level in peatlands is evaporation (E), which represents a loss of water from the ecosystem. During dry conditions, E typically consists of transpiration and surface E from soil and water, while during wet conditions following rainfall, it primarily consists of interception loss (E_{int}) from vegetation surfaces (Coenders-Gerrits et al., 2020). Globally, annual E has been estimated to comprise 80% transpiration, 11% E_{int}, and 7% soil surface E, as well as 2% snow sublimation (Miralles et al., 2011). These water loss pathways need to be studied in order to understand mechanisms causing water table drawdown and C loss in peatlands.

Since so much of the Earth's soil C is concentrated in a very small area, increasing risks of peatland degradation due to drainage, fires, vegetation removal, and climatic warming and drying (Dohong et al., 2017; Harris et al., 2021) could have a major impact on the global climate. This is because peatland C sequestration has caused a net cooling effect on the global

climate over thousands of years (Frolking & Roulet, 2007), therefore any C losses are likely to counteract this effect. Recent work by Helbig et al. (2020) has shown that *E* from boreal peatlands increases with increasing atmospheric vapour pressure deficit (VPD), suggesting an increased risk of peatland water table drawdown due to future climatic drying. Under such conditions, it is possible that a decrease in ecosystem net C uptake or a switch to a net C loss could occur, as has been observed in peatlands responding to drought-related water table drawdown (e.g., Aurela et al., 2007; Lund et al., 2012; Gažovič et al., 2013). Therefore, investigating dry and wet canopy *E* regimes may be crucial to understanding current peatland hydrology and C sequestration, as well as future impacts under climatic warming and drying.

1.1 Thesis aim and objectives

The aim of this study is to gain a better understanding of dry and wet canopy *E* regimes at Kopuatai bog, Aotearoa New Zealand, an ecosystem dominated by the very water-conservative plant species *Empodisma robustum*. This will firstly involve examining seasonal variability in *E* and equilibrium evaporation (E_{eq}), energy partitioning, and the response of *E* to increasing VPD at Kopuatai relative to a shrub and moss-dominated Northern Hemisphere peatland. Secondly, the magnitude of E_{int} will be quantified at Kopuatai using a canopy water balance small plot experiment and two E_{int} models.

1.1.1 Peatland evaporation across hemispheres: contrasting controls and sensitivity to climate warming driven by plant functional types

The aim of this chapter is to examine an 11-year eddy covariance (EC) *E* dataset collected from Kopuatai bog to determine whether *E. robustum* has a notable influence on long-term variability in *E*, with a particular focus on the response of *E* to increasing VPD due to climatic warming and drying. The majority of this analysis will pertain to dry canopy conditions; however, a small component examines wet canopy energy balance partitioning. In order to isolate the effect of *E. robustum* on *E*, this analysis is replicated on a 20-year dataset from Mer Bleue bog, Canada - a 'typical' shrub and *Sphagnum* moss-dominated Northern Hemisphere peatland.

The objectives of this analysis are to compare the following between Kopuatai and Mer Bleue:

- Climate and hydrological conditions
- Seasonal variability in E and E_{eq}
- Seasonal variability in dry canopy energy balance partitioning
- Daily energy balance partitioning in dry and wet canopy conditions
- The response of dry canopy E, evaporative fraction (EF), and canopy conductance (g_c) to increasing VPD.

The hypothesis for this section is that differences in seasonal E limitations, energy balance partitioning, and responses of E to VPD, such that more water is conserved at Kopuatai relative to Mer Bleue, can be attributed to differences in vegetation functional type. If this hypothesis is correct, it is possible that *E. robustum* may enable greater resistance of the hydrological regime and resilience of C stores to future climatic drying compared to Northern Hemisphere peatlands.

1.1.2 Quantifying interception loss at Kopuatai bog

The aim of this chapter is to quantify E_{int} at Kopuatai bog, thereby improving our current understanding of wet canopy E regimes in this ecosystem. This will be done by collecting net precipitation (P_n) data using a small plot field experiment and applying two models to the 11-year EC dataset collected at Kopuatai to estimate E_{int}. As such, the objectives of this section are to:

- Develop a P_n measurement method applicable to dense vegetation lacking a trunk (i.e., *E. robustum*), where the use of sub-canopy rain gauges and stemflow collars is impractical
- Calculate E_{int} and canopy storage capacity (S) for the *E. robustum* canopy using the field experiment results and the two modelling approaches at rain event to annual timescales

- Determine whether rain event characteristics, vegetation features, and meteorological conditions affect E_{int} at Kopuatai
- Describe seasonal variability in E_{int} using modelled results.

The hypothesis for this section is that E_{int} will be high compared to other ecosystems dominated by short vegetation due to the dense canopy structure of *E. robustum*, and that E_{int} will constitute a larger proportion of total E during wetter months.

1.2 Thesis outline

Chapter 2 consists of a literature review which details the formation of peatlands, the relationship between peatland carbon uptake and hydrology, controls on E, and E_{int} measurement techniques. In addition, current knowledge of the vegetation, hydrology, and C balance of Kopuatai bog is summarised.

Chapters 3 and 4 are structured in the form of journal papers. Chapter 3 compares the E regimes at Kopuatai bog, Aotearoa New Zealand, and Mer Bleue bog, Canada, with a focus on characterising the E-limiting effect of *E. robustum* at Kopuatai. In addition, the response of E to increasing VPD is compared at these two peatlands. Chapter 4 describes the results of a small plot experiment carried out at Kopuatai to quantify E_{int}, comparing the results of this experiment to those of two modelling approaches. Furthermore, factors influencing E_{int} are identified and seasonal variability in E_{int} is described.

Chapter 5 presents the conclusions drawn from this research, as well as providing recommendations for further research.

Chapter 2

Literature Review

2.1 Peatland formation

Peatlands are wetland ecosystems that have been formed through the accumulation of dead and decaying organic matter, called peat, which mostly consists of plant litter (Page & Baird, 2016). Peat accumulation occurs when plant litter production exceeds the rate of its decomposition, an imbalance that results from limitations imposed on decomposition by waterlogged conditions (Joosten & Clarke, 2002). This occurs because waterlogging creates low oxygen conditions, which are particularly important for inhibiting the breakdown of decomposition-limiting phenolic compounds found within plant material (Freeman et al., 2001; Fenner & Freeman, 2011).

Peatland formation can be initiated through two processes – paludification and terrestrialization; the former occurs when a hydrological change causes a previously dry ecosystem to transition into a wetland, while the latter results from the infilling of a water basin, e.g., a shallow lake, with organic matter accumulated in the anoxic aquatic environment (Temmink et al., 2022). Two main types of peatlands may be formed throughout the peatland development process – minerotrophic and ombrotrophic peatlands (also referred to as fens and bogs, respectively; Lindsay, 2018), which differ in terms of their hydrology, nutrient status, and pH (Charman, 2009). Raised bogs in particular only receive water through precipitation (*P*) in the form of rain, snow, dew, mist, and fog, as they form due to the accumulation of a thick layer of peat that isolates the system from groundwater (Lindsay, 2018). Fens, on the other hand, receive surface water and groundwater inputs in addition to *P*, which has implications for peatland nutrient status and pH, as surface water and groundwater contain nutrients through contact with mineral soils (Charman, 2009). However,

P cannot be enriched in this manner, resulting in a lower nutrient content and pH in raised bog ecosystems (Charman, 2009).

2.2 The connection between hydrology and the carbon sink

Peatland carbon (C) sequestration is influenced by environmental factors, such as light availability, soil temperature, and water table depth (WTD), and by biological characteristics of the ecosystem, such as the dominant plant species (Blodau, 2002; Lafleur, 2009). WTD is a particularly important influence on the peatland C balance, as water table drawdown due to drought or drainage can reduce net C uptake due to (a) decreased carbon dioxide (CO_2) gain through photosynthesis and/or (b) enhanced CO_2 loss through soil respiration (Lafleur, 2009; Lund et al., 2012; Gažovič et al., 2013; Ma et al., 2022b). Conversely, water table drawdown can mitigate some C losses through lower methane (CH_4) emissions and dissolved organic carbon (DOC) export, however in many cases this is insufficient to prevent a decrease in net C uptake or a switch to a net C source in response to water table drawdown (e.g., Gažovič et al., 2013; Kwon et al., 2022). Therefore, WTD has a major influence on peatland C accumulation, and factors affecting WTD, such as evaporation (*E*), in turn have an important indirect influence on the C balance.

2.3 Evaporation: importance and controls

The water balance of raised bog peatlands consists of precipitation (*P*) inputs, with evaporation (*E*) and surface runoff and groundwater (*Q*) outputs, the balance of which causes changes in water storage (ΔS; Rydin & Jeglum, 2013b). As stated above, inputs of surface and groundwater can occur in fens, while in raised bogs such inputs do not occur. The water balance of raised bogs can therefore be described by the following equation:

$$\Delta S = P - E - Q \qquad (2.1)$$

Water loss via *E* has an important indirect influence on WTD, as it reduces the available water within a peatland. Evaporative fluxes primarily consist of transpiration, interception loss (E_{int}), and soil surface *E* components, which have been estimated to constitute 80%, 11%, and 7% of

total *E* at a global scale, respectively (Miralles et al., 2011). The magnitude of *E* is influenced by a number of meteorological (e.g., solar radiation, vapour pressure deficit (VPD), atmospheric turbulence) and surface factors (e.g., vegetation type, WTD) at diurnal to interannual timescales (Takagi et al., 1999; Shimoyama et al., 2003; Wu et al., 2010). The occurrence of specific weather phenomena can also affect *E*; for example, fog has been observed to limit solar radiation receipt and VPD in a Newfoundland blanket bog, resulting in very low *E* rates (Price, 1991). Therefore, there are a number of factors that affect *E* rates from peatlands, the most important of which are discussed below. In particular, this discussion will demonstrate the important role of peatland vegetation in determining *E* rates.

2.3.1 Net radiation

The surface energy balance applicable to all ecosystems is described using the following equation:

$$R_n = LE + H + G + Q \quad (2.2)$$

where R_n is net radiation, which is the net sum of all incoming and outgoing fluxes of shortwave and longwave radiation, *LE* is the latent heat flux, which is the energy used to evaporate water, *H* is the sensible heat flux, defined as the transfer of heat between the surface and atmosphere, *G* is the ground heat flux, or the energy gained or lost by soil as heat, and *Q* is the energy storage in biomass, the air below the measurement height, the soil above the measurement depth, and plant metabolic processes (Lafleur, 2008; Anderson & Wang, 2014). The key component of the energy balance linked to the water balance is *LE*, which represents the *E* rate through (Oke, 1987):

$$E = LE/L_v \quad (2.3)$$

where L_v is the latent heat of vaporisation (2.45 MJ kg^{-1} at 20 °C).

Therefore, as *LE* is directly linked to R_n through the energy balance, R_n is an intrinsically important driver of *E*. As a result, correlations between R_n (or available energy, R_n–*G*) and *E*

have previously been observed in a number of peatlands (Lafleur & Roulet, 1992; Kurbatova et al., 2002; Brümmer et al., 2012; Peichl et al., 2013; Wang et al., 2020).

2.3.2 Vapour pressure deficit

In any ecosystem, VPD appears to have two possible opposing effects on *E* - increases in VPD raise the atmospheric demand for water, either driving higher *E*, or decreasing plant transpiration rates (and therefore *E*) by triggering stomatal closure (Novick et al., 2016; Massman et al., 2019). Factors affecting the direction of the VPD-*E* relationship include the climate, vegetation type, and soil moisture content of an ecosystem (Massman et al., 2019; Tong et al., 2022). Positive relationships between *E* and VPD have been shown at half-hourly, daily, and monthly scales in a number of peatlands (Admiral et al., 2006; Wu et al., 2010; Peichl et al., 2013; Wang et al., 2020), in addition to observations of control over interannual variability in *E* (Shimoyama et al., 2003). The strength of these relationships has been shown to depend on R_n (Wang et al., 2020), WTD, and surface dryness; the latter impacts the source partitioning of *E* between mosses and vascular vegetation, each of which cause contrasting responses of *E* to high VPD (Admiral et al., 2006; Admiral & Lafleur, 2007). The influence of vegetation type on the response of peatland *E* to VPD is discussed further in the following section.

2.3.3 Vegetation type

Many vegetation groups are found in peatlands, including bryophytes, herbs, graminoids, shrubs, and trees (Rydin & Jeglum, 2013a), each of which have a unique influence on *E*. In particular, vascular (e.g., shrubs) and non-vascular (e.g., bryophytes) peatland vegetation has contrasting effects on the *E* regime, as differences in *E* rates and controls have been observed between these vegetation types (Lafleur & Roulet, 1992; Takagi et al., 1999; Admiral et al., 2006). These differences primarily occur due to the contrasting plant physiology and canopy structure of vascular and non-vascular species.

Peatland vascular plants have been observed to restrict water loss through stomatal closure in response to increasing VPD (Takagi et al., 1999; Admiral & Lafleur, 2007), which causes a reduction in stomatal conductance (g_s), i.e., the rate of water vapour exiting stomata (Jeanguenin et al., 2017). In contrast, the non-vascular *Sphagnum* mosses commonly dominating peatlands only have pseudostomata structures that are not involved in gas exchange (Duckett et al., 2009), and therefore cannot restrict water loss with increasing VPD. As a result, *E* rates from mosses have been observed to increase with increasing VPD, while *E* from vascular vegetation decreases at high VPD due to stomatal closure (Admiral et al., 2006). However, moss *E* can become limited when the water table is too low and the supply of water to the moss surface is restricted (Waddington et al., 2015), or when VPD is too high, as the rate of water transport through mosses may be insufficient to meet the high atmospheric demand (Liljedahl et al., 2011).

In addition to plant physiology, canopy structure also influences *E* rates. For example, the canopy structure of vascular plants may be subject to seasonal changes; in a prairie wetland, it was observed that the contribution of transpiration to *E* was lower during senescence periods compared to the growing season (Burba et al., 1999). Furthermore, *E* can be reduced by changes in vegetation structure in response to severe drought, such as leaf shedding from trees in tropical peat domes of Southeast Asia (Dommain et al., 2010). Therefore, peatland *E* regimes can be significantly affected by the physiology and structure of the dominant vegetation.

2.3.3.1 *Sphagnum* moss

Sphagnum mosses are peat formers which cover a large proportion of boreal peatlands (Rydin et al., 2006). The ability of *Sphagnum* species to form peat is a result of the slow decomposition of dead *Sphagnum*, which is enabled by its low nutrient content, and by the acidic, wet, and anoxic conditions maintained in peatlands by living *Sphagnum* vegetation (Clymo & Hayward, 1982; Rydin et al., 2006). *Sphagnum* plants obtain water through capillary rise from the water table and retain it within capitula - structures that make up the top 2 cm of the plant

- and in hyaline cells, which hold water until emptied by a low soil water pressure (McCarter & Price, 2014).

Evaporative losses from the moss surface have been shown to constitute up to two thirds of total *E* in peatlands, depending on the time of day and the season (Kim & Verma, 1996; Admiral & Lafleur, 2007); therefore, this is an important mechanism of water loss from *Sphagnum*-dominated peatlands. The magnitude of *E* from *Sphagnum* is dependent on its water content (Williams & Flanagan, 1996), which is in turn influenced by *P*, WTD, and species-specific moss properties, such as capitula density and pore geometry (Strack & Price, 2009; Adkinson & Humphreys, 2010; McCarter & Price, 2014). In particular, when the WTD is far from the surface and rainfall is low, the water content of *Sphagnum* capitula decreases and hyaline cells may drain (Strack & Price, 2009; Strack et al., 2009), reducing moss *E* (Lafleur et al., 2005; Admiral & Lafleur, 2007).

2.3.4 Water table depth

Generally, WTD and *E* in peatlands have been found to be only weakly correlated (Sonnentag et al., 2010), or uncorrelated (Humphreys et al., 2006; Parmentier et al., 2009; Wu et al., 2010). Parmentier et al. (2009) proposed that WTD and *E* were not correlated at their site because the peat water content was sufficiently high to maintain *E*, even at a low WTD; this implies that peat water content may be a more important control on *E*. Alternatively, weak correlations of *E* with WTD may have occurred due to differing responses of vascular and non-vascular vegetation; while increases in WTD limit *E* from moss surfaces due to insufficient capillary rise, high *E* rates appear to be maintained via increased local surface temperatures and atmospheric dryness, which enhance vascular plant transpiration rates (Kim & Verma, 1996; Lafleur et al., 2005). However, it is also possible that a WTD–*E* relationship was not observed in the aforementioned studies because significant restrictions on *E* may only occur once the WTD drops below the maximum rooting depth of vascular plants, restricting transpiration (Lafleur et al., 2005). As such, the effect of water table drawdown on peatland *E* is closely linked to the vegetation composition of the ecosystem.

2.4 Interception loss measurement

Interception loss, E_{int}, is the proportion of gross precipitation (P_g) that is detained by and evaporated from the plant canopy (David et al., 2005). The proportion of seasonal or annual P_g returned to the atmosphere as E_{int} can be large, with proportions as high as 45% observed in forest and dryland ecosystems (Carlyle-Moses & Gash, 2011; Magliano et al., 2019a). Therefore, E_{int} can be responsible for substantial water losses from an ecosystem. The magnitude of E_{int} has typically been determined by measuring net precipitation (P_n), i.e., the water that reaches the ground by travelling through vegetation, which consists of throughfall and stemflow components. Throughfall is water which falls through the vegetation canopy and onto the ground, while stemflow involves the flow of water down stems and trunks to the ground surface (Crockford & Richardson, 2000). Having measured P_n, E_{int} can be calculated (Dunkerley et al., 2000):

$$E_{int} = P_g - P_n \quad (2.4)$$

The amount of water travelling through the canopy has typically been quantified using sets of funnels, rain gauges, or troughs for throughfall and collars for stemflow (Dunkerley et al., 2000). While these methods have been applied to both trees (e.g., Marin et al., 2000) and shrubs (e.g., Magliano et al., 2019b), they are more difficult to use when vegetation is short and/or lacks a single trunk. In such cases, alternative methods have been developed; for example, an 'interception flow collection box' was used to collect throughfall and stemflow under a small shrub canopy (Serrato & Diaz, 1998), while collection trays and latex collars were used to collect this data in a grass-covered area (Zou et al., 2015).

Canopy storage capacity (S), defined as the minimum quantity of water needed to saturate the plant canopy, is an important factor influencing E_{int} (David et al., 2005). The value of S has previously been determined using measures of weight gain under artificial rainfall or after submergence in a water tank (Dunkerley et al., 2000), using gamma ray and microwave attenuation methods (David et al., 2005), or most commonly by determining the y-intercept of the linear relationship between P_g and P_n (as done by Campbell & Murray, 1990; Guevara-Escobar et al., 2007; Su et al., 2016; Ma et al., 2022a).

2.5 Peatlands in New Zealand

Peatlands are most abundant in boreal regions of the Northern Hemisphere (Vitt, 2006), however they can also form in temperate climates, where they make up about 10% of the global peatland area (Frolking et al., 2011). In Aotearoa New Zealand, the temperate climate is warmer and drier compared to that of Northern Hemisphere peatlands, and experiences summer water deficits; as such, peatland formation would not be anticipated in this climate (McGlone, 2009). One of the most extensively studied peatlands in New Zealand and the focus of this thesis is Kopuatai bog, an ombrotrophic peatland located in the Waikato region. The following sections will summarise our current understanding of the dominant vegetation species, hydrological characteristics, and C balance of Kopuatai.

2.5.1 *Empodisma robustum* vegetation

The vegetation composition of peatlands in Aotearoa New Zealand differs from that of *Sphagnum*-dominated Northern Hemisphere peatlands due to the common occurrence of species from the Restionaceae ('restiad') family (McGlone, 2009). A particular species of interest from this family is *Empodisma robustum*[1], a peat-forming vascular plant that is found north of the 38° S latitude on Te Ika-a-Māui North Island (Wagstaff & Clarkson, 2012), and is the dominant plant species at the Kopuatai bog research site. *E. robustum* is an evergreen plant consisting of intertwined wiry stems with leaf sheaths located at short intervals (Figure 2.1; Agnew et al., 1993; Wagstaff & Clarkson, 2012). It forms a dense surface mat of white, negatively geotropic roots, the remains of which constitute the majority of new peat material; however, these roots also bind live mosses and dead plant material into the peat (Campbell, 1964; Agnew et al., 1993). In addition, *E. robustum* contains decay-resistant compounds, such as lignins, tannins, and phenolic compounds, which facilitate peat accumulation (Kuder et al., 1998). Due to its ability to initiate fen-bog transitions, *E. robustum* is regarded as an ecosystem engineer in New Zealand peatlands (Hodges & Rapson, 2010).

1 Referred to as *Empodisma minus* in early studies but reclassified to *Empodisma robustum* by Wagstaff & Clarkson (2012).

Figure 2.1. *Empodisma robustum* stems wetted by rain (left), and its canopy structure (right; Photo: David Campbell) at Kopuatai bog.

One of the most important properties of *E. robustum* is its ability to restrict *E* rates; at Kopuatai bog, this feature results in *E* rates that are below those typically observed in Northern Hemisphere peatlands (Campbell & Williamson, 1997). This has been attributed to a number of *E* restriction mechanisms. Firstly, *E. robustum* is able to use its stomata to restrict transpiration (Campbell & Williamson, 1997), like many other plant species. However, *E. robustum* has additional features which enable water retention, such as its dense above-ground root mass, which can hold up to 15 times its dry weight in water (Campbell, 1964). In addition, its dense standing litter layer limits *E* by acting as a 'mulch', providing a barrier to water vapour diffusion and restricting solar radiation at the peat surface; this litter also absorbs a considerable amount of *P*, further enabling water retention (Campbell & Williamson, 1997). It has also been speculated that the low peat nutrient content observed at Kopuatai could be an additional factor limiting *E* rates; this results in a low leaf nitrogen content, which limits C assimilation (Campbell & Williamson, 1997) and therefore transpiration rates.

2.5.2 Hydrology

Hydrological studies at Kopuatai have mainly investigated *E* regimes (Campbell & Williamson, 1997; Thompson et al., 1999), although WTD variations have been examined in connection to the C balance (Ratcliffe et al., 2019). The WTD at Kopuatai is shallow and stable (Ratcliffe et al., 2019), and *E* rates are low, likely due to the restrictions imposed on *E* by *E. robustum* (described above). Rates of *E* at Kopuatai appear to be controlled by VPD and canopy resistance (r_c), based on the low decoupling coefficient value observed (Campbell & Williamson, 1997). Partitioning of *E* has also been attempted at Kopuatai, however this only included transpiration and peat surface *E*, not E_{int}; 65% of *E* was estimated to be derived from the peat surface, with the remaining 35% attributed to transpiration (Campbell & Williamson, 1997). In addition, an important feature of the *E* regime observed at Kopuatai is the contrast in *E* rates between dry and wet canopy conditions – *E* rates were constrained when the vegetation canopy was dry, while during wet canopy conditions *E* rates were considerably higher (Campbell & Williamson, 1997; Thompson et al., 1999).

2.5.2.1 Interception loss

Throughfall and stemflow measurements were previously made at Kopuatai by Agnew et al. (1993) using bottles placed within a canopy of *E. robustum* and *Sporadanthus ferrugineus* (another restiad species). Over a 1-year period, their results showed that 44.8% and 21.3% of rainfall became throughfall and stemflow, respectively, resulting in 33.9% of rainfall being lost as E_{int} (Agnew et al., 1993). In addition, canopy storage capacity (*S*) has previously been estimated to be around 2 mm for the *E. robustum* canopy (Campbell & Williamson, 1997); however, this value was not derived using a replicated experiment. Therefore, E_{int} and *S* measurements for *E. robustum* are few, and further investigation is needed.

2.5.3 Carbon balance

Kopuatai bog is a strong C sink compared to many Northern Hemisphere peatlands. This is likely due to the year-round growing conditions, which enable C uptake to occur over longer

periods of time (Campbell et al., 2014), and the aforementioned *E*-limiting adaptations of *E. robustum* (Goodrich et al., 2017), which contribute to maintaining a high water table, and therefore high C uptake. Individual components of the C balance at Kopuatai have been previously linked to the hydrology of this ecosystem, highlighting the importance of hydrological conditions for regulating C uptake. For example, ecosystem respiration (ER), which represents a C loss, is typically lower when the water table is close to the surface, while C loss via methane (CH_4) emissions is enhanced; in addition, the outflow of dissolved organic carbon (DOC) is mainly driven by the peatland water balance (*P* minus *E*; Goodrich et al., 2017). However, gross primary productivity (GPP), which represents a C gain, does not appear to be significantly impacted by WTD (Goodrich et al., 2017). Therefore, there are strong interdependencies between most components of the C balance and hydrological conditions at Kopuatai.

Chapter 3

Peatland evaporation across hemispheres: contrasting controls and sensitivity to climate warming driven by plant functional types

3.1 Introduction

Global peatlands have accumulated carbon (C) stocks of 500 Pg or more over thousands of years, resulting in a net cooling effect on the climate (Yu et al., 2010; Frolking & Roulet, 2007). This C stock is estimated to make up a third of global soil C (based on a median estimate of 1460.5 Pg), despite only occupying ~3% of Earth's land surface area (Scharlemann et al., 2014; Xu et al., 2018). Carbon accumulation as peat occurs in undisturbed peatlands when the rate of organic matter deposition exceeds decomposition, due to limitations imposed on decomposition by waterlogged conditions and the presence of decay-resistant plant litter (Joosten & Clarke, 2002; Holden, 2005). Therefore, long-term C sequestration in peatlands depends on maintaining a high and stable water table (Kim et al., 2021; Ma et al., 2022b).

Evaporation (E)[2] is an important indirect influence on peat accumulation, as it reduces available water and contributes to water table drawdown. Evaporative fluxes consist of three main components - transpiration, surface E (either from water, soil, or non-vascular plant surfaces), and interception loss from vegetation surfaces, and are influenced by a number of meteorological (solar radiation, vapour pressure deficit (VPD)) and surface factors (vegetation type and water table depth (WTD); Takagi et al., 1999; Shimoyama et al., 2003; Wu et al., 2010). In bog ecosystems, where precipitation is the sole water input (Holden, 2005), conservation of water is particularly important; this occurs through limitations imposed on E by bog

[2] 'Evaporation' refers to "the bulk flux of water, including transpiration". We did not use the term 'evapotranspiration', as both evaporation and transpiration involve transformation of water from a liquid to a vapour (Miralles et al., 2020).

vegetation (Campbell & Williamson, 1997), as well as limitations on lateral and vertical drainage by low hydraulic conductivity in the highly decomposed peat soils (Fraser et al., 2001). As such, vegetation type is often a major factor regulating *E* from bogs (Lafleur & Roulet, 1992; Takagi et al., 1999; Admiral et al., 2006).

The response of *E* to increasing atmospheric demand, i.e., increasing VPD, is of particular interest, as climate change-related warming has been predicted to elevate VPD (Ficklin & Novick, 2017; Fang et al., 2022). As VPD increases, contrasting *E* responses have been observed across different vegetation types (Takagi et al., 1999; Admiral et al., 2006; Massman et al., 2019) and ecosystems (Helbig et al., 2020). For example, using eddy covariance (EC) data from 95 boreal peatland and forest sites, Helbig et al. (2020) demonstrated that *E* rates were elevated by increasing VPD in both ecosystem types, however *E* rates were 30% higher in boreal peatlands than in boreal forests at high VPD. This suggests that the stability of peatland hydrology and C stores may be at risk under future changes to the climate.

Kopuatai bog is a warm-temperate, ombrotrophic peatland on Te Ika-a-Māui North Island of Aotearoa New Zealand. The vegetation at Kopuatai is dominated by the vascular plant *Empodisma robustum*, which has been implicated in severely restricting *E* (Campbell & Williamson, 1997). The hypothesised mechanisms for this are stomatal control of transpiration and limitation of surface *E* due to restricted water vapour diffusion from the substrate through the dense standing litter layer (Campbell & Williamson, 1997; Thompson et al., 1999). Studies on ecosystem C balances have shown that C uptake at Kopuatai is greater than in analogous Northern Hemisphere peatlands, and exhibits resilience to drought (i.e., high annual C uptake rates despite drought disturbance in summer; Goodrich et al., 2017). This could be a result of the year-round growing conditions (Campbell et al., 2014), in contrast to the temperature-limited growing season lengths in Northern Hemisphere peatlands which constrain C uptake (Roehm & Roulet, 2003; Lafleur et al., 2001; Helfter et al., 2015). However, high C uptake rates and drought resilience could also be indirectly attributed to the extremely low *E*, which maximises available water and maintains a high and stable water table. Therefore, the *resilience* of C uptake at Kopuatai could be due to *resistance* of the hydrology to environmental stressors through limitations on *E*, thereby preventing major shifts in the hydrological regime

(resistance and resilience definitions are from Nimmo et al., 2015). As such, *E* limitation could be a very important self-regulation mechanism in this peatland ecosystem type.

Peatlands have formed in warm climates, however the majority of the global peatland area occurs in boreal regions of the Northern Hemisphere (Vitt, 2006). One such peatland is the Mer Bleue bog in Canada, a shrub and *Sphagnum*-dominated ecosystem located in a cool continental climate zone (Moore et al., 2002). As one of the most studied Northern Hemisphere peatlands, Mer Bleue has an extensive record of *E* measurements and knowledge of *E* processes. Daily *E* rates at Mer Bleue are comparable to many other Northern Hemisphere peatlands; *E* has been shown to be reduced by deep water tables (Lafleur et al., 2005), and regulated by available energy, which drives increases in *E*, and by VPD, the effect of which varies depending on the partitioning of *E* between vascular and non-vascular sources (Admiral et al., 2006). The average net annual C uptake at Mer Bleue is much lower than at Kopuatai, primarily due to net C losses during the winter period, and a shorter growing season (Roulet et al., 2007; Goodrich et al., 2017).

Knowledge of *E* at Kopuatai bog is limited to the results of two short-term studies (Campbell & Williamson, 1997; Thompson et al., 1999); therefore, long-term *E* datasets from Kopuatai have not yet been examined, so our understanding of the variability and mechanisms of *E* restriction by *E. robustum* is incomplete. In addition, it is not yet known how these limitations on *E* may affect the response of the ecosystem at Kopuatai to climate warming. Therefore, the aim of this study is to compare the *E* regime at Kopuatai to that of Mer Bleue, as an example of a 'typical' Northern Hemisphere peatland, to better understand the potential relative sensitivity of these systems to hydrological change under continued climate warming. Compared with previous studies, our study benefits from extensive multi-annual data records at each site, thereby analysing *E* characteristics over a wide range of weather conditions. The objectives of this study are to (1) compare seasonal variability in actual *E* and equilibrium *E* (E_{eq}) at Kopuatai and Mer Bleue, (2) investigate energy balance partitioning and (3) examine the responses of *E*, evaporative fraction (EF), and canopy conductance (g_c) to VPD at each site. Our hypothesis is that differences in seasonal *E* limitations, energy balance partitioning, and responses of *E* to VPD, such that more water is conserved at Kopuatai relative to Mer Bleue,

can be attributed to differences in vegetation. If this hypothesis is correct, it is possible that the water-conserving traits of *E. robustum* will enable greater resistance of the hydrological regime, and hence greater resilience of the C stores, to climate warming compared to typical Northern Hemisphere peatlands.

3.2 Methodology

3.2.1 Site descriptions

3.2.1.1 Kopuatai bog

Kopuatai bog is a 96 km^2 ombrotrophic peatland located in a warm-temperate oceanic climate in the Waikato region of Aotearoa New Zealand (37.388° S, 175.554° E). Kopuatai is Aotearoa's largest undisturbed bog, representing a remnant of formerly widespread and diverse lowland wetlands, which have been reduced to 10% of their previous extent due to widespread drainage, primarily for agriculture (McGlone, 2009; Dymond et al., 2021). Probing at the research site showed a mean peat depth of 11 m (maximum depth = 14 m), which has accumulated over the last 11,700 years at an average rate of 0.9 mm $year^{-1}$ (Newnham et al., 1995; Shearer, 1997).

The dominant peat-forming vegetation at Kopuatai is *E. robustum* (Wagstaff & Clarkson, 2012), a vascular, evergreen jointed rush-like plant that is part of the family Restionaceae (known as 'restiads'; Wagstaff & Clarkson, 2012). At the field site, *E. robustum* has a mean leaf area index (LAI) of 1.32 (Goodrich et al., 2015) and mean canopy height of 0.48 m. *E. robustum* forms a dense, negatively geotropic surface root mat approximately 50 mm deep which can hold up to 15 times its dry weight in water (Campbell, 1964; Agnew et al., 1993; Clarkson et al., 2009). In addition, the standing litter of *E. robustum* intercepts a considerable quantity of precipitation (Campbell & Williamson, 1997). It has been hypothesised that this dense standing litter layer (litter biomass = 0.92 kg m^{-2}, where total canopy biomass = 1.80 kg m^{-2}) can also restrict water vapour diffusion from the peat surface by limiting

turbulent transport (Campbell & Williamson, 1997; Keyte Beattie, 2014). However, *E. robustum* can also restrict water loss via transpiration through strong stomatal control (Campbell & Williamson, 1997). The roots of *E. robustum* are the main material from which peat is formed, however live mosses and decayed canopy litter are also bound by the roots for peat formation (Campbell, 1964; Agnew et al., 1993). Other vegetation types found at this site include sedges (*Machaerina* spp. and *Schoenus brevifolius*), isolated shrubs of *Leptospermum scoparium* (manuka) and *Epacris pauciflora*, as well as small patches of *Sporadanthus ferrugineus*, another restiad plant.

3.2.1.2 Mer Bleue bog

Mer Bleue bog is a 28 km^2 ombrotrophic peatland (45.411° N, -75.481° E) located near Ottawa, Canada, in a cool continental climate. Mer Bleue has many features in common with boreal peatlands, but is located near the southern limit of the boreal climate zone (Hember et al., 2005). This peatland was formed 8400 years ago, initially as a fen, transitioning into a bog around 7100–6800 years ago (Roulet et al., 2007). At the research site, Mer Bleue is characterised by a hummock-hollow microtopography, and has peat depths of 5–6 m (Lafleur et al., 2005). The dominant vegetation consists of evergreen ericaceous and deciduous shrubs (e.g., *Chamaedaphne calyculata*, *Rhododendron groenlandicum*, *Kalmia angustifolium*, *Kalmia polifolia*, *Vaccinium myrtilloides*), with *Sphagnum* moss species as the dominant ground cover, including *S. capillifolium*, *S. papillosum*, and *S. magellanicum* (Bubier et al., 2006). The average shrub canopy height is 0.18 m (range = 0.10–0.30 m; Bubier et al., 2006); shrub vegetation makes up 61% of the total biomass on average, while *Sphagnum* capitula make up 30% (Moore et al., 2002). The total biomass ranges between 0.147 and 1.011 kg m^{-2}, while the LAI of dominant vascular species is 1.3 on average (Moore et al., 2002; Bubier et al., 2006).

3.2.2 Data collection and processing

3.2.2.1 Data collection

Data has been collected at both sites for many years - in this study, data collected between 1 January 2012 and 31 December 2022 at Kopuatai and 1 January 1999 and 31 December 2018 at Mer Bleue were used. At each site, 30-minute fluxes of latent heat (*LE*), sensible heat (*H*) and net radiation (R_n), along with data on environmental and weather variables, including air temperature (T_{air}), vapour pressure deficit (VPD), precipitation (*P*), and water table depth (WTD; measured relative to the hummock surface at Mer Bleue), were collected. Latent and sensible heat fluxes were measured using the eddy covariance (EC) technique (Burba, 2022). The EC system at Kopuatai is an open path system (Appendix A) situated at 4.25 m height, with uninterrupted fetch greater than 500 m in all directions. At Mer Bleue, a closed path EC system is situated at 3.0 m height, with a fetch greater than 500 m in all directions except south, where it is 200–300 m. Full details of data processing, quality control, and gap-filling are provided in Goodrich et al. (2017) for Kopuatai. For gap-filling of *LE* and *H*, separate daytime and night-time neural network models used drivers of R_n, T_{air}, VPD, and modelled canopy wetness state (detailed below). At Mer Bleue, gap-filling of *LE* was carried out by developing a linear relationship between available energy (R_a) and *LE* for summer, and calculating a multiplier to adjust the estimated *LE* to observed *LE* over a moving window period (the window width is 100 consecutive available half hours moved in increments of 20 half hours). R_a was calculated as R_n minus the rate of change in energy storage terms (*J*) and the ground heat flux (*G*), which was calculated using peat surface temperature profiles. Sensible heat fluxes were then calculated as the difference between R_a and *LE*.

3.2.2.2 Equilibrium evaporation

To provide a reference E rate at each site, the equilibrium evaporation (E_{eq}) was calculated using gap-filled 24-hour mean data via the following equation:

$$E_{eq} = \frac{s(R_n - G)}{L_v(s + \gamma)} \quad (3.1)$$

where s is the slope of the saturation vapour pressure versus air temperature curve, L_v is the latent heat of vaporisation (dependent on T_{air}), and γ is the psychrometric constant (0.066 kPa °C^{-1}). G was assumed to be 0 W m^{-2} due to the use of 24-hour mean data.

The proportion E/E_{eq}, i.e. the Priestley–Taylor α, was then calculated in order to be able to compare E regimes at the two sites despite differing climates. Gap-filled LE data were converted to $E = LE/L_v$ for this analysis.

E_{eq} was selected as a measure of potential E as it provides a more conservative estimate compared to other methods, such as the Penman equation (Granger, 1989). In addition, E_{eq} is less dependent on energy partitioning compared to Penman open water E (Thompson et al., 1999). As explained by Thompson et al. (1999), due to the high ratio of sensible to latent heat flux (i.e., a high Bowen ratio (β)) at Kopuatai, VPD is potentially larger than it would be above an extensive water surface in the same region, driving Penman open water E to an unrealistic level. Due to the lack of a VPD term in the E_{eq} equation, this effect is mitigated.

3.2.2.3 Energy balance partitioning and VPD analysis

The analysis of energy balance partitioning and the relationships of E, EF, and g_c with VPD involved the use of non-gap-filled E, R_n, LE, H, and VPD data, pre-filtered through quality control processes. These data were then filtered further - firstly, data were filtered by growing season months (May–Oct at Mer Bleue and Sep–May at Kopuatai). In addition, all 30-minute

data from both sites were filtered to select only "middle of day" (MoD) conditions (10:00–14:30 local standard time), and $R_n \geq 200$ W m^{-2}. These 30-minute data were also filtered by dry or wet canopy conditions, which were identified using an antecedent precipitation index (API) at both Kopuatai and Mer Bleue (Appendix B). An API ≤ 0.2 signifies a dry canopy, while API ≥ 1 indicates fully wet canopy conditions. These filtered 30-minute data were then used to calculate MoD means of all variables. Days with less than three acceptable 30-minute data points for all variables were removed to ensure representative MoD means. Overall, this filtering resulted in 56% and 65% of MoD 30-minute data being rejected for Kopuatai and Mer Bleue, respectively.

To analyse energy balance partitioning, the filtered growing season MoD mean *LE* and *H* data were binned by R_n (bin width = 50 W m^{-2}) for each site, taking the mean value of each bin. This was done separately for dry and wet canopy conditions. Seasonal energy balance partitioning was also investigated by calculating monthly means of MoD dry canopy *LE*, *H*, and R_n.

To show the relationship of variables with VPD, filtered dry canopy growing season MoD means of *E*, EF, and g_c were binned by VPD (0.1 kPa intervals), following Helbig et al. (2020), taking the mean of each bin for all variables. EF was used to assess the change in energy balance partitioning into *LE* with increasing VPD, and was calculated as:

$$EF = \frac{LE}{LE + H} \tag{3.2}$$

The denominator $LE + H$ was used rather than R_n to prevent incomplete energy balance closure (Appendix C) from affecting our results. In addition, β was calculated as:

$$\beta = \frac{H}{LE} \tag{3.3}$$

Finally, g_c was calculated as in Campbell & Williamson (1997):

$$\frac{1}{g_c} = \frac{(1 + \beta)\,\rho\, c_p\, VPD}{\gamma\, R_n} + \frac{r_a\, s\, \beta}{\gamma} - r_a \qquad (3.4)$$

where ρ is air density (1.2 kg m^{-3}), c_p is the specific heat of air (1010 J kg^{-1} $°C^{-1}$), and r_a is aerodynamic resistance. Values of r_a were also calculated using the method from Campbell & Williamson (1997), which firstly required calculation of the aerodynamic resistance to momentum transfer from the measurement height to the canopy (r_{aM}):

$$r_{aM} = \frac{u}{u_*^2} \qquad (3.5)$$

where u is the horizontal wind speed and u_* is the friction velocity measured by the sonic anemometer. Then, r_a was calculated as:

$$r_a = \frac{1.6}{k\, u_*} + r_{aM} \qquad (3.6)$$

where k is von Karman's constant (0.4).

3.2.2.4 Energy balance closure

Energy balance closure was imperfect at both sites, with 85% closure at Kopuatai and 89% at Mer Bleue (Appendix C). This could be due to a number of factors, such as mismatch between footprint characteristics for the turbulent and non-turbulent energy balance terms, or increasing uncertainty of surface soil heat flux measurements due to peat accumulation, which increases the depth of soil heat flux plates over time. Energy imbalances could also be a result of a lack of sustained turbulence at these sites (Anderson & Wang, 2014), or due to the use of MoD means of energy balance components rather than 24-hour means (Leuning et al., 2012).

All analyses were carried out using MATLAB R2021b.

3.3 Results

3.3.1 Climate and hydrology

Mean annual precipitation (P) was 1213 ± 147 mm (± 95% confidence interval) at Kopuatai (2012–2022), compared to 879 ± 58.1 mm at Mer Bleue (1999–2018). Mean monthly P ranged between 49–139 mm and 50–100 mm at Kopuatai and Mer Bleue, respectively, with the minimum monthly P occurring during the warm season at Kopuatai and the cool season at Mer Bleue (Figure 3.1a). The mean monthly air temperature (T_{air}) range was much smaller at Kopuatai (9.3–19.0 °C) than at Mer Bleue (-10.0–20.2 °C) (Figure 3.1b), with mean annual temperatures of 14.1 ± 0.27 °C and 6.2 ± 0.31 °C at the two sites, respectively. Mean annual VPD was 0.39 ± 0.013 kPa at Kopuatai and 0.38 ± 0.023 kPa at Mer Bleue, and monthly mean VPD ranged between 0.17–0.68 kPa and 0.07–0.77 kPa (Figure 3.1c). Mean annual WTD was -82.6 ± 14.4 mm at Kopuatai and -377 ± 19.8 mm at Mer Bleue. Monthly mean WTD had narrower ranges and was shallower at Kopuatai than at Mer Bleue year-round; as a result, the WTD ranges at these sites did not overlap (-153 to -28 mm and -460 to -278 mm, respectively; Figure 3.1d).

3.3.2 Evaporation and equilibrium evaporation

Mean annual E and E_{eq} were larger at Kopuatai compared to Mer Bleue, however mean annual E/E_{eq} was lower at Kopuatai (Table 3.1). In addition, growing season and year-round mean E/E_{eq} values were very similar at each respective site. At both sites, mean monthly E was below E_{eq}, except during winter (Figure 3.2). Both variables followed an expected seasonal pattern of low values in winter and high values in summer, mostly driven by radiation receipts. The difference between E_{eq} and E was larger at Kopuatai than at Mer Bleue in non-winter months; the maximum difference between monthly E_{eq} and E was 71 mm in January at Kopuatai, but only 21 mm at Mer Bleue in May. Both E and E_{eq} were close to zero at Mer Bleue during winter

(Dec–Feb), when air temperature was below 0 °C and the bog was snow covered, and both values were similar during spring (March) and autumn (October) months.

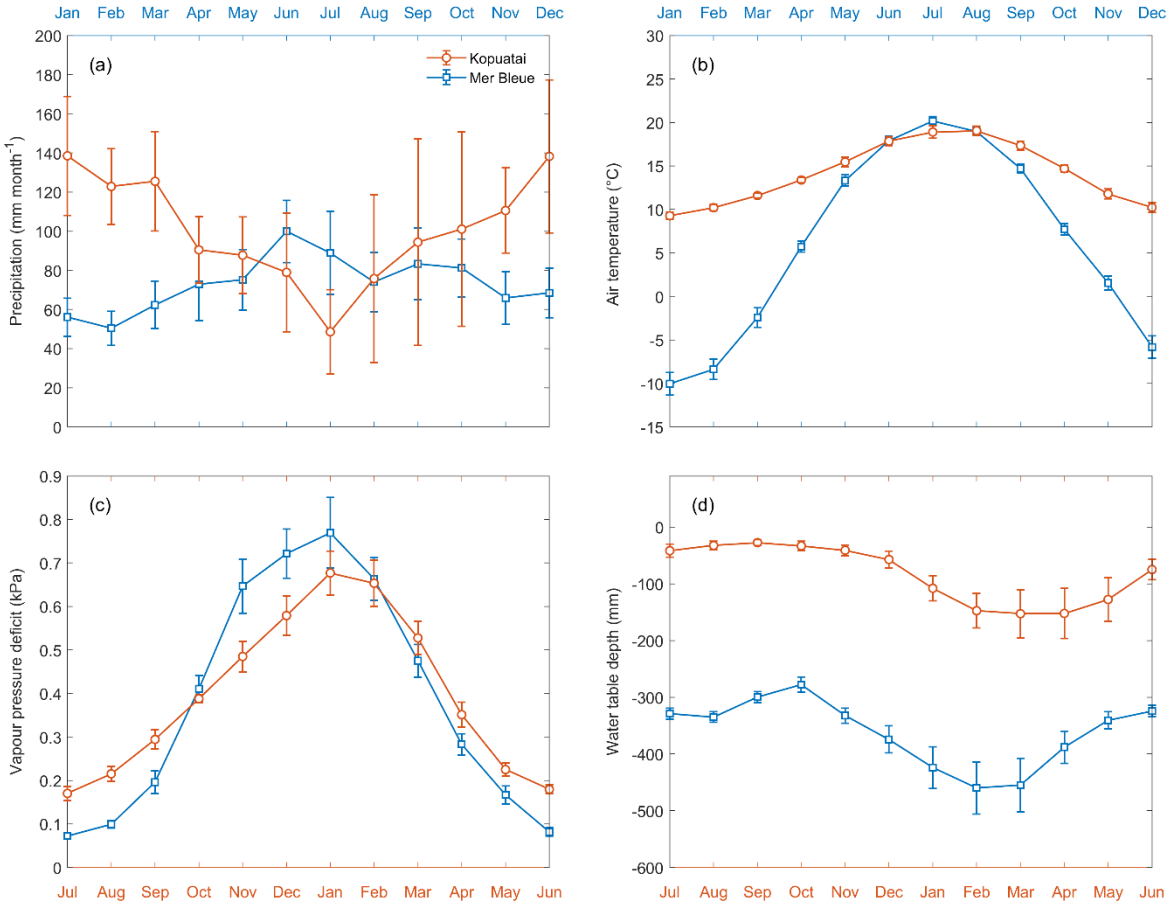

Figure 3.1. Mean monthly (a) precipitation (b) air temperature (c) vapour pressure deficit, and (d) water table depth at Kopuatai (orange) and Mer Bleue (blue). These values were calculated using data between 1999–2018 (inclusive) at Mer Bleue and 2012–2022 (inclusive) at Kopuatai. Error bars are 95% confidence intervals. Note that the Northern and Southern Hemisphere seasons have been aligned by using separate x-axes for each site (Jan–Dec for Mer Bleue and Jul–Jun for Kopuatai).

Table 3.1. Mean annual ecosystem evaporation (E) and equilibrium evaporation (E_{eq}), and means and ranges of their ratios (i.e. Priestley–Taylor α) at each site (n = 11 and 20 years for Kopuatai and Mer Bleue, respectively). These values are given for both year-round data and for the growing season only (Sep–May at Kopuatai and May–Oct at Mer Bleue). Values in parentheses are 95% confidence intervals.

			Annual				**Growing season only**	
Site	***E* (mm)**	***E*$_{eq}$ (mm)**	***E*/*E*$_{eq}$**	***E*/*E*$_{eq}$ range**	***E* (mm)**	***E*$_{eq}$ (mm)**	***E*/*E*$_{eq}$**	***E*/*E*$_{eq}$ range**
Kopuatai	578 (± 13)	910 (± 18)	0.64 (± 0.022)	0.57–0.70	482 (± 11)	816 (± 19)	0.59 (± 0.023)	0.52–0.65
Mer Bleue	450 (± 17)	530 (± 13)	0.85 (± 0.026)	0.76–0.95	388 (± 16)	466 (±11)	0.83 (± 0.027)	0.70–0.94

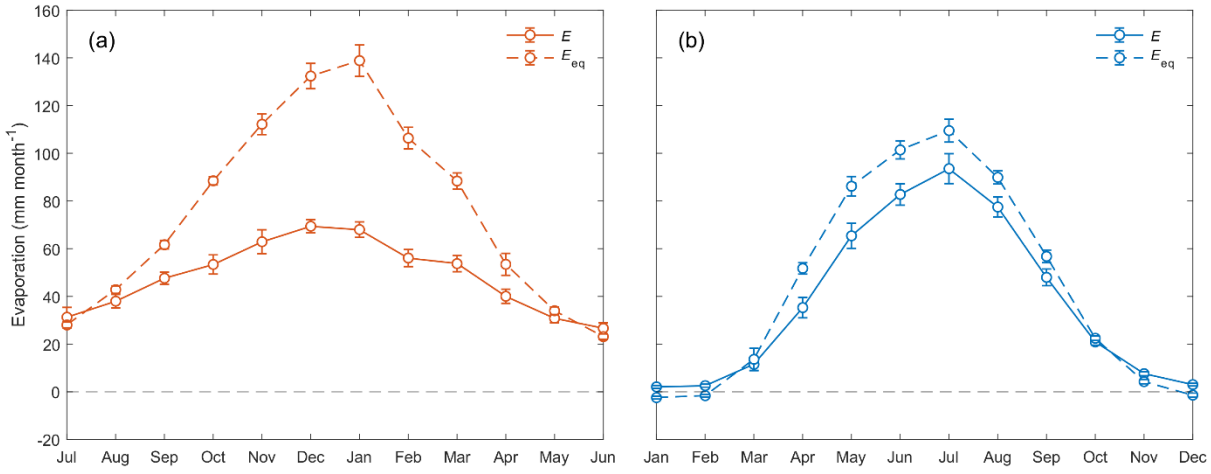

Figure 3.2. Mean monthly E and E_{eq} at (a) Kopuatai and (b) Mer Bleue. Error bars represent 95% confidence intervals. Note that the x-axis for Kopuatai in the Southern Hemisphere starts from July (a six-month offset from the graph for Mer Bleue in the Northern Hemisphere).

3.3.3 Dry canopy energy balance partitioning

Seasonal energy balance partitioning was markedly different at each site. At Kopuatai, *H* was greater than *LE* in most months, with *LE* only comprising 21% of the annual R_n (Figure 3.3). Between autumn and winter (April to August), however, the difference between *H* and *LE* was smaller. In contrast, *LE* was a much larger component of the energy balance at Mer Bleue, representing 43% of the annual R_n due to *LE* exceeding *H* throughout most of the growing season. During the rest of the year, however, *LE* was either less than or similar to *H*. There was also a difference in the seasonality of *LE*, *H*, and R_n between sites - at Kopuatai, all components of the energy balance reached a maximum during summer; *LE* and R_n peaked in mid-summer (January), while *H* peaked a month earlier. At Mer Bleue, *LE* and R_n also peaked during summer (in June and July, respectively), however *H* peaked in the middle of spring (April).

Mean monthly *LE* increased substantially (range = 257 W m^{-2}) towards summer at Mer Bleue, while at Kopuatai, there was less monthly variation in *LE* (range = 79 W m^{-2}). Although the maximum monthly R_n (± 95% confidence interval) at Kopuatai was higher than at Mer Bleue (578 ± 26.0 W m^{-2} and 480 ± 17.7 W m^{-2}, respectively), maximum monthly *LE* at Kopuatai (124 ± 6.45 W m^{-2}) was lower than at Mer Bleue (264 ± 17.0 W m^{-2}). Consequently, the maximum monthly *H* was higher at Kopuatai than at Mer Bleue (304 ± 30.5 W m^{-2} and 191 ± 7.57 W m^{-2}, respectively). In addition, R_n was particularly low in winter at Mer Bleue due to snow cover and the lower solar receipt. During spring, R_n increased steeply (March and April) due to a decrease in albedo resulting from snowmelt. In contrast, Kopuatai does not receive snow, and seasonal albedo does not vary substantially (not shown).

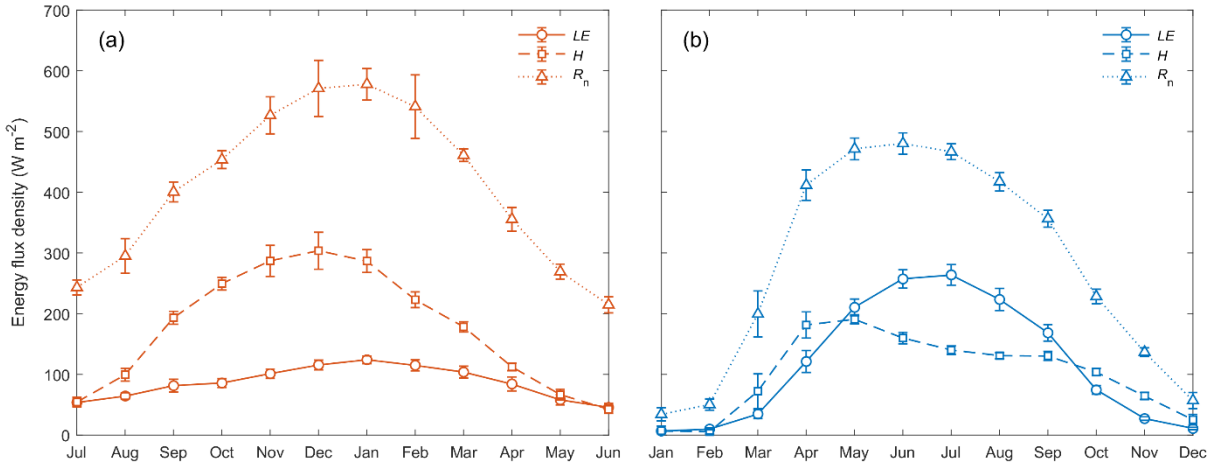

Figure 3.3. Mean monthly *LE*, *H*, and R_n at (a) Kopuatai and (b) Mer Bleue for middle-of-day, dry canopy conditions. Error bars are 95% confidence intervals. Note that the x-axis for Kopuatai starts from July (a six-month offset from the graph for Mer Bleue).

Daily mean energy balance partitioning during dry canopy conditions was also distinctly different between Kopuatai and Mer Bleue (Figure 3.4). At Kopuatai, *H* was a much larger component of the energy balance than *LE* (Figure 3.4a); *H* was greater than *LE* at $R_n \geq$ 250 W m^{-2}, which was reflected in a mean Bowen ratio (β) of 1.96 (β range based on binned *H* and *LE* values was 0.37–2.91). At Mer Bleue, however, *LE* was greater than *H* at $R_n \geq$ 350 W m^{-2} (Figure 3.4b). As a result, mean β was 0.77, with a range of 0.61–1.05.

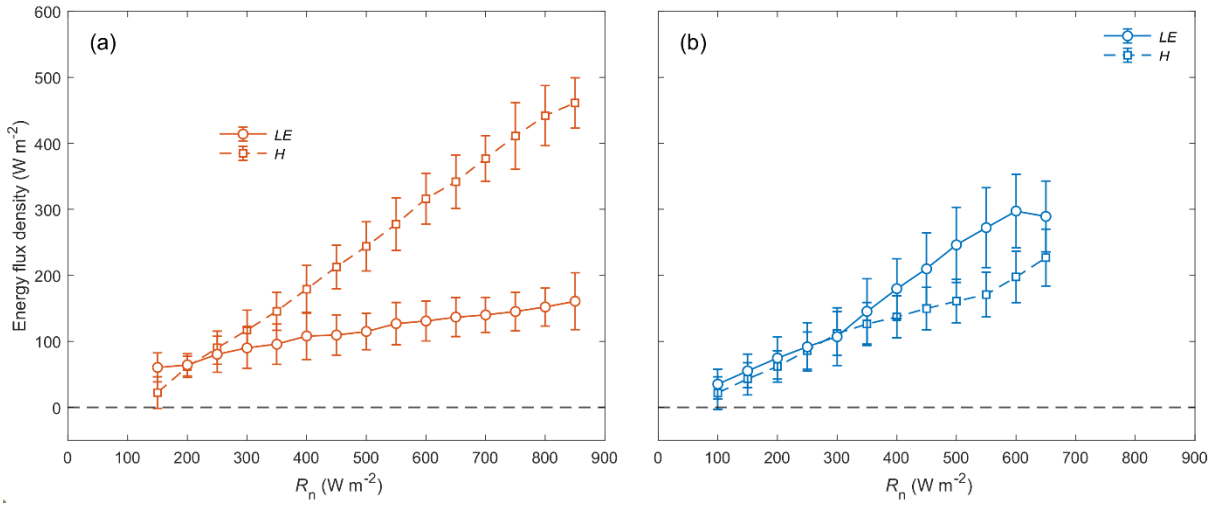

Figure 3.4. Relationship between binned middle-of-day mean *LE*, *H*, and R_n for dry canopy conditions at (a) Kopuatai and (b) Mer Bleue. Values are for the growing season only (Sep–May at Kopuatai and May–Oct at Mer Bleue). Error bars are standard deviations.

3.3.4 Wet canopy energy balance partitioning

During wet canopy conditions, the limitation on *LE* observed at Kopuatai under dry canopy conditions was not apparent (Figure 3.5a); *LE* was greater than *H* at both low and high R_n in these conditions (β ranged between -0.01–0.93, with mean 0.51). Both *LE* and *H* increased at approximately the same rate with increasing R_n. At Mer Bleue, the relationship between *LE*, *H*, and R_n under wet canopy conditions was similar to dry canopy conditions, with a lower mean β of 0.57 and a range of -0.38–0.83 (Figure 3.5b).

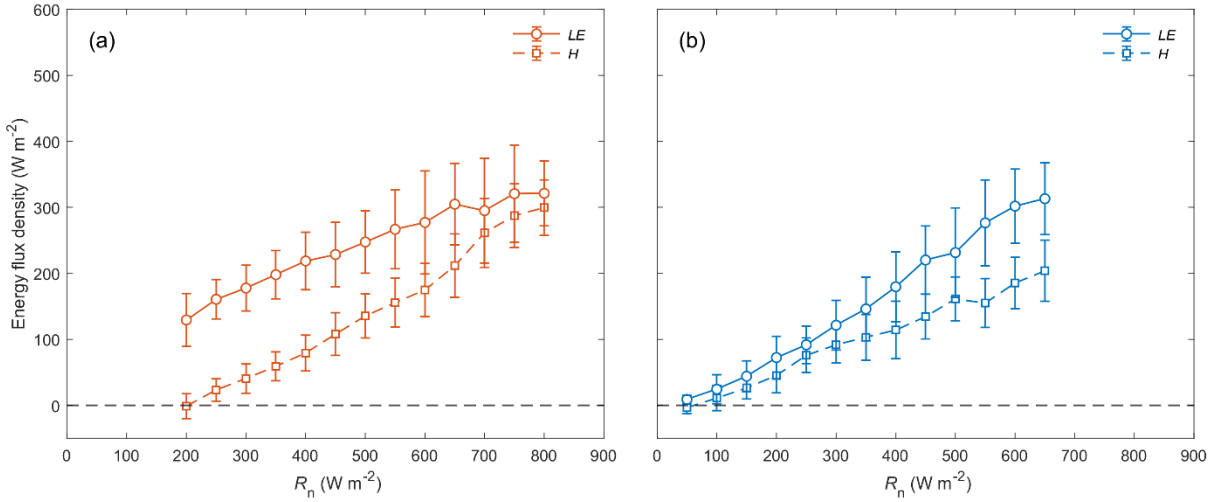

Figure 3.5. Relationship between binned middle-of-day mean *LE*, *H*, and R_n for wet canopy conditions at (a) Kopuatai and (b) Mer Bleue. Values are for the growing season only (Sep–May at Kopuatai and May–Oct at Mer Bleue). Error bars are standard deviations.

3.3.5 Response of *E*, EF, and g_c to VPD

E increased with increasing VPD at both sites, i.e. greater water loss occurred at high VPD (Figure 3.6). Below 2.0 kPa, the rate of increase in *E* with increasing VPD was 3.7 times larger at Mer Bleue (0.221 mm hr^{-1} / kPa) than at Kopuatai (0.060 mm hr^{-1} / kPa). This resulted in a higher *E* of 0.44 mm h^{-1} at VPD = 2.0 kPa at Mer Bleue, compared to only 0.23 mm h^{-1} at the same VPD at Kopuatai. Beyond VPD = 2.0 kPa, *E* showed little or no change with increasing VPD at both sites.

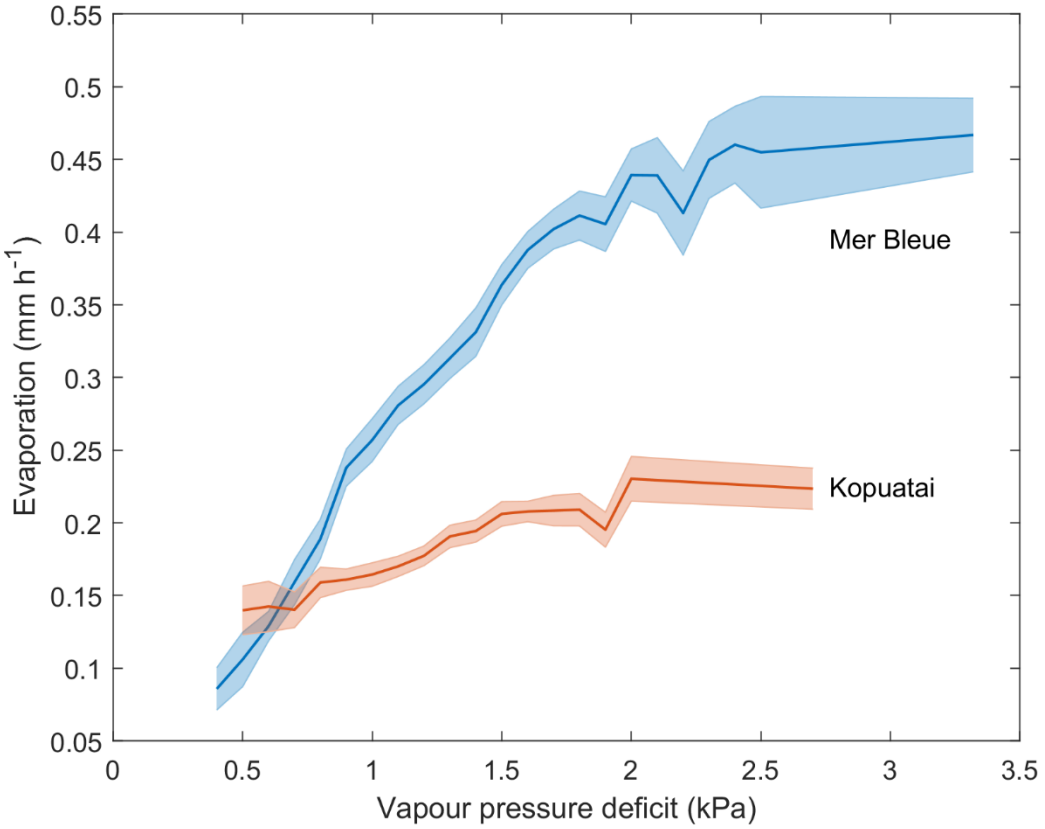

Figure 3.6. Middle-of-day mean growing season *E* for 0.1 kPa bins of VPD during dry canopy conditions at Kopuatai and Mer Bleue. Shaded areas represent 95% confidence intervals.

At Kopuatai, EF decreased in response to increasing VPD, while the opposite trend was observed at Mer Bleue (Figure 3.7). This contrast in responses of EF to increasing VPD was also evident in 30-minute data (Appendix D). At Kopuatai, mean MoD EF decreased from 0.44 at VPD = 0.5 kPa to 0.28 at 2.7 kPa, and increased from 0.31 at 0.4 kPa to 0.66 at 3.3 kPa at Mer Bleue bog. At both sites, the rate of increase or decrease in EF was reduced at VPD > 1.0 kPa.

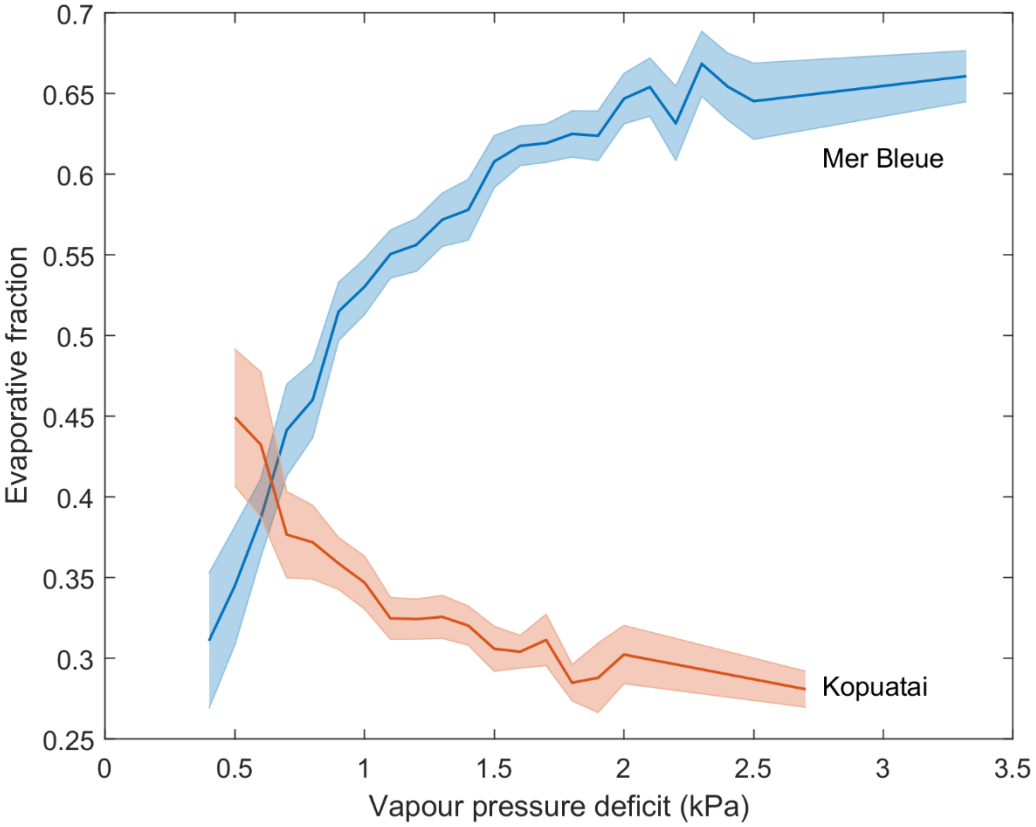

Figure 3.7. Middle-of-day mean growing season EF for 0.1 kPa bins of VPD during dry canopy conditions at Kopuatai and Mer Bleue. Shaded areas represent 95% confidence intervals.

There was a steep decline in g_c with increasing VPD at Kopuatai (Figure 3.8); mean g_c decreased from a maximum of 10.6 mm s^{-1} at a VPD of 0.5 kPa to a minimum of 2.57 mm s^{-1} at 2.7 kPa. In contrast, the pattern of declining g_c with increasing VPD was weak at Mer Bleue, decreasing from 9.10 mm s^{-1} at 0.4 kPa to 6.23 mm s^{-1} at 3.3 kPa.

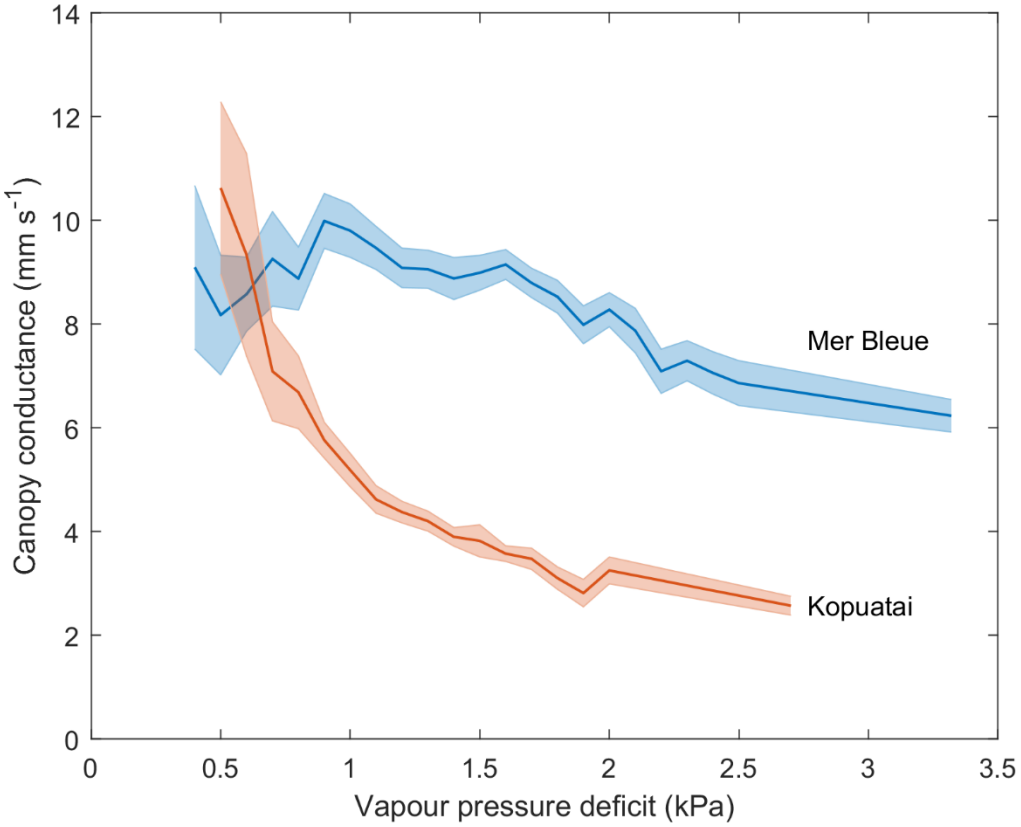

Figure 3.8. Middle-of-day mean growing season g_c for 0.1 kPa bins of VPD during dry canopy conditions at Kopuatai and Mer Bleue. Shaded areas represent 95% confidence intervals.

3.4 Discussion

3.4.1 Evaporation regimes

Our study demonstrates the crucial importance of vegetation characteristics in controlling water loss from peatlands. Kopuatai and Mer Bleue, two ombrotrophic bogs with different vegetation communities, display strikingly different E regimes, energy balance partitioning, and responses of E, EF, and g_c to VPD. Despite being in a warmer climate zone with warm winters, the E regime at Kopuatai was more conservative than at Mer Bleue. Although mean annual E and E_{eq} were 25% and 53% higher at Kopuatai than at Mer Bleue, mean annual E/E_{eq} (i.e, Priestley–Taylor α) was 28% lower at Kopuatai. This occurred because the mean annual E was 45% lower than mean annual E_{eq} at Kopuatai, while at Mer Bleue there was only a 16% difference. The large difference between E and E_{eq} at Kopuatai occurred due to the relatively high E_{eq}, resulting from the higher R_n (due to latitudinal differences), warmer climate, and

longer growing season compared to Mer Bleue. These results indicate that greater surface limitations were imposed on E at Kopuatai relative to Mer Bleue. The difference in E/E_{eq} between the two sites is highly likely to be a result of differences in vegetation, as different vegetation communities, even at the same peatland, have been shown to result in different E regimes (Takagi et al., 1999; Strilesky & Humphreys, 2012). The limitations on E at Kopuatai likely occurred due to the physiological and canopy structural features of the dominant vascular plant, *E. robustum*. However, some limitation on E was observed at Mer Bleue, as evidenced by the decrease in E/E_{eq} towards mid-summer. It is possible that this occurred due to stomatal closure in the shrub vegetation in response to high VPD (Admiral et al., 2006). However, this limitation was weaker than at Kopuatai, likely due to high surface E from *Sphagnum* carpets (Admiral et al., 2006).

At Kopuatai, the range of E/E_{eq} values tended to be lower than at most Northern Hemisphere peatlands, while the E/E_{eq} range at Mer Bleue overlapped with the lower end of most of these ranges (Table 3.2). However, there were some sites with E/E_{eq} ranges that were closer to those of Kopuatai. For example, a tree-dominated peatland in Canada had a lower E/E_{eq} than at Kopuatai, which could be attributed to stomatal limitation of transpiration (Brümmer et al., 2012), i.e., the same mechanism of E limitation as exhibited at Kopuatai, but to a greater extent. Of interest is also the Fäjemyr bog in Sweden, which had lower growing season E/E_{eq} values than most peatlands in Table 3.2 (but not Kopuatai), possibly due to a low water table and low surface conductance (Alekseychik et al., 2018). In addition, in an earlier study of E rates at Kopuatai, Thompson et al. (1999) reported lower E/E_{eq} values than those in this study; this could have occurred due to measurements being made only during summer, when limitations on E are most prominent. Apart from these outliers, the E/E_{eq} values in Table 3.2 are generally much greater than at Kopuatai bog, indicating that *E. robustum* may be more adept at restricting E than the vascular and non-vascular vegetation in most Northern Hemisphere peatlands.

Table 3.2. Ranges of E/E_{eq} calculated for peatlands globally (including this study), with a description of the type of variability covered in the range of E/E_{eq} values, and the time period for which they were calculated.

Location	Dominant vegetation types	E/E_{eq} (i.e., Priestley–Taylor α)	Range type	Time period	Reference
Kopuatai bog, Aotearoa	*Empodisma robustum*	0.57–0.70	Interannual variability	Year-round	This study
		0.52–0.65	Interannual variability	Growing season (Sep–May)	This study
	Empodisma robustum	0.34	N/A	Growing season (Nov-Mar)	Thompson et al. (1999)
	Sporadanthus ferrugineus [a]	0.58	N/A	Summer period (Jan–Mar)	Thompson et al. (1999)
Mer Bleue bog, Canada	Shrubs and *Sphagnum* moss	0.76–0.95	Interannual variability	Year-round	This study
		0.70–0.94	Interannual variability	Growing season (May–Oct)	This study

Location	Dominant vegetation types	E/E_{eq} (i.e., Priestley–Taylor α)	Range type	Time period	Reference
Plotnikovo, Russia	Sedges, shrubs, and *Sphagnum* moss	0.99–1.29 (1999) 0.96–1.07 (2000)	Seasonal variability	Growing season (Apr–Oct)	Shimoyama et al. (2004)
Sandhill fen, Canada	Trees, shrubs, and brown moss	0.79–1.04	Interannual variability	Snow-free periods (May-Nov)	Sonnentag et al. (2010)
Alberta, Canada	Trees, shrubs, and various mosses	0.55–0.57	Interannual variability	Year-round	Brümmer et al. (2012)
Degerö Stormyr, Sweden	Shrubs, grasses, and *Sphagnum* moss	0.86–1.17	Interannual variability	Year-round	Peichl et al. (2013)
Siikaneva-1 & Siikaneva-2, Finland	Shrubs, sedges, and *Sphagnum* moss	1.09–1.21 & 1.11–1.13	Interannual variability	Growing season (May–Oct)	Alekseychik et al. (2018)
Fäjemyr bog, Sweden	Shrubs, sedges, *Sphagnum* moss, and sparse trees	0.66–0.71	Interannual variability	Growing season (May–Oct)	Alekseychik et al. (2018)

Location	Dominant vegetation types	E/E_{eq} (i.e., Priestley–Taylor α)	Range type	Time period	Reference
Seven peatlands in Canada	Shrubs, sedges, mosses (all peatlands), trees, and herbs (some peatlands)	0.82–1.05	Spatial variability	Midsummer period (Jul–Aug)	Humphreys et al. (2006)

[a] *A tall restiad plant that dominates portions of Kopuatai bog, but is not present at the EC site.*

3.4.2 Controls on evaporation

The steep decline in EF with increasing VPD at Kopuatai suggests strong surface controls on *E* at this site. A similar negative relationship between midsummer LE/R_n and VPD was shown by Takagi et al. (1999) at a section of a peatland invaded by vascular vegetation, which was attributed to stomatal closure. This is also likely to be the main factor limiting *E* from Kopuatai due to the non-linear decrease in canopy conductance (g_c) with increasing VPD, a trend that has also been observed in other peatlands (Humphreys et al., 2006; Peichl et al., 2013; Runkle et al., 2014; Alekseychik et al., 2018). However, it has also been hypothesised that the standing litter layer formed by *E. robustum* reduces *E* (Campbell & Williamson, 1997); this canopy feature has been observed to limit *E* in marsh, restored wetland, and dryland ecosystems (Goulden et al., 2007; Villegas et al., 2010; Eichelmann et al., 2018). Standing litter restricts *E* by decoupling the subcanopy environment from atmospheric turbulence, and by preventing solar radiation from reaching the surface, which minimises the variability of T_{air} and VPD below the litter layer (Goulden et al., 2007; Eichelmann et al., 2018). Although the results of this study cannot separate the effect of stomatal closure and standing litter on *E*, it is likely that both of these factors act in tandem to severely restrict *E* at Kopuatai.

At Mer Bleue, *E* rates were almost double those of Kopuatai at high VPD, and there was a greater absolute increase in dry canopy *LE* with increasing R_n at Mer Bleue than at Kopuatai (an increase of 254 W m^{-2} compared to 93 W m^{-2}, respectively), indicating weaker water loss restrictions at Mer Bleue. Weak restrictions likely occurred because of the large contribution of *Sphagnum* moss *E* during well-watered conditions, as moss *E* is enhanced substantially by increasing VPD (Admiral & Lafleur, 2007). Since *LE* increased with increasing R_n and *E* and EF increased with increasing VPD, both of these factors were important controls on *E* and energy partitioning at Mer Bleue. Similar positive correlations between *LE* and R_n (or available energy, R_n–*G*) at daily and monthly scales have previously been observed at other peatlands (Lafleur & Roulet, 1992; Kurbatova et al., 2002; Brümmer et al., 2012), in addition to positive relationships between daily *E* and VPD (Wu et al., 2010; Peichl et al., 2013; Wang et al., 2020).

There were also reduced rates of increase in *E* and EF with increasing VPD at Mer Bleue (i.e., a 'saturating' effect; also observed by Peichl et al., 2013), which only became evident at high VPD (above ~2.0 kPa for *E* and ~1.0 kPa for EF; Figs. 6 and 7). This relatively weak *E* limitation was likely caused by stomatal control of transpiration by vascular vegetation (Admiral et al., 2006), as a slight decrease in g_c was observed with increasing VPD. A similar relationship between surface conductance and VPD has previously been observed at Mer Bleue (Humphreys et al., 2006). It has also been suggested that *E* may become limited at high VPD if the transport rate of water through mosses is insufficient to meet the atmospheric demand (Liljedahl et al., 2011). While we cannot determine whether this occurred at Mer Bleue using the data available, it is possible that this may have been a contributing factor to limitations on *E*.

While there was almost no difference in energy balance partitioning between dry and wet canopy conditions at Mer Bleue, the canopy wetness state had a major effect at Kopuatai. During dry canopy conditions, *H* was the dominant convective flux, as the rate of increase in *LE* with increasing R_n was suppressed. However, *LE* became dominant over *H* during wet canopy conditions, with a much greater rate of increase in *LE* with increasing R_n compared to dry canopy conditions. A previous study at Kopuatai also reported dominance of *LE* over *H*

when the canopy was rain-wetted, and vice versa during dry canopy conditions (Campbell & Williamson, 1997). This indicates that the restrictions on *E* imposed by *E. robustum* break down in wet canopy conditions, likely due to high interception loss. It is possible that interception loss is much higher at Kopuatai relative to Mer Bleue due to the greater canopy height (means 48 cm and 18 cm, respectively) and density.

The responses of *E* and EF to increasing VPD at Mer Bleue were consistent with previous findings by Helbig et al. (2020), which synthesised data from 35 boreal peatlands, including Mer Bleue; however, the response at Kopuatai bog was closer to that of the boreal forests included in their study. As such, the response of *E* to VPD at Kopuatai bog is distinctive compared to boreal peatlands. This may be a critical adaptation that allows peat formation in a climate zone that is uncharacteristic for ombrotrophic peatlands (McGlone, 2009) due to the combination of moderate precipitation and a higher mean annual temperature than at Northern Hemisphere peatlands. Tropical peatlands also experience higher temperatures, however annual precipitation tends to be much higher than at Kopuatai (>2500 mm in Southeast Asia, for example; Page et al., 2006), which maintains adequately wet conditions. Therefore, it is likely that the dominance of *E. robustum* at Kopuatai is crucial to the persistence of this peatland in its unusual climate zone due to restrictions imposed on transpiration and sub-canopy *E*, as these adaptations likely contribute to maintaining a shallow and stable water table.

3.4.3 Implications for future peatland water balances

Northern Hemisphere peatlands, such as Mer Bleue, may be at risk of increased evaporative water loss as VPD increases due to climate warming (Helbig et al., 2020). This could lead to more frequent low water tables and water deficits, which in turn may reduce net C uptake (Zhong et al., 2020; Kwon et al., 2022). The effect of low water tables on the C balance has previously been observed at Mer Bleue, where decreases in water levels at a beaver pond near the EC site caused a decrease in C uptake; further modelling also predicted that a beaver pond water table below ~1.7 m would cause Mer Bleue to switch from a C sink to a source (He et al., 2022). A lower mean water table at a drained *E. robustum* bog near Kopuatai also caused

lower C uptake rates compared to Kopuatai, but likely remained a C sink due to the tolerance of *E. robustum* to a low and fluctuating water table (Ratcliffe et al., 2019). Therefore, the C uptake of both peatlands could be impacted by decreased water tables; however, under increased VPD due to climate warming, it appears that Kopuatai may be able to retain more water than Northern Hemisphere peatlands through strong constraints on *E*. This greater water retention at Kopuatai could enable current high and stable net annual C uptake rates (Goodrich et al., 2017) to be maintained despite warmer and potentially drier conditions in the future (Lawrence et al., 2022). Therefore, we propose that the previously observed *resilience* of C uptake at Kopuatai to dry conditions (Goodrich et al., 2017) primarily results from "hydrological resistance" to increasing VPD driven by the properties of the *E. robustum* canopy.

3.5 Conclusions

We compared ecosystem *E* regimes, energy balance partitioning, and the response of *E* to VPD at two peatlands - Kopuatai bog in Aotearoa New Zealand and Mer Bleue bog in Canada. Our motivation was to determine whether regulation of water losses in these peatlands with different vegetation communities enables hydrological resistance to climatic drying. Our results demonstrated that the *E* regime was much more conservative at Kopuatai than at Mer Bleue at high VPD because of greater limitations on *E* due to reduced g_c. At Mer Bleue, *E* was only weakly limited at high VPD, as the impacts of reduced shrub g_c were likely offset by water loss from non-vascular moss surfaces. The greater limitations on *E* observed at Kopuatai indicate hydrological resistance of this vascular plant-dominated ecosystem to hydro-climatic change. Importantly, this resistance likely contributes to resilience of the net C sink at Kopuatai, despite being located in a warm-temperate climate zone, and thus could be a key self-regulation mechanism. As a result, it appears that Kopuatai may be better equipped to conserve water and maintain high C uptake rates than Mer Bleue, and perhaps other Northern Hemisphere peatlands, in the face of climate change-induced warming and drying. Further investigation of *E* partitioning into transpiration, interception loss, and peat surface *E*, and the role of the dense standing litter layer for *E* regulation at Kopuatai may yield additional insights into this observed hydrological resistance.

Chapter 4

Quantifying interception loss at Kopuatai bog

4.1 Introduction

Interception loss (E_{int}) represents the quantity of gross precipitation (P_g) that is detained on vegetation surfaces and returned to the atmosphere through evaporation (E; David et al., 2005). At the global scale, 6.0–8.6% of annual P_g becomes E_{int}, providing 11% of annual E (Miralles et al., 2011; Lian et al., 2022). However, E_{int} can be much higher at an ecosystem scale; for example, a review of forest E_{int} studies showed that up to 45% of P_g can be returned to the atmosphere over a season-long or annual time period (Carlyle-Moses & Gash, 2011). Substantial E_{int} has also been observed in peatlands - at a maritime raised bog, E_{int} constituted 9–15% and 20–36% of P_g for tree and shrub vegetation, respectively (Exler & Moore, 2022). Therefore, as it can be responsible for significant water losses from peatlands and other ecosystem types, E_{int} needs to be quantified to better understand the E regimes of these ecosystems.

The magnitude of E_{int} during and after a rain event depends on the rain event characteristics (e.g., rain event size, intensity, duration, frequency, continuity), meteorological conditions (e.g., vapour pressure deficit (VPD), wind speed), and vegetation features (e.g., age, height, leaf or plant area index (LAI or PAI, respectively); Llorens & Domingo, 2007; Staelens et al., 2008; Toba & Ohta, 2008; Carlyle-Moses & Gash, 2011; Ochoa-Sánchez et al., 2018 [Table 2]). With the exception of meteorological conditions, the dominant factors influencing E_{int} differ from those regulating dry canopy E (i.e., transpiration and surface E), particularly in relation to vegetation due to the lack of plant physiological control over E_{int} and the greater importance of canopy structure (e.g., Llorens & Domingo, 2007). One important structural feature of vegetation that influences the magnitude of E_{int} is the canopy storage capacity (S), defined as the quantity of water needed to fully saturate the canopy (David et al., 2005). The value of S

itself is determined by the properties of individual species, such as vegetation density and leaf water retention properties (dependent on the leaf angle and degree of hydrophobicity), and by the percentage of canopy cover within an ecosystem (David et al., 2005; Carlyle-Moses & Gash, 2011). Furthermore, the quantity of E_{int} can be linked to ecosystem type, as water yield in forests has been observed to be lower (i.e., E_{int} is higher) than in scrub, tussock, and grass-dominated areas of Aotearoa New Zealand (Dymond et al., 2012).

At Kopuatai bog in Aotearoa New Zealand, E_{int} has previously been estimated to constitute 33.9% of P_g, based on a 1-year small plot experiment (Agnew et al., 1993). In addition, an unreplicated experiment reported by Campbell & Williamson (1997) provided an S estimate of 2 mm. However, further measurements have not been made at Kopuatai, nor have E_{int} models been applied to this ecosystem. Therefore, the aim of this study is to quantify E_{int} and S at Kopuatai using a replicated field experiment and two modelling approaches, thereby improving our current understanding of wet canopy E regimes in this ecosystem. The objectives of this study are to (1) develop a field experimental setup for quantifying E_{int} that is applicable to *Empodisma robustum*, the dominant vegetation species at Kopuatai, (2) calculate E_{int} and S for the *E. robustum* canopy using the field experiment results and the two modelling approaches at rain event to annual timescales, (3) identify controls on E_{int}, and (4) describe seasonal variability in E_{int} using modelled results. The hypothesis for this section is that E_{int} will be high compared to other ecosystems dominated by short vegetation due to the dense canopy structure of *E. robustum*, and that E_{int} will constitute a larger proportion of total E during wetter months.

4.2 Methodology

4.2.1 Collection tray experiment

4.2.1.1 Design and data collection

At Kopuatai, the magnitude of E_{int} was determined indirectly by measuring net precipitation (P_n), then subtracting this from P_g to estimate the quantity of water remaining on the canopy

($E_{int} = P_g - P_n$). A tipping bucket rain gauge was used to measure P_g, while P_n was collected using trays below the plant canopy and stored in buckets set into the peat. The magnitude of P_n was quantified using continuous water level measurements within the buckets. These measurements were made between 12 August 2022 and 30 June 2023 at two to six-week long intervals, between which the buckets were emptied and water level measurements restarted. Overall, there were nine periods during which data were collected.

Collection trays have been used in a small number of studies for P_n measurement (or for separate measurement of throughfall and stemflow; e.g., Serrato & Diaz, 1998; Yimam et al., 2015; Zou et al., 2015). This method was selected to determine E_{int} at Kopuatai due to the density of the *E. robustum* canopy and lack of a central trunk, which does not allow for the more common methods (e.g., throughfall gauges and stemflow collars) of P_n measurement to be used. It is important to note that the collection tray method used in this study does not allow for throughfall and stemflow to be measured separately.

Four sites were selected for P_n collection, ensuring sufficient variability in canopy height. Spatial variability of canopy heights at Kopuatai was assessed using three 10 m transects (Figures 4.1 and 4.2), giving a mean canopy height of 0.48 m, and a range of 0.21–0.71 m. The mean litter layer height was 0.25 m (range = 0–0.47 m). Canopy heights at the four measurement sites are given in Table 4.1; Site 1 had the highest maximum canopy height, while Site 3 had the lowest.

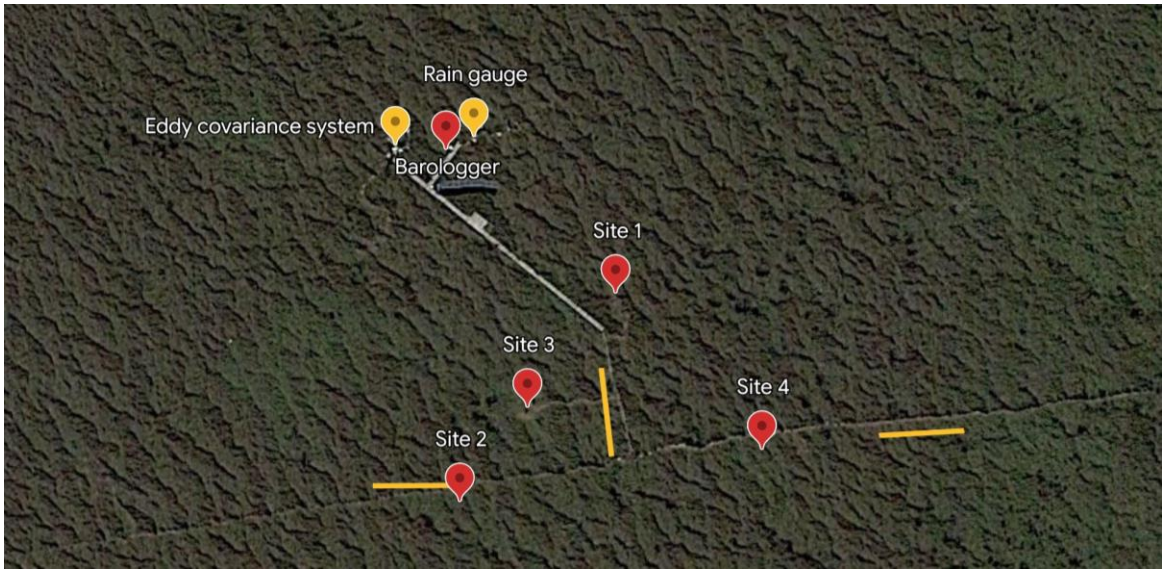

Figure 4.1. Aerial image showing the location of transects (yellow lines), field sites, the Barologger, the rain gauge, and the eddy covariance tower (Image: Google Earth, *11/03/2016*).

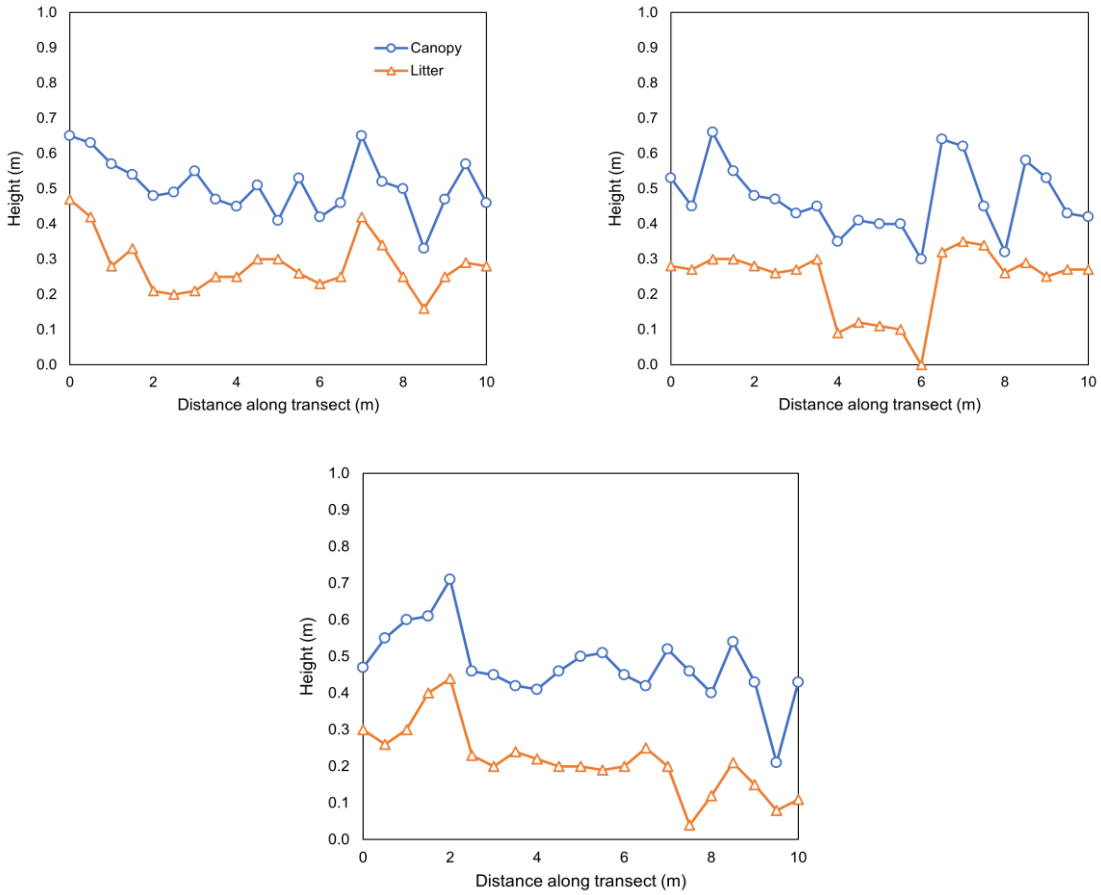

Figure 4.2. Canopy and standing litter height distributions of *Empodisma robustum* across three 10-m transects.

The experimental setup at each site consisted of four rectangular ~0.05 m^2 trays (Figure 4.3), connected by tubing to a lidded 20 litre water collection bucket embedded in the peat (Figure 4.4). Installation of the trays at each site was carried out by cutting stems of the *E. robustum* canopy with hedge shears and placing each tray underneath the canopy at a 5–11° angle (Table 4.1) to ensure the flow of water down the tray during rainfall events. Leakage of water outside the trays was prevented by applying silicone sealant at the joints between tray components, and mesh was placed over the water outlet to mitigate blockages by plant litter in the tubing. To prevent the collection buckets embedded in the peat from floating, each bucket was weighed down with a 20 litre bucket filled with water. An additional tube was connected to each collection bucket in order to allow for air displacement as water filled the buckets.

Table 4.1. Tray angles and canopy heights at the front and rear ends of each tray at each P_n measurement site.

Site	Tray	Tray angle (°)	Canopy height at front of tray (m)	Canopy height at rear of tray (m)
1	A	8	0.23	0.57
	B	9	0.20	0.57
	C	7	0.15	0.40
	D	8	0.11	0.36
	Mean	**8**	**0.17**	**0.48**
2	A	7	0.20	0.50
	B	8	0.20	0.38
	C	7	0.15	0.38
	D	7	0.20	0.40

Site	Tray	Tray angle (°)	Canopy height at front of tray (m)	Canopy height at rear of tray (m)
	Mean	**7.25**	**0.19**	**0.42**
3	A	5	0.23	0.35
	B	6	0.25	0.35
	C	11	0.20	0.45
	D	10	0.26	0.40
	Mean	**8**	**0.24**	**0.39**
4	A	10	0.15	0.33
	B	7	0.45	0.45
	C	7	0.27	0.50
	D	9	0.20	0.37
	Mean	**8.25**	**0.27**	**0.41**

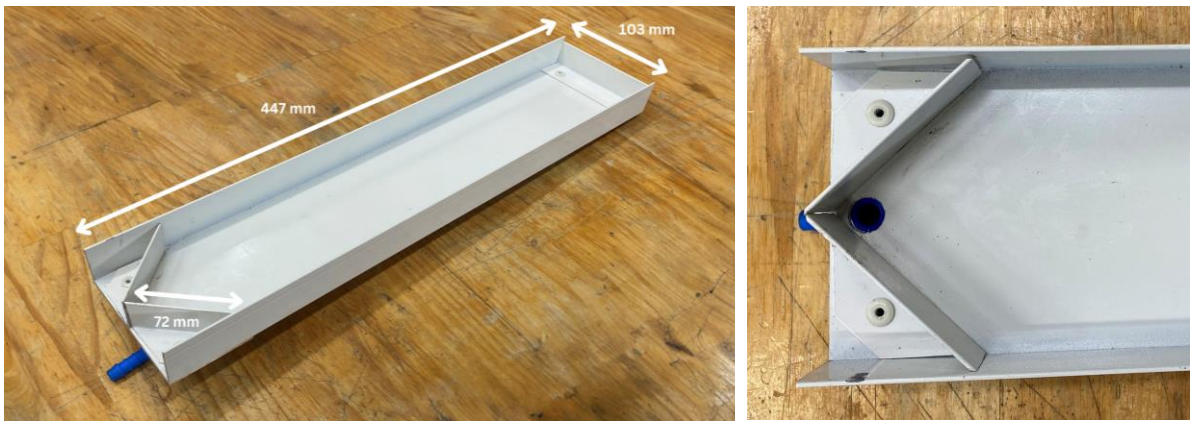

Figure 4.3. Design of the collection trays, showing average tray dimensions (left) and the water outlet (right).

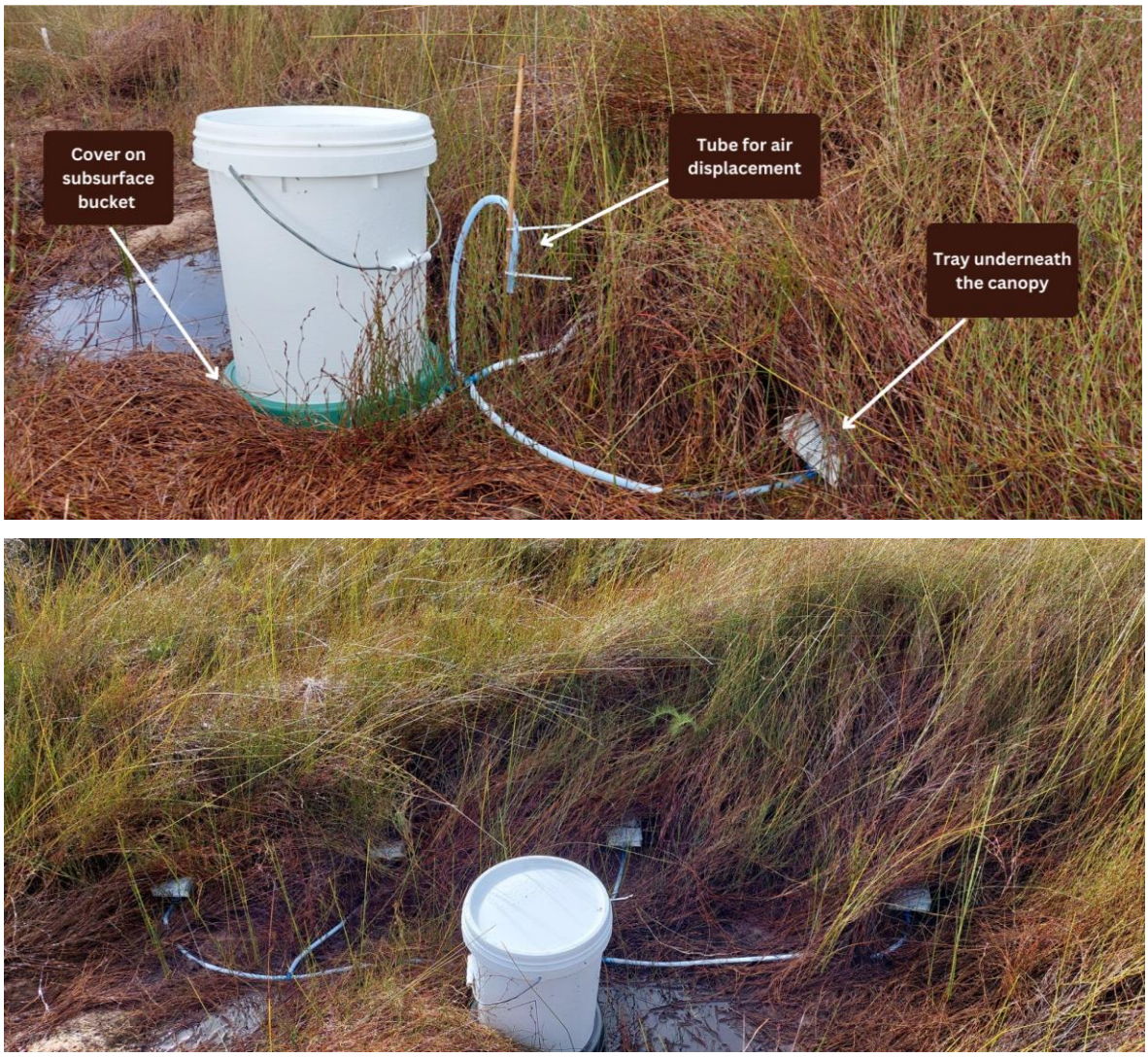

Figure 4.4. Experimental setup for P_n measurement, consisting of four trays and two buckets at each site. The top bucket was water-filled and used as ballast to hold the sealed collection bucket in place, which was embedded to its rim in the peat.

A self-logging water level transducer (Levelogger model 3001, Solinst Ltd Georgetown, ON Canada) was suspended inside each storage bucket to determine the water level (cm), with measurements being made every 30 minutes. As these water level measurements are influenced by atmospheric pressure, barometric compensation of the measurements was carried out (measured water level minus barometric pressure in cm). Initially, barometric pressure measurements from the eddy covariance (EC) flux tower were used for barometric compensation, however this produced very noisy water level data; this is likely because the EC barometric pressure represents a mean of 1800 measurements taken during each half hour,

whereas the water level transducer only provided one measurement per half hour. To reduce this effect, a Solinst Barologger was installed in a vented PVC tube, which was embedded in the peat at approximately the same depth as the pressure transducers in the buckets. Barologger measurements were used for barometric compensation from the third period of data collection onwards, reducing noise in the data significantly. Sample water level data are shown in Figure 4.5, including data compensated with EC barometric pressure (Figure 4.5a) and Barologger measurements (Figure 4.5b).

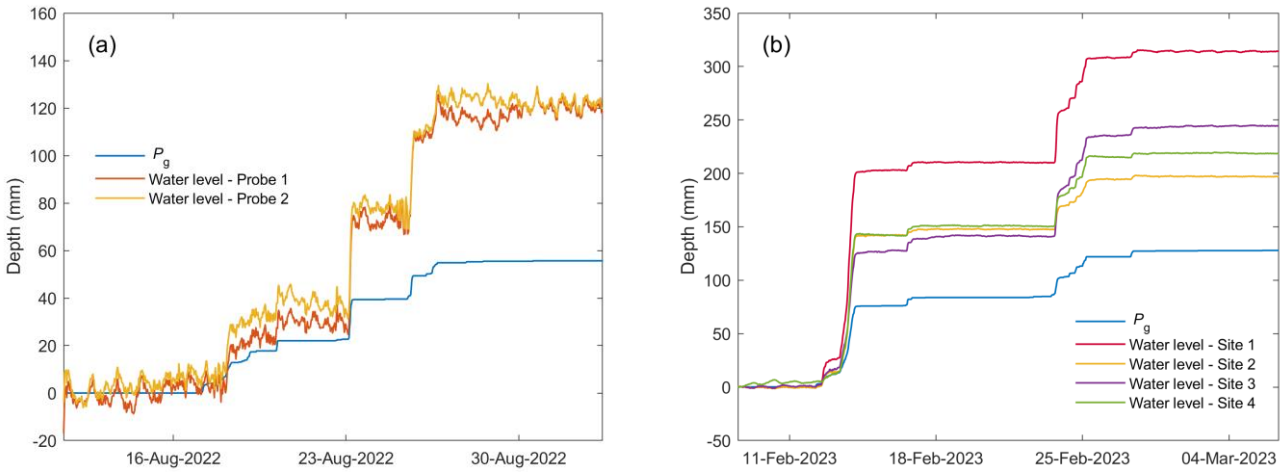

Figure 4.5. Examples of cumulative P_g and bucket water level measurements for (a) Period 1, compensated with eddy covariance barometric pressure measurements, and (b) Period 7, compensated using Barologger data.

Testing the water level transducers in the laboratory showed that the accuracy of measurements was reduced at very low water levels. To prevent this issue, 2–4 cm of water was left in each bucket to begin each set of measurements, taking a manual measurement of the exact water depth. When the buckets were close to being full, another manual measurement was made, and buckets were emptied and reset with 2–4 cm of water. The resulting pressure transducer data were modified to start from zero (Figure 4.5), as the starting water depth was not accumulated due to rainfall. Pressure transducer and manual measurements of stored water depth were generally within 5% of each other, however there was a small number of periods where this difference was larger (up to 18%). This likely occurred due to human error when measuring water depth manually, as this issue did not occur consistently for one pressure transducer or one particular measurement period.

4.2.1.2 Data analysis

Following barometric compensation, water level data were converted into stored water volume using the stable relationship between depth (d) and volume (V):

$$V = 2 \times 10^{-5} d^2 + 0.0557d + 0.0029 \quad (4.1)$$

This volume-depth relationship was obtained using the dimensions of the buckets and the equation for the volume of a frustum, as the walls of the buckets were slightly sloping:

$$V = \frac{1}{3}\pi h\,(R^2 + Rr + r^2) \quad (4.2)$$

where h is the height of water in the bucket, R is the radius of the water surface at a given water level in the bucket, and r is the radius of the bottom of the bucket.

The cosine of the mean tray angle (8°) was multiplied by the mean tray length to estimate the projected horizontal length exposed to P_n when the trays were at an angle underneath the canopy. Based on this projected length, the combined projected horizontal area of the trays receiving P_n was approximately 0.1925 m^2 at each site, which includes their triangular outlet sections. At each site, P_n was calculated by dividing the volume of stored water (m^3) by this total tray area and converting to mm depth. Due to the nature of these measurements, the P_n data were in a cumulative form. Therefore, cumulative E_{int} was calculated by subtracting cumulative P_n from cumulative P_g for each measurement period (sample data are shown in Figure 4.6).

Inspection of the cumulative data showed that the water level transducer at Site 4 recorded gradual decreases in water levels between rain events during Periods 4, 5, 8, and 9. Therefore, these data were excluded from further calculations.

Interception loss fractions (E_{int}/P_g) were calculated for each measurement period by dividing the final cumulative E_{int} by the final cumulative P_g; the former was calculated as an average over the last rain-free section of each period due to fluctuation in the data (Figure 4.6). In

addition, E measured using the EC system was used to calculate the contribution of E_{int} to total E (E_{int}/E) for each period, where E data were filtered then gap-filled using a neural network.

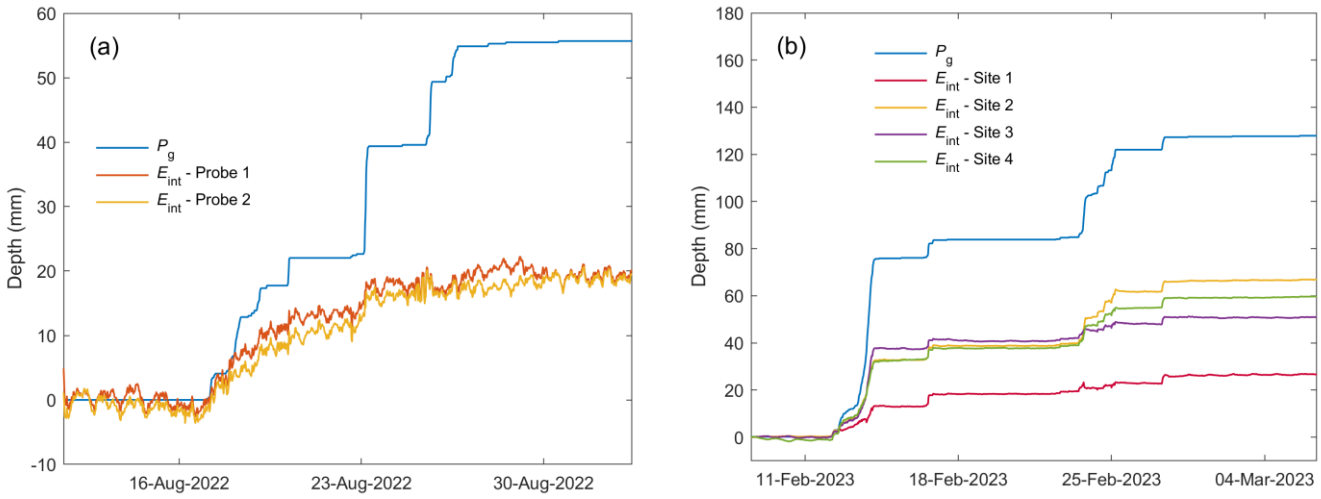

Figure 4.6. Sample of cumulative E_{int} and P_g for Periods (a) 1 and (b) 7. Note that cumulative E_{int} decreased during one rain event throughout Period 7 at Sites 1 and 3 due to a brief period where $P_n > P_g$ (either due to measurement uncertainty for the rain gauge or collection trays, or due to spatial variability in P_g).

These E_{int}/P_g and E_{int}/E fractions were also calculated for selected rain events; it was necessary that these rain events started when the canopy was dry, in order to remove the influence of water from previous rain events on interception estimates. Suitable rain events were identified using the 24-hour Antecedent Precipitation Index (API; Appendix B), which enables separation of dry and wet canopy conditions. However, rain events were rejected from our dataset if they had no effect on bucket water levels.

The remaining rain event data were analysed in two ways - at the sub-rain event and whole rain event timescales. Sub-rain event data only included the initial pulse of rainfall, before canopy drying began according to the 24-hour API function. On the other hand, whole rain event data included the entire rain event, regardless of whether drying occurred throughout. The end of each whole rain event period was identified as the time at which rainfall stopped, provided that this was followed by complete canopy drying according to the 24-hour API function.

Sub-rain event E_{int}/P_g was very high, likely because the initial pulse of precipitation was primarily directed towards filling the canopy store, resulting in less precipitation penetrating the canopy and reaching the trays as P_n. At the whole rain event scale, however, the canopy had likely been completely wetted, resulting in more efficient delivery of P_n to the collection trays, and therefore lower E_{int}/P_g. Therefore, as sub-rain event data did not appear to accurately represent rain event E_{int}/P_g, only whole rain event E_{int}/P_g results were used in this study.

Further analysis involved determining the relationship between rain event size and whole rain event E_{int}/P_g, which was compared to a theoretical relationship (as in Campbell & Murray, 1990) representing the lower boundary of E_{int}/P_g:

$$\begin{aligned} P_g \leq S&: E_{int}/P_g = 100\% \\ P_g > S&: E_{int}/P_g = S/P_g * 100 \end{aligned} \tag{4.3}$$

Canopy storage capacity, S, was given by the y-intercept of the linear relationship between rain event P_g and P_n at each site (following Campbell & Murray, 1990). Only sub-rain event data were used to construct this relationship, as S was likely overestimated at the whole rain event scale due to canopy drying. In addition, to prevent skewing the P_n–P_g relationship with small rain events that did not completely saturate the canopy, such rain events (< 3.5 mm for Sites 1 and 2, < 1.5 mm for Site 3, and < 2.5 mm for Site 4) were removed when plotting this relationship.

4.2.2 Modelling E_{int}

4.2.2.1 Czikowsky & Fitzjarrald (2009) method

The methodology developed by Czikowsky & Fitzjarrald (2009) uses EC evaporative flux data to calculate E_{int} at a rain event scale. This involves generating an ensemble of E for dry days, then subtracting these values from E occurring during and after rain events at corresponding times of day to obtain an estimate of E_{int}. As EC data are used, this E_{int} value represents water evaporating from both the plant canopy and the ground surface (Czikowsky & Fitzjarrald, 2009). In addition, this method assumes that transpiration remains constant before, during, and after each rain event; therefore, transpiration is not expected to affect E_{int} estimates (Czikowsky & Fitzjarrald, 2009).

In this study, gap-filled EC evaporative flux data (2012–2022, inclusive) were used to calculate E_{int} using a modified version of the Czikowsky & Fitzjarrald (2009) method ('C-F method' henceforth); see Goodrich et al. (2017) for information on the gap-filling processes used at Kopuatai. Firstly, dry canopy ensemble E rates were calculated using the original C-F method; however, in contrast with the original method, a 48-hour API function was used to identify dry canopy conditions (conservatively defined as API ≤ 0.2; Appendix B). Dry canopy E ensembles were constructed for each season to account for the large seasonal differences in daytime E (Figure 4.7a).

Before calculating E_{int}, dry canopy E ensembles needed to be corrected for differences in R_n between dry and wet days, as R_n tends to be lower when it is raining (Czikowsky & Fitzjarrald, 2009). Czikowsky & Fitzjarrald (2009) devised a method to correct for these differences by multiplying dry canopy ensemble E by a ratio of mean rain event R_n to mean dry canopy ensemble R_n (Figure 4.7b) for the duration of the rain event. However, our modified method used the *instantaneous* R_n during each half hour of a rain event and the corresponding half hourly dry canopy ensemble R_n values (rather than calculating means over the whole rain event) for this correction. These R_n corrections were only implemented during the day, as

night-time E is not affected by R_n; in this study, daytime data were defined as periods when R_n exceeded 10 W m^{-2}.

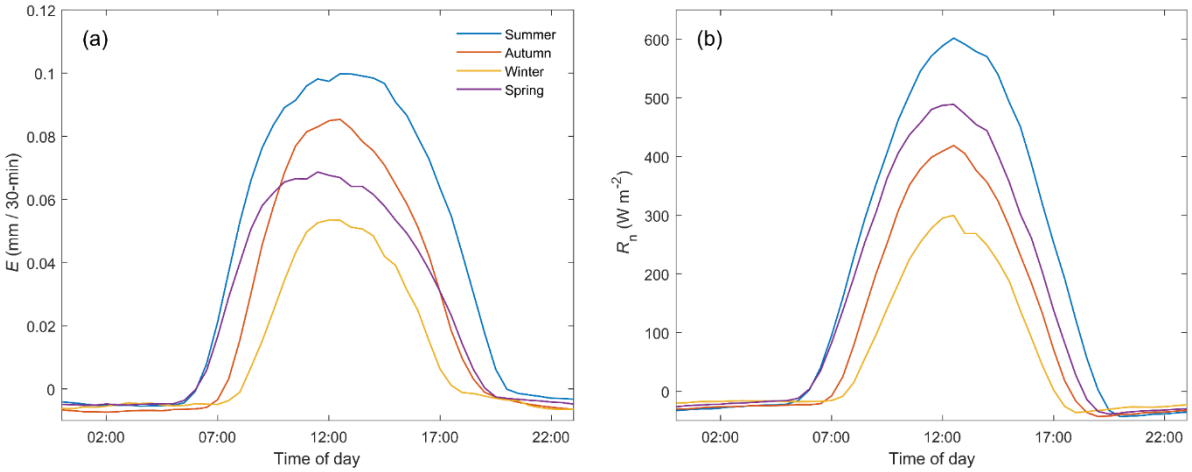

Figure 4.7. Seasonal ensembles of 30-minute dry canopy (a) E rates and (b) net radiation (R_n). Summer data consists of Dec–Feb months, autumn of Mar–May, winter of Jun–Aug, and spring of Sep–Nov.

For each half hour of data, the season during which it occurred was identified. This was done so that the corresponding dry canopy E and R_n ensembles could be used for corrections. As within-season variability of sunset times occurred for all seasons, there were times when sunset was earlier (or later) on the day of the rain event than indicated by the dry canopy ensemble R_n, causing the rain event R_n to be considerably lower (or higher) than the dry canopy R_n towards sunset. This resulted in unusually small (or large) or negative correction ratios, causing a downward (or upward) spike in the dry canopy E data. This issue was corrected by setting all ratios greater than 2 and less than -2 to 1, which substantially reduced the number of spikes in the data.

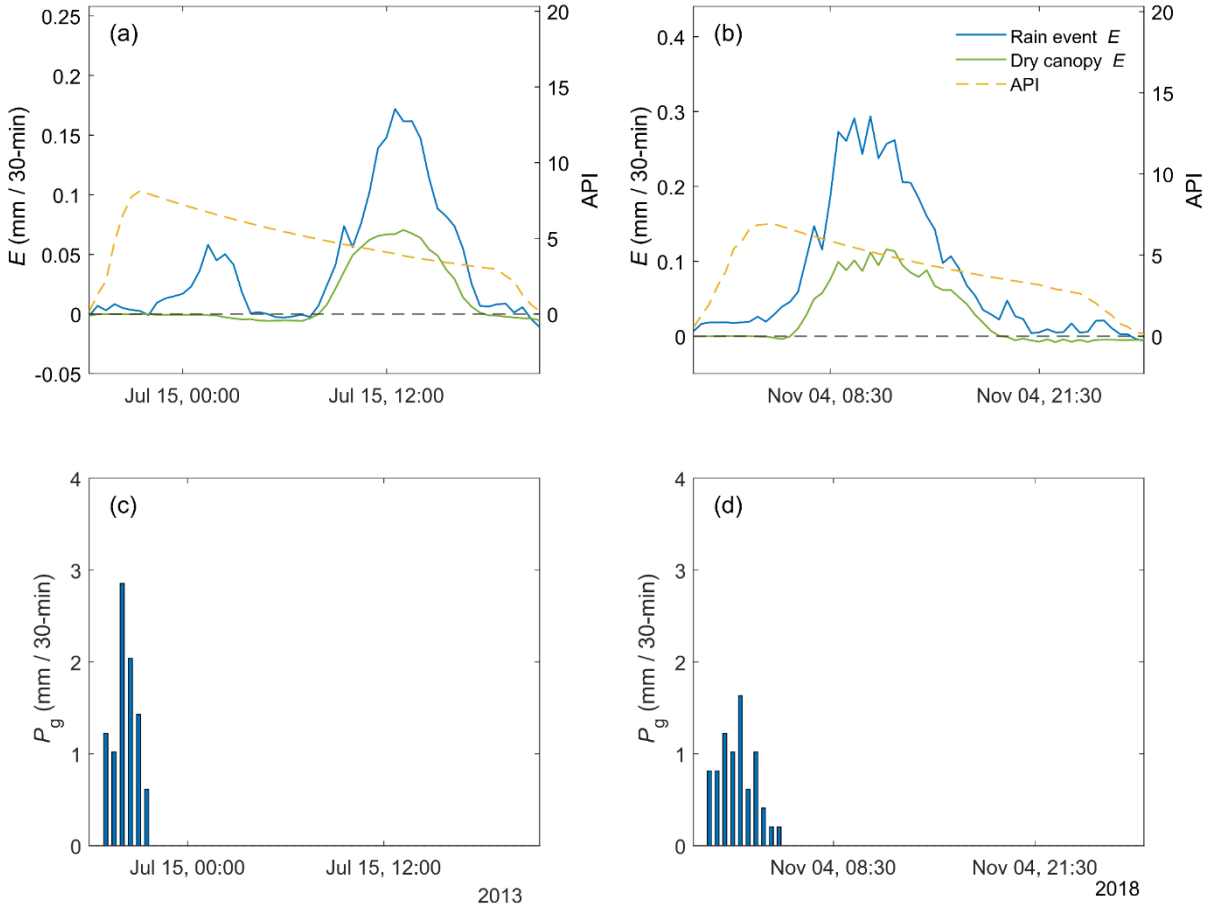

Figure 4.8. Two sample rain events showing rain event *E*, dry canopy ensemble *E* calculated using the C-F method (corrected by net radiation), and the antecedent precipitation index (API) in (a) and (b), while (c) and (d) show gross precipitation (P_g) per half hour.

Another difference between the original C-F method and our modified version pertains to identification of rain events. Czikowsky & Fitzjarrald (2009) isolated rain events by ensuring a minimum 4-hour separation period between them. However, as canopy drying takes approximately 18 hours for the upper canopy of *E. robustum* at Kopuatai (Keyte Beattie, 2014), we used a conservative 24-hour API function to predict the rate of canopy drying[3]. Rain events were isolated using the API function by identifying the start of each rain event (when API ≥ 1, i.e., the canopy was wetted) and the end of the post-rain drying period, when the canopy

[3] Note that the drying time predicted by the 24-hour API function can be slightly shorter or longer than 24 hours, but generally only differs by one to two half hours. For most rain events, the drying time is not dependent on rain event size. However, the drying time for very small rain events (less than 0.5 mm) tends to be significantly shorter than 24 hours.

was predicted to have dried completely (API ≤ 0.2). However, rain events were discarded from the dataset if more than one pulse of rainfall occurred, as incomplete canopy drying between pulses would have affected *S* estimates. These data were filtered further to remove rain events smaller than 1 mm, which tended to produce E_{int}/P_g values greater than 100%. As a result, only 49 suitable rain events (10 in summer, 9 in autumn, 5 in winter, and 25 in spring) were identified within the Kopuatai dataset, which were used to derive a mean rain event E_{int}/P_g for Kopuatai. Two sample rain events that were processed using the C-F method are shown in Figure 4.8.

4.2.2.2 Rutter et al. (1971) model

Rutter et al. (1971) modelled a running water balance for a forest canopy in order to calculate E_{int}. In this study, the Rutter model was modified by removing the drainage coefficient (*b*) and free throughfall coefficient (*p*) - the former was removed for simplicity, while the latter was unnecessary due to the high canopy density, which results in minimal canopy gaps (diffuse light availability at the peat surface has previously been measured as only 0.1–0.2% under an *E. robustum* canopy; Wilson, 2020). The Rutter model also requires a value of *S* to be specified as an input parameter, which in this study was the mean *S* value obtained from the collection tray experiment at the sub-rain event scale.

Canopy cover is very high at Kopuatai, as no bare peat was observed in this study or in previous canopy height measurements (Keyte Beattie, 2014). However, a proportion of canopy cover was still specified in our model (as done by Valente et al., 1997) to account for areas where E_{int} is lower due to a lack of standing litter. As such, the proportion of 0 cm litter height measurements to the total number of litter height measurements made in this study (98.4%; Figure 4.2) was specified as the percentage canopy cover in this model. In contrast to the method used by Valente et al., (1997), however, *S* was *multiplied* by the canopy cover fraction in this study, as *S* would be expected to be lower over an area with sparser canopy cover.

In the Rutter model, potential E (E_p) is used to estimate E_{int}, and was calculated using the Penman–Monteith equation from Rutter et al. (1975):

$$E_p = \frac{s\,R_n + \rho\,c_p\,VPD/r_a}{L_v\,(s + \gamma)} \quad (4.4)$$

where s is the slope of the saturation vapour pressure versus temperature curve, ρ is air density (1.2 kg m^{-3}), c_p is the specific heat of air (1010 J kg^{-1} $°C^{-1}$), VPD is the vapour pressure deficit, r_a is the aerodynamic resistance, L_v is the latent heat of vaporisation (dependent on air temperature), and γ is the psychrometric constant (0.066 kPa $°C^{-1}$). The r_a term of this equation was calculated using Equations 3.5 and 3.6 in Chapter 3 of this thesis.

A schematic for the simplified Rutter model used in this study is shown in Figure 4.9. As is evident from this diagram, E_p was multiplied by the actual canopy storage (C) divided by S if the canopy store was not full, as done in the original model (Rutter et al., 1971). In addition, if E predicted by the Penman–Monteith equation was greater than the water available on the canopy, it was limited to $C(t\text{-}1) + P_g$ (as done by van Dijk et al., 2015). Furthermore, only positive E values were subtracted from C to avoid increases in C overnight. This model was run for the same 49 rain events that were identified for the C-F method, and the same two sample rain events are shown in Figure 4.10.

One issue with the Rutter model was that the output S was typically lower than the original input value, with the gap between input and output S becoming larger with increasing S (Appendix E; Figure E1). This occurred because the Rutter model predicted a slow rate of C depletion by E following rainfall (as E from a partially wet canopy depended on C/S; Figure 4.9). This frequently resulted in C values greater than zero at the start of many rain events, producing a lower output S value than expected. This problem was also highlighted by van Dijk et al. (2015), who removed the C/S fraction from their model; however, this fraction was retained for our analysis due to the intermediate surface resistance observed for a partially wet canopy compared to completely dry and wet canopy conditions (Shuttleworth, 1976), indicating that some reduction in E_{int} rates occurs as the canopy dries.

To account for the slow C depletion, the Rutter model was run continuously across all years of data and rain event data extracted from this time series. This was done instead of running

the model for each rain event and assuming that C started at zero. To account for differences between C at the start and end of each rain event, the absolute difference between the starting and final C values was subtracted from the total E_{int} if the starting value was greater than the final value, and added to the total E_{int} if the opposite was true. This ensured the water balance of each rain event was closed.

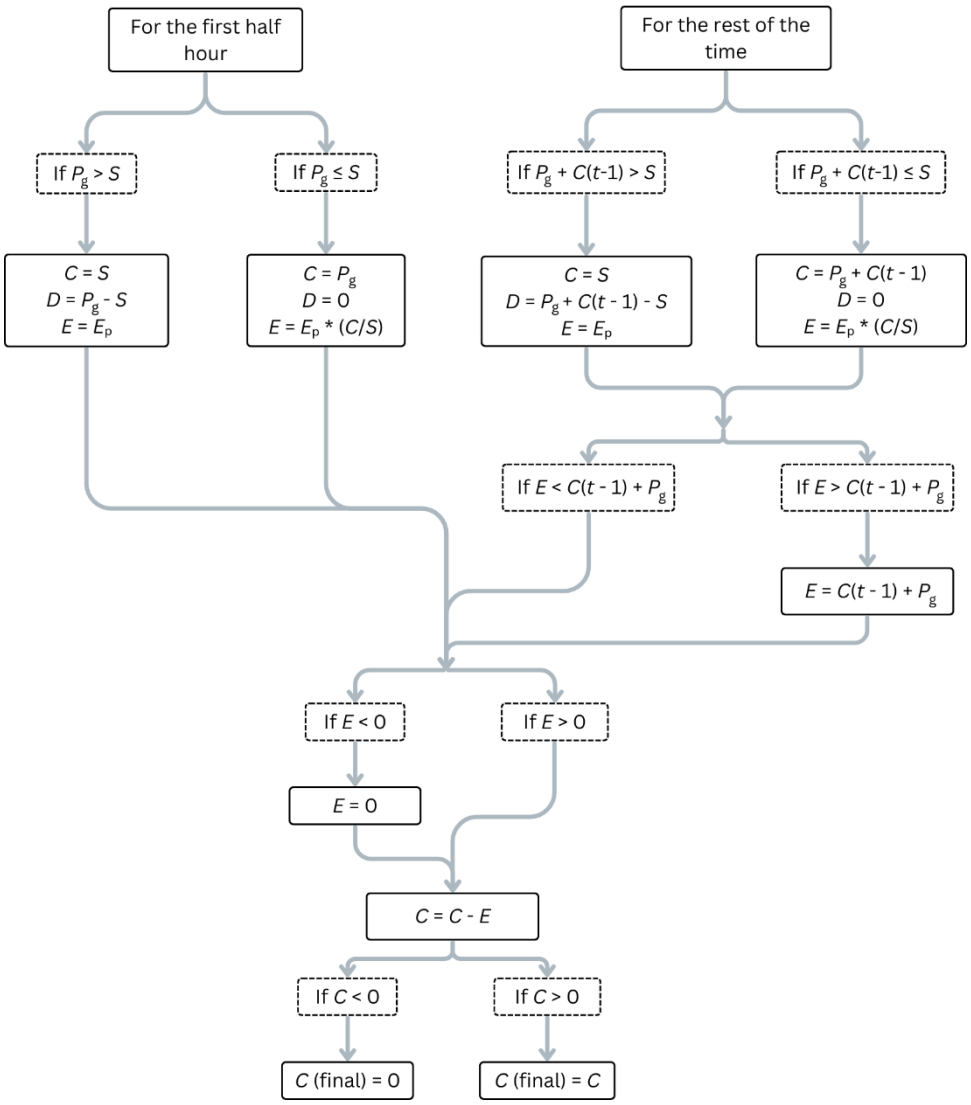

Figure 4.9. Flow chart demonstrating the process of calculating a running water balance for each half hour of data using the Rutter model, where S is the canopy storage capacity, C is actual canopy storage, and D is drainage through the canopy. $C(t\text{-}1)$ represents the water stored on the canopy during the previous half hour.

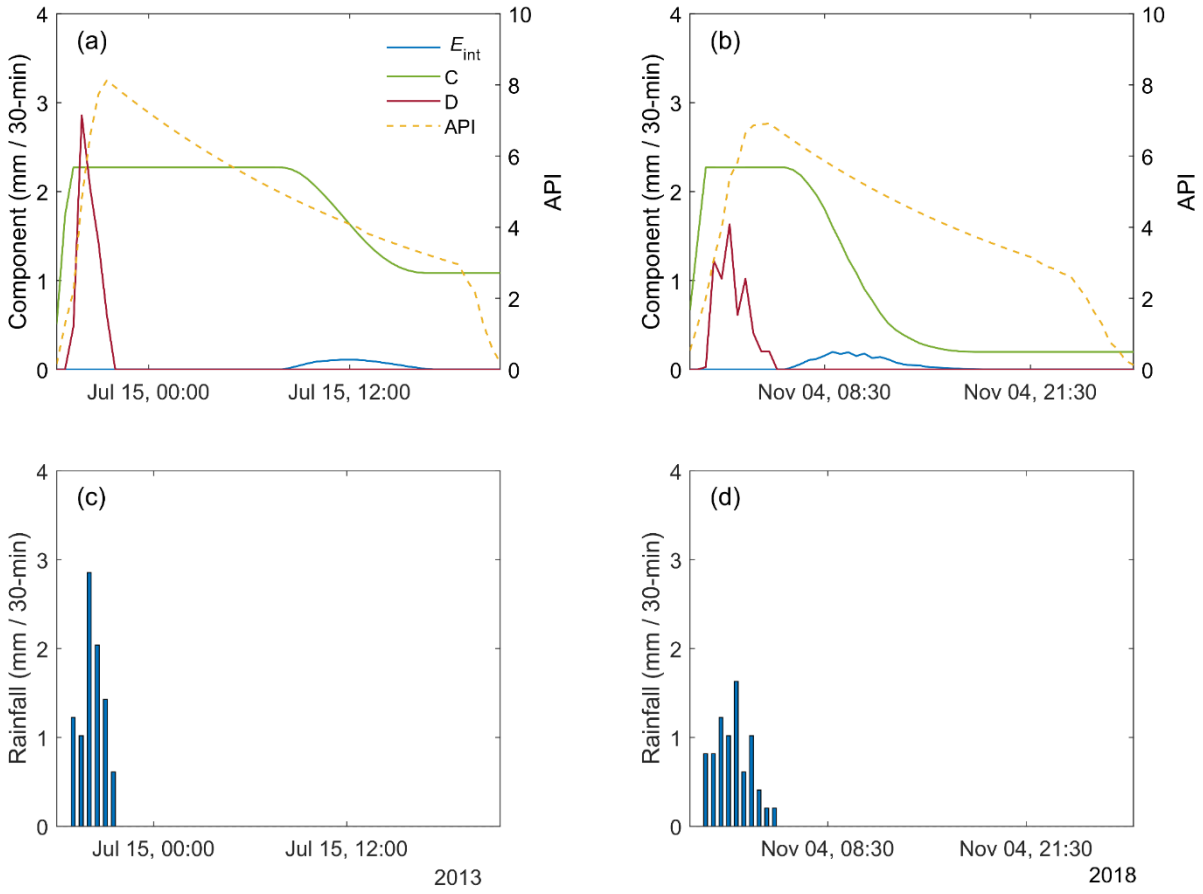

Figure 4.10. Two sample rain events, with Rutter model E_{int}, canopy storage (C), drainage rate (D; i.e., P_n), and antecedent precipitation index (API) shown in (a) and (b). The bar graphs in (c) and (d) show rainfall per half hour.

To complete this analysis, using both models, E_{int}/P_g and E_{int}/E were calculated for the 49 rain events from the Kopuatai dataset, the "periods" during which field data was collected, and for annual time periods (2012–2022). In addition, for each model, the relationship between E_{int}/P_g and P_g was plotted and compared to the theoretical, and S was calculated at the rain event scale using the relationship between P_g and P_n, as done for the collection tray data. However, rain events with $P_n = 0$ were excluded from the S calculation, as they skewed the relationship between P_g and P_n. Finally, seasonal trends in Rutter model E_{int} were demonstrated to determine variability in the contribution of E_{int} to total E (measured using the EC system) and to loss of P_g to the atmosphere.

All analyses were carried out using MATLAB R2021b and Microsoft Excel.

4.3 Results

4.3.1 Collection tray experiment

4.3.1.1 Rain event E_{int} and S

At the whole rain event scale, the mean collection tray interception loss fraction (E_{int}/P_g; ± 95% confidence interval) was 61.6 ± 6.7% (Table 4.2). At each site, mean E_{int}/P_g values decreased in the order of Site 4 > Site 2 > Site 1 > Site 3. Mean E_{int}/E values (where E was measured using the EC system and gap-filled using a neural network) are not shown due to the large values produced, which at times exceeded 1000%. At this timescale, there was no correlation between meteorological variables (i.e., R_n and VPD) and E_{int}/P_g (not shown).

Mean collection tray S (i.e., the negative y-intercept of the relationship between P_n and P_g) was 2.31 ± 1.36 mm at the sub-rain event scale (Table 4.2). The slope of the relationship between P_n and P_g at each site ranged between 0.53 and 0.94, with a mean slope of 0.71 (Appendix F). As observed for E_{int}/P_g, the lowest S value occurred at Site 3. However, the other S values did not follow the site-to-site variability of E_{int}/P_g.

Table 4.2. Interception loss fractions (E_{int}/P_g) at the whole rain event scale and canopy storage capacity (S) at the sub-rain event scale for each collection tray site. E_{int}/P_g values greater than 100% were included in the mean, while rain events smaller than 1 mm were removed from the E_{int}/P_g dataset to ensure consistency with filtering of modelled data (see Methods).

	Whole rain event E_{int}/P_g (%)	**Sub-rain event S (mm)**
Site 1	59.4	3.87
Site 2	64.6	3.04
Site 3	53.3	0.88
Site 4	69.2	1.45
Mean	61.6	2.31
95% CI	6.7	1.36

4.3.1.2 Period-scale E_{int}

Across all field sites and measurement periods (excluding periods where errors occurred; Table 4.3), mean and median period-scale E_{int}/P_g fractions were 47.0 ± 4.4% and 47.7%, respectively, which is lower than at the whole rain event scale. On average, E_{int}/P_g was highest at Site 4 (mean = 52.0%) and lowest at Site 3 (mean = 38.1%), corresponding with the whole rain event scale findings. Temporal variability in E_{int}/P_g also occurred, with mean values for each measurement period ranging between 35.7% and 56.8%; this temporal variability correlated well with mean R_n (Figure 4.11; $R^2 = 0.657$, $p < 0.01$, $t = 3.66$), VPD, and air temperature (not shown due to collinearity of these variables with R_n) for each period.

Table 4.3. Collection tray E_{int}/P_g (%) for each measurement period at each site. Only values in **bold** were included when calculating mean E_{int}/P_g and 95% confidence intervals, as the remaining values were affected by measurement errors. Dashes indicate that data were not collected.

	Period										
	1	2	3	4	5	6	7	8	9	*Mean*	*95% CI*
	Aug–Sep	*Sep*	*Sep–Oct*	*Oct–Nov*	*Nov–Dec*	*Dec–Jan*	*Feb–Mar*	*Mar–Apr*	*Apr–Jun*		
Site 1	**35.7**	12.8	**36.9**	**62.4**	**59.1**	11.7	20.9	**50.1**	24.5	48.8	10.8
Site 2	-	**41.4**	**37.5**	**51.1**	**61.5**	**54.0**	**52.2**	**52.3**	**42.5**	49.1	5.5
Site 3	-	-	**32.0**	37.1	**47.7**	**41.6**	39.9	**30.8**	14.8	38.1	7.9
Site 4	-	-	-	62.6	68.4	**57.5**	**46.6**	48.7	47.6	52.0	10.7
Mean	35.7	41.4	35.5	56.8	56.1	51.0	49.4	44.4	42.5		
95% CI	*N/A*	*N/A*	3.4	11.1	8.3	9.4	5.5	13.4	*N/A*		

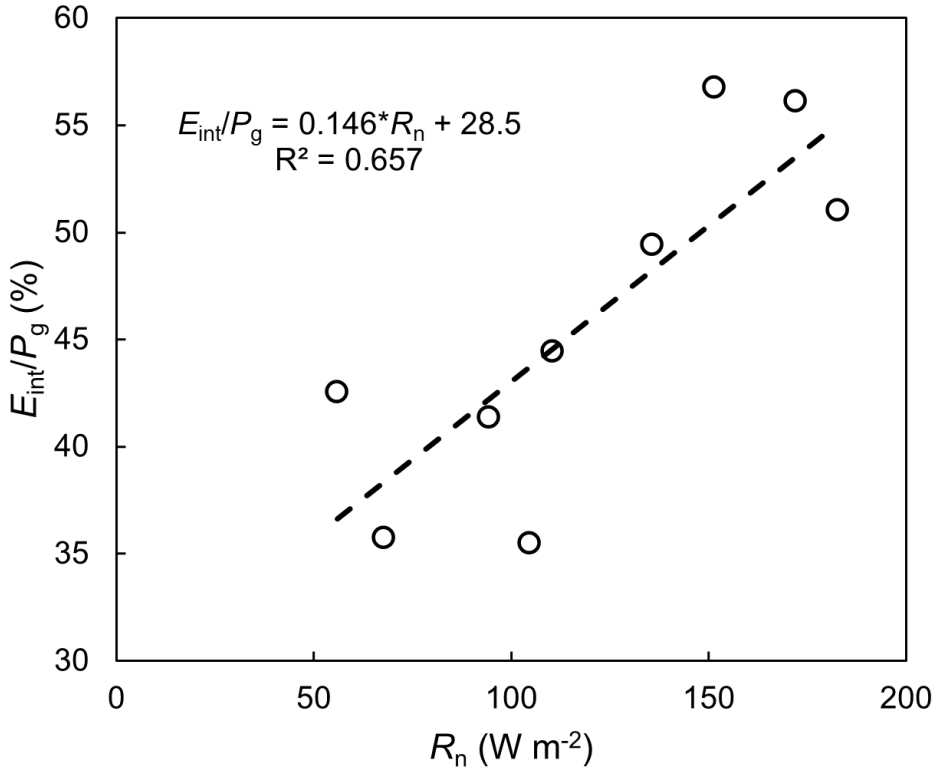

Figure 4.11. Relationship between mean net radiation (R_n) and interception loss fractions (E_{int}/P_g) for each time period when data was collected during the field experiment.

In contrast to E_{int}/P_g, period-scale E_{int}/E fractions were often larger than 100%, resulting in high mean and median values of 95.4 ± 17.6% and 87.5%, respectively (Table 4.4). Values for individual periods ranged between 37.9% and 222.6%.

Table 4.4. Collection tray E_{int}/E (%) for each measurement period at each site. Only values in **bold** were included when calculating mean E_{int}/E and 95% confidence intervals, as the remaining values were affected by measurement errors. Dashes indicate that data were not collected.

	Period										
	1	2	3	4	5	6	7	8	9	*Mean*	*95% CI*
	Aug-Sep	*Sep*	*Sep-Oct*	*Oct-Nov*	*Nov-Dec*	*Dec-Jan*	*Feb-Mar*	*Mar-Apr*	*Apr-Jun*		
Site 1	**73.0**	68.5	**128.4**	**106.8**	**86.8**	17.2	46.0	**61.6**	56.9	91.3	23.4
Site 2	-	**222.6**	**130.5**	**87.5**	**90.3**	**79.4**	**115.0**	**64.4**	**98.8**	111.0	34.3
Site 3	-	-	**111.5**	63.5	**70.2**	**61.2**	87.9	**37.9**	34.4	70.2	30.1
Site 4	-	-	-	107.2	100.4	**84.6**	**102.5**	59.8	110.6	93.5	17.6
Mean	73.0	222.6	123.4	97.1	82.4	75.1	108.7	54.6	98.8		
95% CI	*N/A*	*N/A*	11.8	18.9	12.2	13.9	12.2	16.4	*N/A*		

4.3.2 Modelled E_{int}

4.3.2.1 Comparison of period-scale E_{int} between methods

For the same two to six-week periods during which field data was collected, E_{int}/P_g values calculated using the C-F method (mean = 18.8 ± 4.0%) and the Rutter model (mean = 20.6 ± 4.9%) were not significantly different, but were much lower than the mean period-scale E_{int}/P_g calculated based on the collection tray data (Figure 4.12). In addition, in contrast to the collection tray results, there was no significant relationship between period-scale E_{int}/P_g and R_n for the C-F model ($p = 0.258$, $R^2 = 0.178$, $t = 1.23$) and the Rutter model ($p = 0.306$, $R^2 = 0.149$, $t = 1.11$). The C-F and Rutter model E_{int}/P_g values were very similar for most periods (except Period 8), despite the different variables and calculations used in each model.

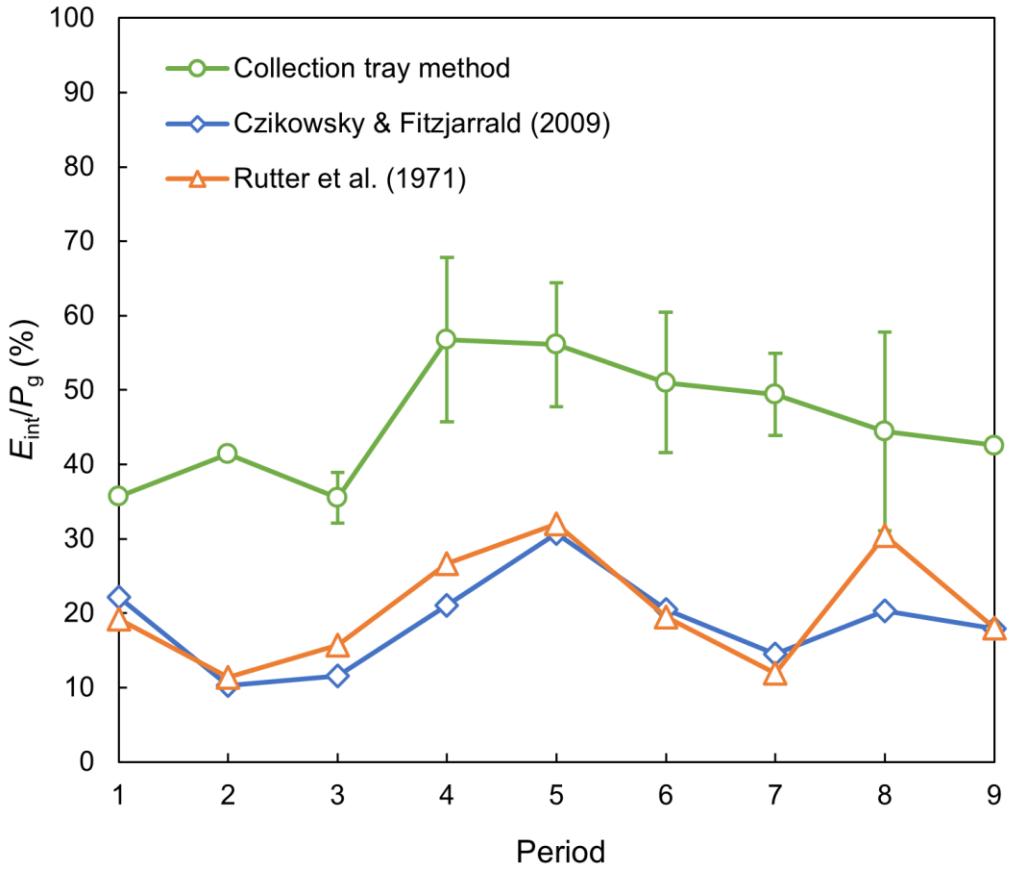

Figure 4.12. Comparison of mean E_{int}/P_g calculated using the collection tray method, C-F method, and Rutter model at the period scale. Error bars for the collection tray method represent 95% confidence intervals, which show variability across Sites 1–4; there are no error bars for periods 1, 2, and 9 because valid data was only available from one site.

Similar to E_{int}/P_g, period-scale E_{int}/E values calculated using the C-F method (mean = 39.0 ± 5.4%) and the Rutter model (mean = 42.5 ± 6.6%) were significantly lower than the mean E_{int}/E for the collection tray method (Figure 4.13); the difference between measured and modelled values was particularly large during Period 2. However, the modelled means were not significantly different.

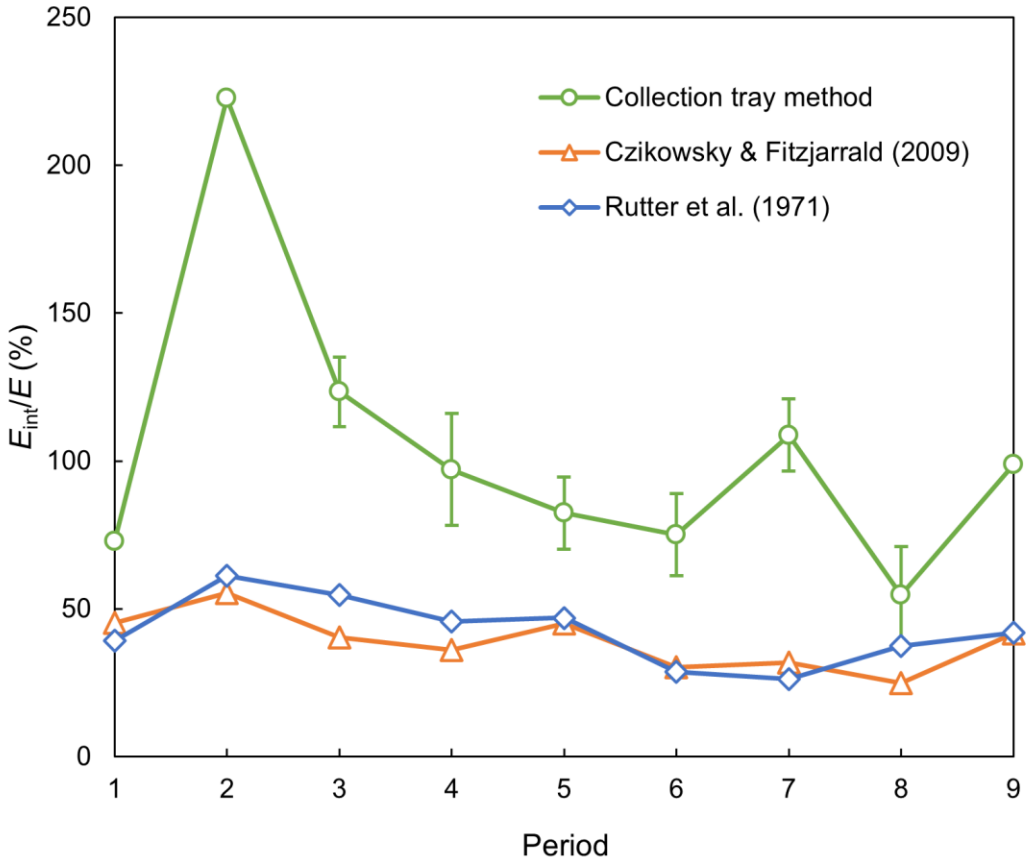

Figure 4.13. Comparison of mean E_{int}/E calculated using the collection tray method, C-F method, and Rutter model at the period scale. Error bars for the collection tray method represent 95% confidence intervals, which show variability across Sites 1–4; there are no error bars for periods 1, 2, and 9 because valid data were only available from one site.

4.3.2.2 Rain event E_{int} and S

Across a set of 49 rain events extracted from the Kopuatai dataset (see Methods), the C-F method produced a mean E_{int}/P_g of 38.5 ± 6.8%, with a median of 37.5%. Mean and median Rutter model E_{int}/P_g values across the same rain events were 41.0 ± 8.5% and 32.3%, respectively. Both modelled mean rain event E_{int}/P_g values were significantly lower than at the rain event scale for the collection tray experiment.

Mean rain event E_{int}/E for the C-F method was 55.4 ± 3.5%, with a median of 58.8%, while mean and median E_{int}/E for the Rutter model were 56.3 ± 6.8% and 53.4%, respectively. These mean E_{int}/E values were not significantly different, but were vastly lower than the rain event E_{int}/E obtained from the collection tray experiment.

Most modelled rain event E_{int}/P_g and E_{int}/E values were between 0% and 100%, however one rain event resulted in negative fractions when using the C-F method (E_{int}/P_g = -1.9% and E_{int}/E = -39.9%). This occurred because the majority of the drying period after this rain event occurred at night, during which E measured using the EC system was negative and below the dry canopy ensemble E. As a result, the sum of rain event E was lower than the dry canopy E in the C-F model, causing E_{int} to be negative. As E_{int} cannot be negative, this rain event was removed from the dataset.

Modelled P_n and measured P_g were used to estimate S, which was 1.50 mm based on the C-F method and 2.02 mm for the Rutter model (Figure 4.14). These estimates were lower than the mean collection tray S (Table 4.2). In addition, the slopes of the P_n–P_g relationships were much closer to 1 than the collection tray data (Appendix F).

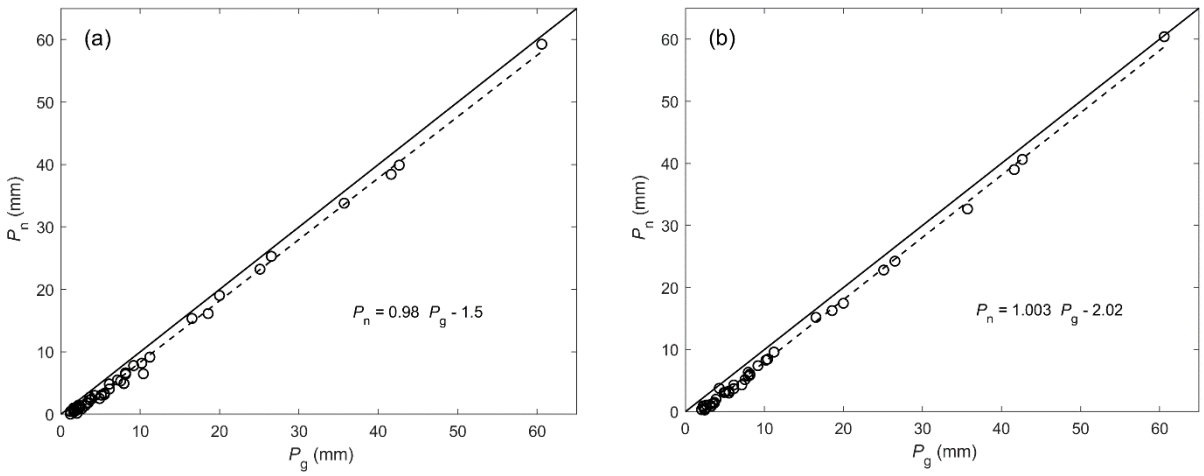

Figure 4.14. Relationship between P_g and P_n for rain events extracted from the Kopuatai dataset, using (a) the C-F method and (b) the Rutter model to calculate P_n. Rain events with P_n = 0 were removed to minimise skew in the P_n–P_g relationship. A 1:1 (solid black) line is shown.

4.3.2.3 Annual E_{int}

Both the C-F and Rutter models were able to provide estimates of annual E_{int}/P_g (15.5 ± 1.2% and 18.3 ± 1.8%, respectively), which were not significantly different. In addition, annual E_{int}/E values were 31.3 ± 1.9% and 36.6 ± 2.2% for the C-F and Rutter models, respectively; however, these values were significantly different (Table 4.5). All annual E_{int}/P_g and E_{int}/E estimates were lower than at the rain event and period scales for each respective model.

Table 4.5. C-F and Rutter model estimates of mean annual E_{int}, E_{int}/P_g, and E_{int}/E at Kopuatai for 2012–2022, with mean annual P_g and E totals provided.

	C-F method		**Rutter model**	
	Mean	**95% CI**	**Mean**	**95% CI**
E_{int} (mm y^{-1})	180.7	13.9	211.1	14.2
P_g (mm y^{-1})	1191.2	159.7	1191.2	159.7
E (mm y^{-1})	575.8	12.8	575.8	12.8
E_{int}/P_g (%)	15.5	1.2	18.3	1.8
E_{int}/E (%)	31.3	1.9	36.6	2.2

4.3.3 Relationship between P_g and E_{int}/P_g

For both the measured and modelled data at the rain event scale, E_{int}/P_g had a negative relationship with P_g (Figures 4.15 and 4.16); all of these relationships fitted well to an exponential curve. Modelled rain event E_{int}/P_g values were very close to the theoretical interception loss rate, while collection tray E_{int}/P_g values were typically higher than the theoretical rate, increasingly so with increasing P_g. At the annual scale, E_{int}/P_g and P_g had a negative *linear* relationship for both the C-F and Rutter models, which had the same slope but different intercepts (Figure 4.16). The difference in E_{int}/P_g between low and high annual

rainfall years (900–1700 mm) was less than 10% for both models, indicating low interannual variability. At both rain event and annual scales, the decreasing trend in E_{int}/P_g was primarily caused by an increase in P_g, rather than a decrease in E_{int}.

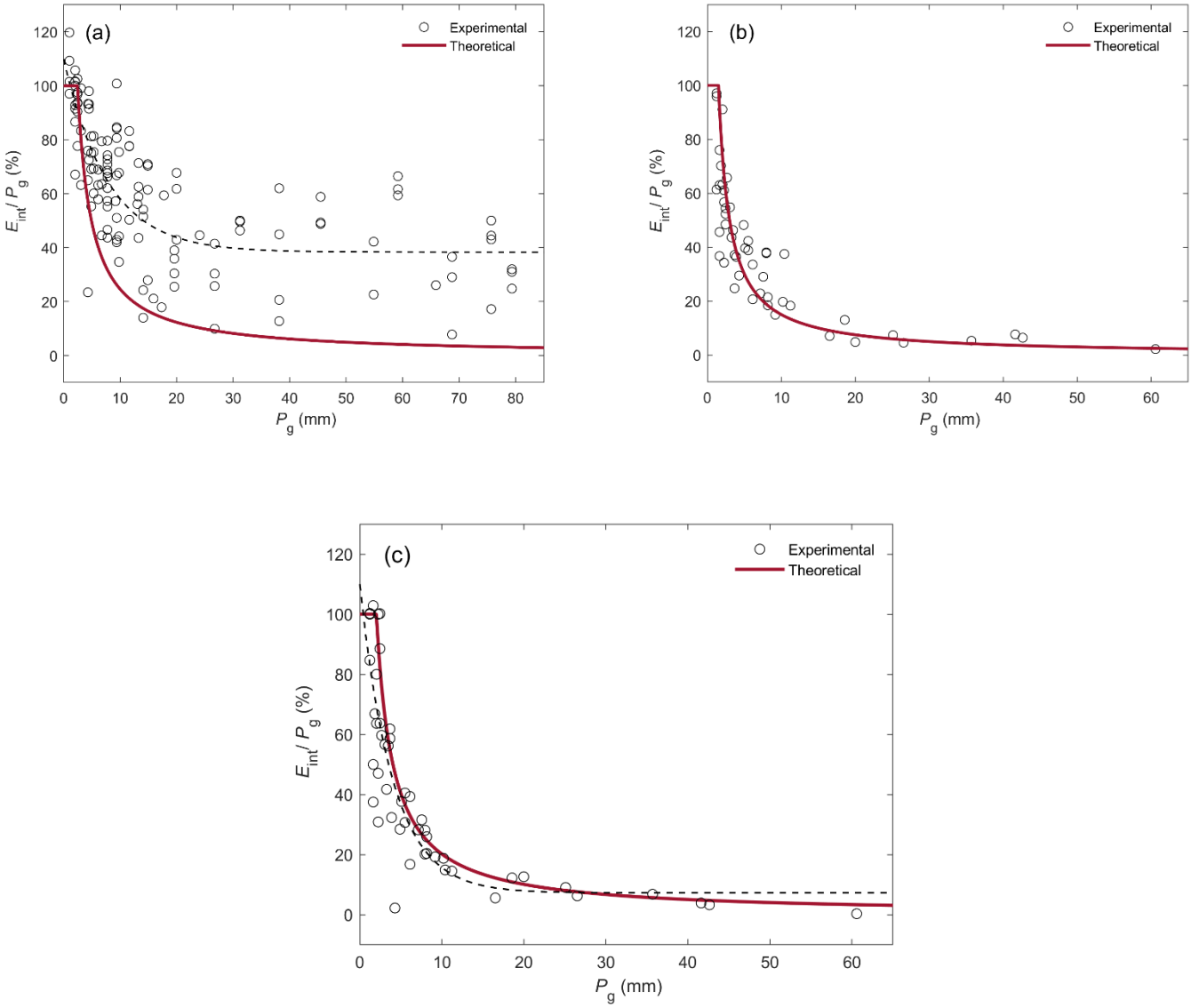

Figure 4.15. The relationship between P_g and E_{int}/P_g for (a) whole rain event data obtained from the collection tray experiment, and for 49 rain events extracted from the Kopuatai dataset, using (b) the C-F method and (c) the Rutter model to calculate E_{int}. The S values used to generate these theoretical relationships corresponded to those calculated using each respective method.

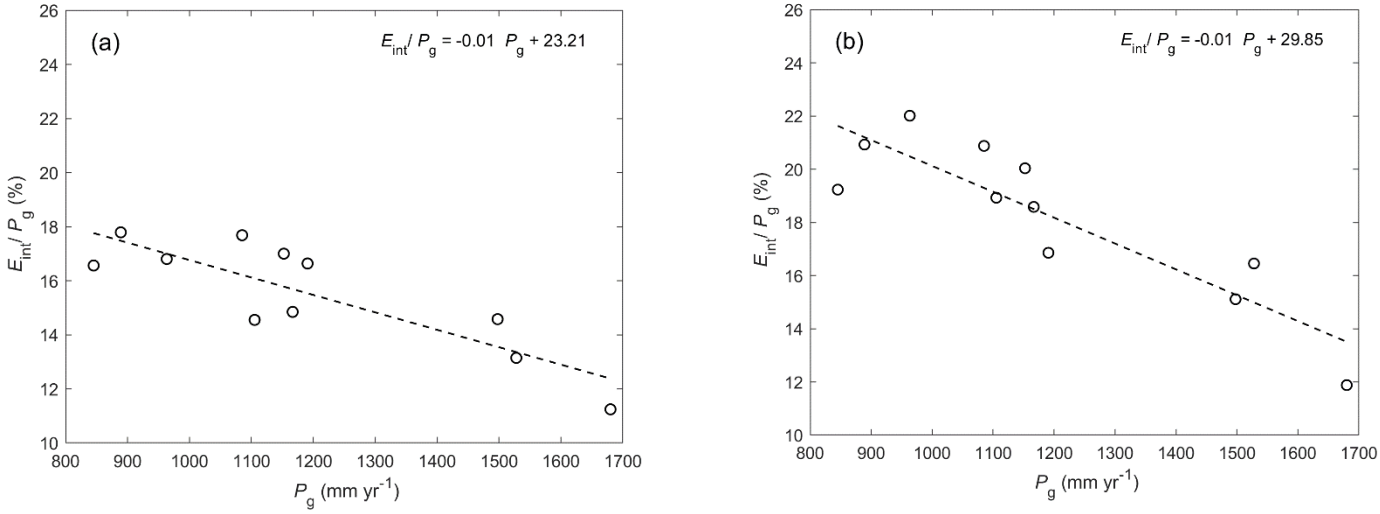

Figure 4.16. The relationship between P_g and E_{int}/P_g at an annual scale, calculated using (a) the C-F method, and (b) the Rutter model.

4.3.4 Seasonal variability in Rutter model E_{int}

Mean monthly P_g varied seasonally at Kopuatai, with a minimum of 47 ± 24 mm month^{-1} occurring mid-summer (January) and a maximum of 145 ± 31 mm occurring mid-winter (July; Figure 4.17). Conversely, the lowest mean monthly total E (measured using the EC system and gap-filled) occurred in winter (27 ± 3 mm in June) and peaked in summer (68 ± 4 mm in January). However, mean monthly Rutter model E_{int} did not follow a clear seasonal trend, instead increasing slightly during the transition between summer and autumn (February to April) and winter and spring (June to September). Monthly E_{int} was relatively low, remaining near a mean of 18 mm month^{-1} throughout the year (range = 11–25 mm month^{-1}).

The contribution of E_{int} to total E (i.e., E_{int}/E) was highest during the mid-winter period (65 ± 8% in July) and lowest in mid-summer (17 ± 5% in January) (Figure 4.18); the seasonal variability of E_{int}/E values was large due to variability in total E, rather than E_{int} (Figure 4.17). However, the proportion of P_g returned to the atmosphere through E_{int} (E_{int}/P_g) had a much smaller range of seasonal variability (15–33%) than E_{int}/E (17–65%), with the lowest losses occurring in winter and highest losses in summer. Similar to E_{int}/E, this variability was driven by changes in P_g, rather than E_{int}.

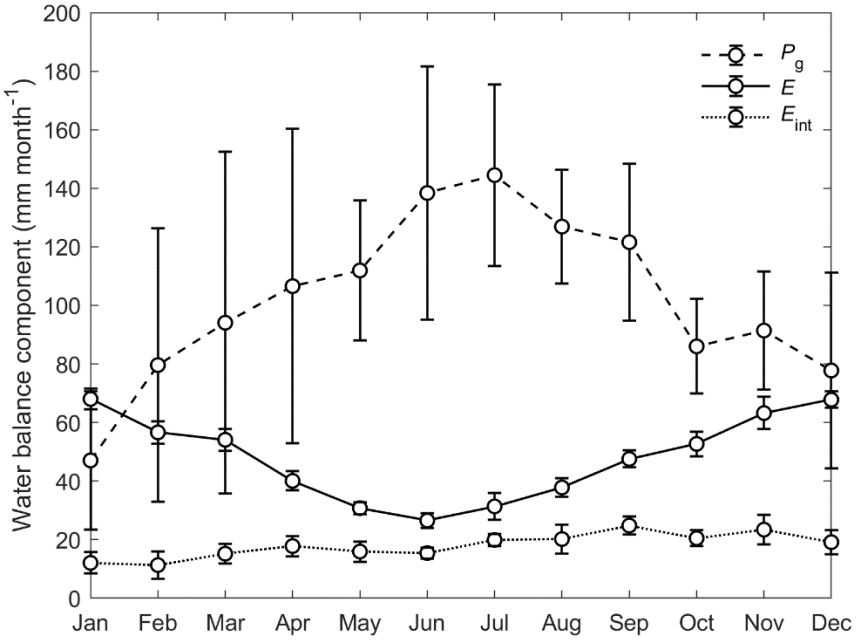

Figure 4.17. Seasonal variability in gross precipitation (P_g), gap-filled evaporation (E) measured using the eddy covariance technique, and Rutter model interception loss (E_{int}) at Kopuatai. Error bars represent 95% confidence intervals.

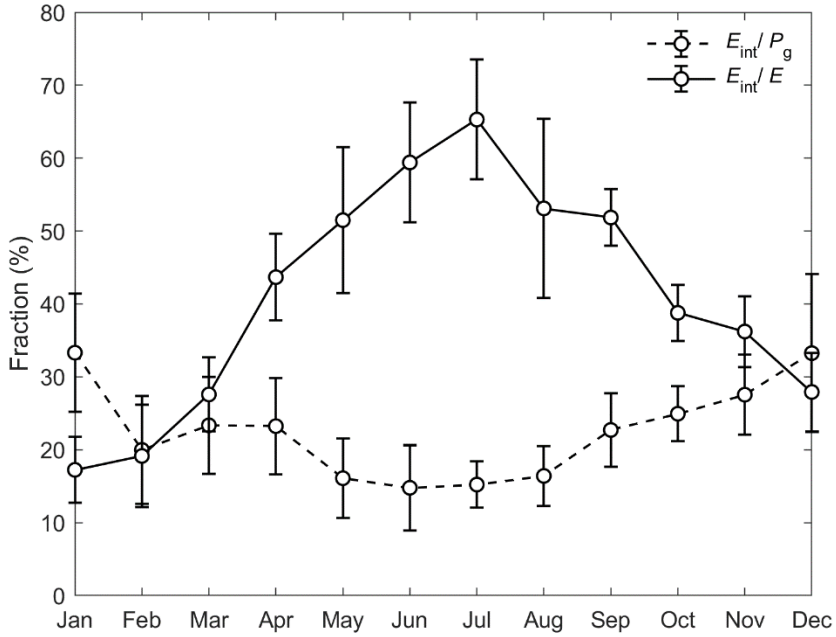

Figure 4.18. Seasonal variability in Rutter model E_{int}/P_g and E_{int}/E at Kopuatai. Error bars represent 95% confidence intervals.

4.4 Discussion

A wide range of measured and modelled E_{int}/P_g estimates were produced across a number of different timescales in this study (Figure 4.19). For each respective method used to calculate E_{int}/P_g, its value was lower at longer timescales, in addition to having smaller 95% confidence intervals. All mean period-scale values (i.e., for the approx. month-long periods during which field data were collected) were significantly lower than at the rain event scale (according to the 95% confidence intervals, which did not overlap). In addition, mean annual C-F and Rutter model E_{int}/P_g values were lower than at the period scale, but not significantly. Mean E_{int}/P_g estimates could have been lower at longer timescales due to the decreasing effect of rain event magnitude on E_{int}, particularly reducing the impact of small, high E_{int}/P_g rain events on mean E_{int}/P_g. The smaller 95% confidence intervals occurred due to lower inter-period and interannual variability in E_{int}/P_g compared to variability between rain events. In terms of the canopy storage capacity, S, the rain event scale data produced estimates of 1.50 mm (C-F model) and 2.31 mm (field experiment).

4.4.1 Errors in measured and modelled E_{int}/P_g

There was no significant difference between the C-F and Rutter model E_{int}/P_g means at the rain event scale, however mean collection tray E_{int}/P_g at the same timescale was significantly higher than both of these modelled means (Figure 4.19). Similarly, at the period scale, both models produced mean E_{int}/P_g and E_{int}/E values that were not significantly different, while the collection tray means were significantly higher. Interestingly, mean period-scale collection tray E_{int}/E was almost 100%, which is not plausible for month-long time periods. Therefore, the agreement between the results of the two models and the unrealistically high collection tray E_{int}/E indicate that the collection tray method may have overestimated E_{int}. Possible mechanisms resulting in E_{int} overestimation will be discussed below.

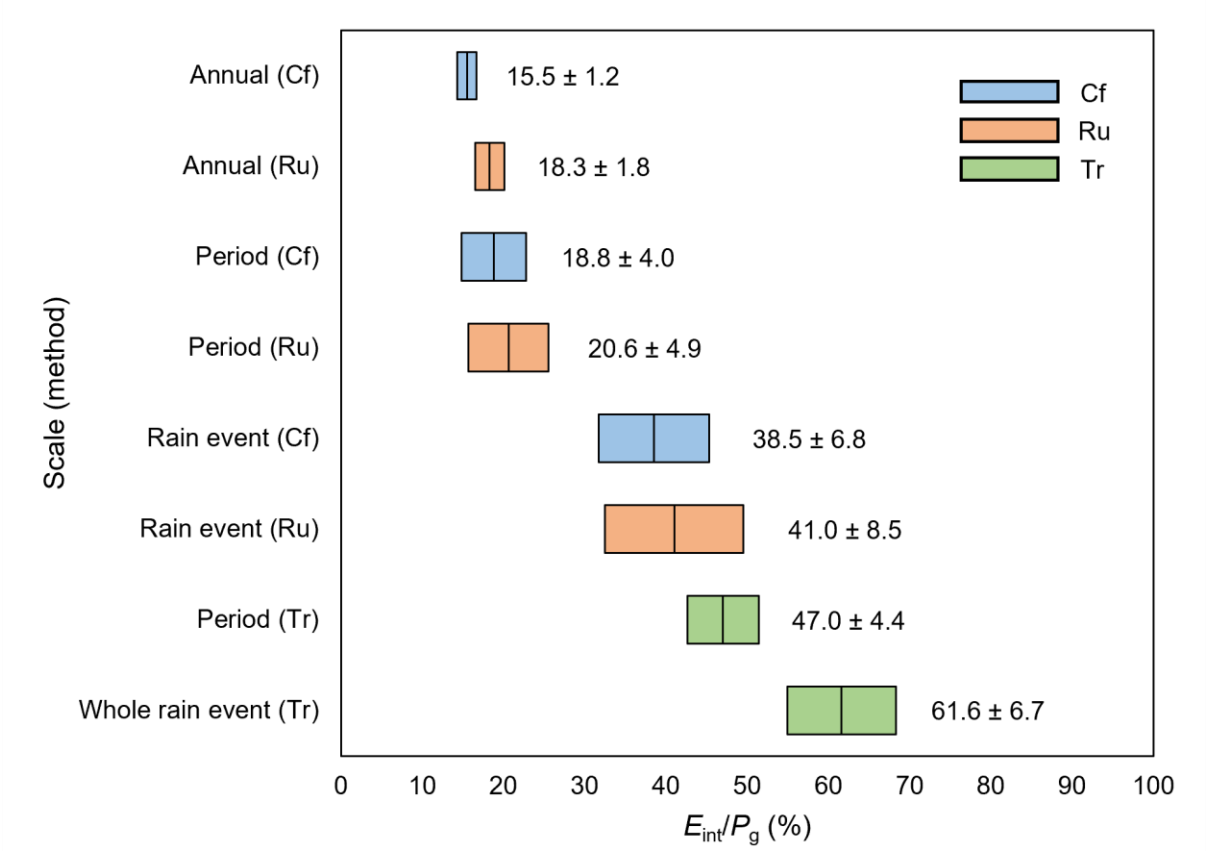

Figure 4.19. Summary of E_{int}/P_g means (and 95% confidence intervals) produced in this study using different methods (Tr = collection tray method, Cf = C-F method, and Ru = Rutter model) and at different timescales (rain event to annual), arranged in order of lowest to highest mean estimate.

Similar to this study, significant disagreement has previously been observed between E_{int} calculated using the water budget method (i.e., field experiments) and the Penman–Monteith equation (used in the Rutter model), where the former tends to produce higher E_{int} estimates than the latter (van Dijk et al., 2015). This could be partially attributed to spatial sampling errors when applying the water budget method, which may underestimate P_n and therefore overestimate E_{int} (van Dijk et al., 2015). In this study, measurements were biased towards high and dense plant canopies - while some spatial variability was accounted for by placing sites in areas with varying canopy heights and using multiple trays for each site, this still excluded areas with a very sparse canopy (or no canopy) due to the impracticality of placing trays in such areas. These portions of the peatland would be expected to experience lower E_{int} than the four sites sampled by the collection trays. Therefore, the bias towards higher and denser

canopies in the collection tray data could have caused E_{int}/P_g and S to be overestimated. In contrast, lower E_{int} estimates were likely produced by the two modelling approaches because the input data is representative of the entire EC footprint, including low canopy and bare peat areas.

At the rain event scale, the gap between measured and modelled E_{int}/P_g could have also occurred due to the use of data from different rain events. The mean modelled E_{int}/P_g was calculated using 49 rain events extracted from the Kopuatai dataset, which were selected on the basis that incomplete canopy drying and subsequent re-wetting did not occur throughout (see Methods). In contrast, almost all rain events that occurred throughout the collection tray experiment were used for E_{int}/P_g calculations, regardless of canopy drying throughout, due to limited data availability. Therefore, partial canopy drying in between pulses of rain within one wetting event could have caused collection tray E_{int}/P_g to be overestimated. However, there was still a significant difference between measured and modelled E_{int}/P_g at the period scale, indicating that the use of different rain event datasets was not the only factor causing this contrast in E_{int}/P_g.

An additional cause of E_{int}/P_g overestimation could have been P_n undercatch resulting from tube blockages by plant litter, which were observed to cause tray overflow from Period 5 onwards. However, mean E_{int}/P_g across Periods 1–4 (before blockages were observed) was 42.4% ± 7.9%, which is not significantly lower than the mean for Periods 5–9 (49.7 ± 4.8%). This indicates that other factors are more likely to be responsible for the differences between measured and modelled E_{int}/P_g. However, tray overflow could have still contributed to errors during large rain events if the rainfall rate exceeded the rate of drainage through the tubing. Additional measurement errors could have resulted from structural changes in the vegetation canopy due to the installation of trays, which could have modified normal throughfall and stemflow dynamics, affecting E_{int}/P_g estimates; however, the impact of this could not be determined.

There was also a frequent error which caused unexpectedly low period-scale E_{int}/P_g values to be produced by the collection tray method (these values were excluded from the analysis;

Table 4.3). This occurred because, at times, P_n exceeded P_g (or the rate of increase in P_n exceeded that of P_g), causing decreases in cumulative E_{int} (as $E_{int} = P_g - P_n$). For example, this occurred at Site 1 during Periods 2 and 6 (Figure 4.20), producing much lower E_{int}/P_g values than expected (Table 4.3). Despite the proximity of the four collection tray sites to the rain gauge, it is possible that spatial variability in P_g caused P_n at some sites to briefly exceed the P_g measured at the rain gauge. In addition, as this issue mostly arose during large, intense rain events, it is also possible that P_n exceeded P_g due to undercatch by the rain gauge, which could have been caused by the loss of splash droplets, deflection of rainfall by wind, and E during rainfall (New et al., 2001). However, it is also likely that P_n undercatch occurred during such rain events due to the loss of water via splash droplets and/or tray overflow. While decreases in cumulative E_{int} did not affect final E_{int}/P_g values in this study due to the removal of such data, it is important to mitigate this issue in future iterations of this experiment.

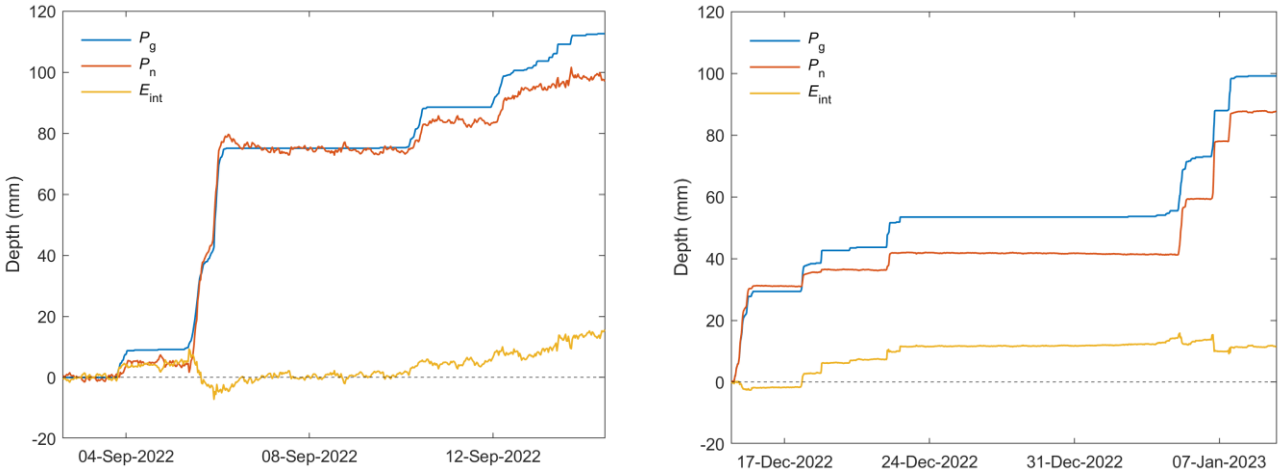

Figure 4.20. Examples of decreases in cumulative interception loss (E_{int}) occurring when net precipitation (P_n) exceeded gross precipitation (P_g) at Site 1 during Periods 2 and 6.

In addition to E_{int} overestimation by the collection tray method, it is also possible that underestimation of modelled E_{int} occurred, contributing to the large difference between measured and modelled E_{int}/P_g. For example, Penman–Monteith E_{int} could have been underestimated because the heat release from biomass and the air below the measurement height (Q) and the ground heat flux (G) were not included as energy sources for E_{int} (van Dijk et al., 2015). Across the 128 FLUXNET sites studied by van Dijk et al. (2015), heat release from

biomass and air was negligible for short vegetation, while heat release from soil was small but non-negligible; therefore, not accounting for the effect of G at Kopuatai may have caused Penman–Monteith E_{int} to be underestimated. Alternatively, lower Rutter model E_{int} values may have been produced if the input S value from the collection tray data was underestimated (Appendix E, Figure E2; van Dijk et al., 2015). However, the evidence in this section suggests *overestimation* of collection tray E_{int}/P_g (and therefore S), indicating that Rutter model E_{int}/P_g may have been overestimated via the input S value, rather than underestimated.

Underestimation of C-F E_{int}/P_g may have occurred due to underestimates of EC evaporative fluxes during and shortly after rainfall, as observed by van Dijk et al. (2015) at 128 FLUXNET EC sites. Measurements during rainfall have previously been problematic due to a large proportion of data loss for open path gas analysers and due to increased noise in sonic anemometer measurements during high intensity rainfall (Mizutani et al., 1997; van Dijk et al., 2015), which could have potentially affected EC measurements during rainfall at Kopuatai. Conversely, C-F E_{int} may have been overestimated due to downward spikes in dry canopy E, which were caused by differences in sunset times between rain events and the dry canopy ensembles (see Methods). While large upward and downward spikes in the data were removed, small predominantly downward spikes still remained, potentially causing E_{int} to be higher than expected. As such, the above sources of error could have caused C-F E_{int}/P_g and S to be either underestimated or overestimated; however, the actual impact of these potential errors could not be quantified.

4.4.2 Errors in measured and modelled *S*

Mean collection tray S (2.31 mm) was 13% and 43% higher than the Rutter and C-F model estimates, respectively. The greater similarity between the collection tray and Rutter model S occurred because the collection tray value was used for the S parameter in the Rutter model. Therefore, as the Rutter model S value is not independent from the collection tray method, it is not accepted as a possible estimate of S for Kopuatai. In contrast, S values obtained through the collection tray and C-F methods are independent; therefore, it is valid to compare them.

A potential issue affecting the collection tray S is the slope of the P_n–P_g relationship. The regression method for determining S is expected to produce a slope of 1, assuming that rain events completely wet the canopy (ensured by removal of small rain events from the P_n–P_g relationship), that rain events are continuous, and that negligible E_{int} occurs during each rain event (Campbell & Murray, 1990). For the Rutter model, the relationship between P_g and P_n was almost 1:1 because the calculation of the drainage term (i.e., P_n) partially depended on the value of P_g. Similarly, the C-F method P_n was also dependent on P_g ($P_n = P_g - E_{int}$), producing a slope close to unity. However, the mean slope for the collection tray P_n–P_g relationship was 0.71 (Appendix F); therefore, it is possible that E_{int} occurred during rainfall throughout the sub-rain event periods. In addition, the slope below unity could have resulted from tray overflow during large, intense rain events (or due to tube blockages), which would have caused P_n undercatch. Susceptibility to tray overflow may have depended on S itself, as the slope of the P_n–P_g relationship was furthest from unity for sites with the lowest S (Appendix F). This indicates that tray overflow may have been higher at sites with less canopy storage by enabling more rainfall to reach the trays. Overall, the combined effect of E_{int} during rainfall and tray overflow during large rain events is likely to have caused S to be overestimated. This is because P_n would have been underestimated, causing the y-intercept of the P_n–P_g relationship to be further from zero than expected.

4.4.3 Controls on E_{int}/P_g

Collection tray E_{int}/P_g was positively correlated with R_n at the period scale, while modelled period-scale data and collection tray data at the rain event scale were not. The correlation for period-scale collection tray data likely occurred due to seasonal variability in R_n, however it is unclear why there was no correlation at the rain event scale or for modelled period-scale data. The available evidence of the importance of R_n for driving E_{int} appears limited and conflicting; in one real and one simulated forest ecosystem, R_n was an important source of energy for E during wet canopy conditions (Klaassen, 2001; Cisneros Vaca et al., 2018), while in two other forests, R_n did not appear to be a major factor regulating E_{int} (Kelliher et al., 1992; Staelens et al., 2008). However, the importance of R_n for driving E_{int} could be location-specific, as one study found that R_n was likely a dominant control on E_{int} at a forest in Russia, while E_{int}

from a forest in Japan was only partially driven by R_n (Toba & Ohta, 2005). Other possible energy sources for E_{int} include downward sensible heat fluxes and heat release from canopy air, biomass, and the soil below (Mizutani et al., 1997; Toba & Ohta, 2005; Herbst et al., 2008; van Dijk et al., 2015; Cisneros Vaca et al., 2018). These alternative energy sources may have been important drivers of E_{int} at Kopuatai, but were not investigated in this study.

Measured and modelled rain event E_{int}/P_g decreased non-linearly with increasing P_g, as has been previously observed in a number of E_{int} measurement studies (e.g., Genxu et al., 2012; Zhang et al., 2015; Li et al., 2015; Ochoa-Sánchez et al., 2018). In addition, similar to our annual scale results, a negative linear relationship between annual E_{int}/P_g and P_g was shown across 24 modelled forest sites with the same vegetation properties (Komatsu et al., 2008). The relationship between E_{int}/P_g and P_g for the rain event collection tray data showed that E_{int}/P_g was mostly above the theoretical S-dependent rate (Figure 4.15a), while modelled values were at or very close to this rate (Figures 4.15b and 4.15c). This indicates that E_{int}/P_g was likely overestimated when using the collection tray method, as suggested above.

Canopy height and density appeared to have an impact on E_{int} at Kopuatai, as Site 3 had a low and sparse canopy, which likely resulted in the lowest E_{int}/P_g and S being observed at this site. In a review of tree and shrub data in Mediterranean Europe, forest stand properties, including LAI, age, height, diameter at breast height, and basal area were negatively correlated with throughfall (Llorens & Domingo, 2007), suggesting an increase in E_{int} with increases in these properties. Similarly, E_{int} has been observed to increase as the plant area index (PAI) of a forest increased (Toba & Ohta, 2008). In addition, the fraction of direct throughfall and leaf area index (LAI) of a forest canopy have been shown to explain 59% and 12% of variability in E_{int}, respectively (Fleischbein et al., 2005). Therefore, vegetation characteristics can have an important influence on the partitioning of P_g between E_{int} and P_n. However, for future collection tray experiments, many more sites would be needed to determine the nature of the relationship between E_{int}/P_g (or S) and canopy height, as there was no clear trend in this study.

4.4.4 E_{int}/P_g at Kopuatai compared to other ecosystems

Given the low 95% confidence intervals and the large amount of data included, the mean annual C-F and Rutter model E_{int}/P_g and E_{int}/E estimates were likely the most realistic. Therefore, E_{int}/P_g and E_{int}/E at Kopuatai are likely to be in the range 15.5–18.3% and 31.3–36.6%, respectively. This range of annual E_{int}/P_g is much lower than the previous estimate made by Agnew et al. (1993) at Kopuatai, which was 33.9%.

Compared to other peatland ecosystems, E_{int}/P_g at Kopuatai does not appear particularly low or high (Table 4.6). Very few E_{int} studies have been carried out in pristine peatlands, with the majority examining E_{int} in disturbed or burned ecosystems (Exler & Moore, 2022). However, two studies at pristine peatlands in Canada observed E_{int}/P_g values of 43.9 ± 7.3% (Baisley, 2012) and 9–15% for trees, as well as an E_{int}/P_g range of 20–36% for shrubs (Exler & Moore, 2022). The modelled E_{int}/P_g range obtained from Kopuatai is lower compared to the shrub vegetation, but was located between the two E_{int}/P_g estimates for trees at these peatlands. The differences in E_{int}/P_g between the vegetation at Kopuatai and these two peatlands could not be explained by differences in vegetation height (Table 4.6).

In relation to most other ecosystem types with short vegetation, our modelled E_{int}/P_g values from Kopuatai were relatively low (Table 4.6). This could be a result of the greater vegetation heights in these ecosystems (up to 2.7 m) than at Kopuatai, with lower aerodynamic resistance leading to higher E_{int} (David et al., 2005). However, minimum vegetation heights are typically low in these ecosystems (as low as 0.24 m; Table 4.6), despite resulting in higher E_{int}/P_g compared to Kopuatai. Similarly, lower E_{int}/P_g values were measured for trees at Burns bog (Exler & Moore, 2022) than for trees at another peatland in Canada (Baisley, 2012), despite much greater tree heights at the former (Table 4.6). Furthermore, the study at Burns bog found lower E_{int}/P_g from trees than from shorter shrubs (Exler & Moore, 2022). All of the above observations highlight the fact that vegetation height is not the only factor determining E_{int}; therefore, the exact cause of differences in E_{int}/P_g between Kopuatai and other ecosystems, including peatlands, is likely complex.

Table 4.6. E_{int}/P_g ranges measured in peatlands and ecosystems with short vegetation, in addition to modelled annual E_{int}/P_g at Kopuatai. Ecosystem vegetation heights and the duration of E_{int} measurements are specified for each study.

Ecosystem name/type	**E_{int}/P_g (%)**	**Vegetation height (m)**	**Measurement duration**	**Reference**
Kopuatai bog, New Zealand	15.6–18.3	0.48	Annual	This study
Burns bog, Canada	9.0–15.0 (trees) 20.0–36.0 (shrubs)	4.3–18.8 (trees) 0.33–1.1 (shrubs)	1 year	Exler & Moore (2022)
Trees at a bog in Canada	43.9 ± 7.3	2.3	1 year	Baisley (2012)
Two shrub types in China	16.7–22.3	0.64–1.45	3 growing seasons	Zhang et al., (2015)
Three Mediterranean shrub species	36.5 (juniper) 25.2 (rosemary) 33.0 (thyme)	0.72–0.78 (juniper) 0.53–0.64 (rosemary) 0.24–0.27 (thyme)	3 years	Serrato & Diaz (1998)
Dryland shrubs	16.6–40.0	0.6–2.7	4 months to 4 years	Magliano et al. (2019b)

4.5 Conclusions and recommendations

This study aimed to build on the limited knowledge of wet canopy E, dominated by E_{int}, at Kopuatai bog in Aotearoa New Zealand. Using a canopy water balance experiment and two models, E_{int} was quantified at rain event to annual timescales. The results of this analysis demonstrated a large gap between measured and modelled E_{int}, suggesting overestimation of E_{int} by the field experiment, or underestimation by the models. However, the modelled E_{int} estimates were more realistic than those obtained from the field data, suggesting that overestimation of E_{int} by the field experiment was more likely. Therefore, the best estimates of E_{int} at Kopuatai were those that were modelled at the annual scale, constituting 15.5–18.3% of P_g and 31.3–36.6% of total E. In addition, an S value of 1.5 mm was estimated using the C-F model. These modelled E_{int}/P_g and S values were lower than previously estimated at Kopuatai, suggesting that past field experiments also overestimated E_{int}.

The results of this analysis indicate that our hypothesis was only partially correct. Firstly, seasonal variability in E_{int} was minimal at Kopuatai, however E_{int}/E varied due to seasonal changes in E, reaching a maximum in winter. This indicates that E_{int} itself is relatively stable, but is a more dominant component of E during the wetter winter months. Therefore, this part of our hypothesis was correct. However, mean annual E_{int}/P_g modelled at Kopuatai was at the low end of ranges observed for other short vegetation types, contrary to our hypothesis.

Considering the results of this study, the use of models appears more favourable for calculation of E_{int}/P_g and E_{int}/E at all timescales compared to the collection tray experiment. However, there are a number of possible sources of error affecting the modelled results that need to be mitigated; for example, the Rutter model results could be improved by accounting for all possible energy sources driving E_{int} when applying the Penman–Monteith equation. Nevertheless, the collection tray method could be used to obtain better estimates of E_{int} and S in the future, provided that more measurement sites are used to account for greater spatial variability in canopy height, and that tray overflow is mitigated. Building on this research,

future work at Kopuatai could include partitioning E into transpiration and peat surface E, as well as determining the relative importance of various controls on E_{int} using statistical models.

Chapter 5

Conclusions

To better understand dry and wet canopy *E* processes at Kopuatai bog in Aotearoa New Zealand, this study compared its long-term *E* regimes, energy balance partitioning, and the response of *E* to VPD to Mer Bleue bog, Canada, and determined the magnitude of E_{int} at Kopuatai using a field experiment and two modelling approaches. This research has shown that strong dry canopy stomatal restriction of *E* by *E. robustum* enables greater water retention at Kopuatai, suggesting greater "hydrological resistance" to climatic warming and drying than at Mer Bleue. In future, the higher water retention at Kopuatai may facilitate greater resilience of C stores to climate warming compared to Mer Bleue and other Northern Hemisphere peatlands. During wet canopy conditions, however, about 16–18% of annual precipitation at Kopuatai was estimated to be lost to the atmosphere via E_{int}, making up about 31–37% of total annual *E*. Therefore, while the dry canopy *E* regime is extremely conservative at Kopuatai, moderately large evaporative losses can still occur when the canopy is wet. Interestingly, E_{int} did not appear to vary seasonally, however its contribution to total *E* varied substantially between summer (17%) and winter (65%) due to seasonal variability in *E*. Therefore, E_{int} appears to be a relatively stable component of the water balance at Kopuatai throughout the year. To further understand dry and wet canopy *E* regimes at Kopuatai, future studies could focus on modelling the effect of projected climate change on the water balance of this ecosystem. In addition, *E* limitation by the dense standing litter layer of *E. robustum* could be quantified, and partitioning of *E* between transpiration and peat surface *E* components could be investigated.

References

Adkinson, A. C., & Humphreys, E. R. (2011). The response of carbon dioxide exchange to manipulations of *Sphagnum* water content in an ombrotrophic bog. *Ecohydrology, 4*(6), 733-743. doi:10.1002/eco.171

Admiral, S. W., & Lafleur, P. M. (2007). Partitioning of latent heat flux at a northern peatland. *Aquatic Botany, 86*(2), 107-116. doi:10.1016/j.aquabot.2006.09.006

Admiral, S. W., Lafleur, P. M., & Roulet, N. T. (2006). Controls on latent heat flux and energy partitioning at a peat bog in eastern Canada. *Agricultural and Forest Meteorology, 140*(1-4), 308-321. doi:10.1016/j.agrformet.2006.03.017

Agnew, A. D. Q., Rapson, G. L., Sykes, M. T., & Bastow Wilson, J. (1993). The functional ecology of *Empodisma minus* (Hook, f.) Johnson & Cutler in New Zealand ombrotrophic mires. *New Phytologist, 124*, 703-710.

Alekseychik, P., Mammarella, I., Lindroth, A., Lohila, A., Aurela, M., Laurila, T., . . . Vesala, T. (2018). Surface energy exchange in pristine and managed boreal peatlands. *Mires and Peat, 21*, 1-26. doi:10.19189/MaP.2018.OMB.333

Anderson, R. G., & Wang, D. (2014). Energy budget closure observed in paired Eddy Covariance towers with increased and continuous daily turbulence. *Agricultural and Forest Meteorology, 184*, 204-209. doi:10.1016/j.agrformet.2013.09.012

Aurela, M., Riutta, T., Laurila, T., Tuovinen, J.-P., Vesala, T., Tuittila, E.-S., . . . Laine, J. (2007). CO_2 exchange of a sedge fen in southern Finland - the impact of a drought period. *Tellus B: Chemical and Physical Meteorology, 59*(5). doi:10.1111/j.1600-0889.2007.00309.x

Baisley, S. A. (2012). *Effect of drying induced afforestation on peatland ecohydrology: implications for wildfire vulnerability.* (MSc). McMaster University, Hamilton, ON, Canada.

Blodau, C. (2002). Carbon cycling in peatlands: A review of processes and controls. *Environmental Reviews, 10*(2), 111-134. doi:10.1139/a02-004

Bonn, A., Allott, T., Evans, M., Joosten, H., & Stoneman, R. (2016). Peatland restoration and ecosystem services: an introduction. In A. Bonn, T. Allott, M. Evans, H. Joosten, & R. Stoneman (Eds.), *Peatland Restoration and Ecosystem Services: Science, Policy and Practice* (pp. 1-16). Cambridge, UK: Cambridge University Press.

Brümmer, C., Black, T. A., Jassal, R. S., Grant, N. J., Spittlehouse, D. L., Chen, B., . . . Wofsy, S. C. (2012). How climate and vegetation type influence evapotranspiration and water use efficiency in Canadian forest, peatland and grassland ecosystems. *Agricultural and Forest Meteorology, 153*, 14-30. doi:10.1016/j.agrformet.2011.04.008

Bubier, J. L., Moore, T. R., & Crosby, G. (2006). Fine-scale vegetation distribution in a cool temperate peatland. *Canadian Journal of Botany, 84*(6), 910-923. doi:10.1139/b06-044

Burba, G. (2022). *Eddy Covariance Method for Scientific, Regulatory, and Commercial Applications*. Lincoln, Nebraska, USA: LI-COR Biosciences.

Burba, G. G., Verma, S. B., & Kim, J. (1999). Surface energy fluxes of *Phragmites australis* in a prairie wetland. *Agricultural and Forest Meteorology, 94*, 31-51. doi:10.1016/S0168-1923(99)00007-6

Campbell, D. I., & Murray, D. L. (1990). Water balance of snow tussock grassland in New Zealand. *Journal of Hydrology, 118*, 229-245. doi:10.1016/0022-1694(90)90260-5

Campbell, D. I., Smith, J., Goodrich, J. P., Wall, A. M., & Schipper, L. A. (2014). Year-round growing conditions explains large CO_2 sink strength in a New Zealand raised peat bog. *Agricultural and Forest Meteorology, 192-193*, 59-68. doi:10.1016/j.agrformet.2014.03.003

Campbell, D. I., & Williamson, J. L. (1997). Evaporation from a raised peat bog. *Journal of Hydrology, 193*, 142-160. doi:10.1016/S0022-1694(96)03149-6

Campbell, E. O. (1964). The restiad peat bogs at Motumaoho and Moanatuatua. *Transactions of the Royal Society of New Zealand : Botany, 2*(16).

Carlyle-Moses, D. E., & Gash, J. H. C. (2011). Rainfall Interception Loss by Forest Canopies. In D. Levia, D. Carlyle-Moses, & T. Tanaka (Eds.), *Forest Hydrology and Biogeochemistry* (pp. 407-423). Dordrecht: Springer.

Charman, D. J. (2009). Peat and Peatlands. In G. E. Likens (Ed.), *Encyclopaedia of Inland Waters* (pp. 541-548): Academic Press.

Cisneros Vaca, C., van der Tol, C., & Ghimire, C. P. (2018). The influence of long-term changes in canopy structure on rainfall interception loss: a case study in Speulderbos, the Netherlands. *Hydrology and Earth System Sciences, 22*(7), 3701-3719. doi:10.5194/hess-22-3701-2018

Clarkson, B. R., Schipper, L. A., & Silvester, W. B. (2009). Nutritional niche separation in coexisting bog species demonstrated by ^{15}N-enriched simulated rainfall. *Austral Ecology*. doi:10.1111/j.1442-9993.2009.01939.x

Clymo, R. S., & Hayward, P. M. (1982). The Ecology of *Sphagnum*. In A. J. E. Smith (Ed.), *Bryophyte Ecology*. London: Chapman and Hall.

Coenders-Gerrits, M., Schilperoort, B., & Jiménez-Rodríguez, C. (2020). Evaporative Processes on Vegetation: An Inside Look. In I. Van Stan, J. T., E. Gutmann, & J. Friesen (Eds.), *Precipitation Partitioning by Vegetation* (pp. 35-48): Springer Cham.

Crockford, R. H., & Richardson, D. P. (2000). Partitioning of rainfall into throughfall, stemflow and interception: effect of forest type, ground cover and climate. *Hydrological Processes, 14*, 2903-2920. doi:10.1002/1099-1085(200011/12)14:16/17<2903::AID-HYP126>3.0.CO;2-6

Czikowsky, M. J., & Fitzjarrald, D. R. (2009). Detecting rainfall interception in an Amazonian rain forest with eddy flux measurements. *Journal of Hydrology, 377*(1-2), 92-105. doi:10.1016/j.jhydrol.2009.08.002

David, J. S., Valente, F., & Gash, J. H. C. (2005). Evaporation of Intercepted Rainfall. In M. G. Anderson & J. J. McDonnell (Eds.), *Encyclopedia of Hydrological Sciences*: John Wiley & Sons, Ltd.

Dohong, A., Aziz, A. A., & Dargusch, P. (2017). A review of the drivers of tropical peatland degradation in South-East Asia. *Land Use Policy, 69*, 349-360. doi:10.1016/j.landusepol.2017.09.035

Dommain, R., Couwenberg, J., & Joosten, H. (2010). Hydrological self-regulation of domed peatlands in south-east Asia and consequences for conservation and restoration. *Mires and Peat, 6*.

Duckett, J. G., Pressel, S., P'Ng K, M. Y., & Renzaglia, K. S. (2009). Exploding a myth: the capsule dehiscence mechanism and the function of pseudostomata in *Sphagnum*. *New Phytol, 183*(4), 1053-1063. doi:10.1111/j.1469-8137.2009.02905.x

Dunkerley, D. (2000). Measuring interception loss and canopy storage in dryland vegetation: a brief review and evaluation of available research strategies. *Hydrological Processes, 14*, 669-678. doi:10.1002/(SICI)1099-1085(200003)14:4<669::AID-HYP965>3.0.CO;2-I

Dymond, J. R., Ausseil, A. G., Ekanayake, J. C., & Kirschbaum, M. U. (2012). Tradeoffs between soil, water, and carbon -- a national scale analysis from New Zealand. *J Environ Manage, 95*(1), 124-131. doi:10.1016/j.jenvman.2011.09.019

Dymond, J. R., Sabetizade, M., Newsome, P. F., Harmsworth, G. R., & Ausseil, A. (2021). Revised extent of wetlands in New Zealand. *New Zealand Journal of Ecology, 45*(2), 1-8. doi:10.20423/nzjecol.45.32

Eichelmann, E., Hemes, K. S., Knox, S. H., Oikawa, P. Y., Chamberlain, S. D., Sturtevant, C., . . . Baldocchi, D. D. (2018). The effect of land cover type and structure on evapotranspiration from agricultural and wetland sites in the Sacramento–San Joaquin River Delta, California. *Agricultural and Forest Meteorology, 256-257*, 179-195. doi:10.1016/j.agrformet.2018.03.007

Exler, J. L., & Moore, R. D. (2022). Quantifying throughfall, stemflow and interception loss in five vegetation communities in a maritime raised bog. *Agricultural and Forest Meteorology, 327*. doi:10.1016/j.agrformet.2022.109202

Fang, Z., Zhang, W., Brandt, M., Abdi, A. M., & Fensholt, R. (2022). Globally Increasing Atmospheric Aridity Over the 21st Century. *Earth's Future, 10*(10). doi:10.1029/2022ef003019

Fenner, N., & Freeman, C. (2011). Drought-induced carbon loss in peatlands. *Nature Geoscience, 4*(12), 895-900. doi:10.1038/ngeo1323

Ficklin, D. L., & Novick, K. A. (2017). Historic and projected changes in vapor pressure deficit suggest a continental-scale drying of the United States atmosphere. *Journal of Geophysical Research: Atmospheres, 122*(4), 2061-2079. doi:10.1002/2016jd025855

Fleischbein, K., Wilcke, W., Goller, R., Boy, J., Valarezo, C., Zech, W., & Knoblich, K. (2005). Rainfall interception in a lower montane forest in Ecuador: effects of canopy properties. *Hydrological Processes, 19*(7), 1355-1371. doi:10.1002/hyp.5562

Fraser, C. D. J., Roulet, N. T., & Lafleur, P. M. (2001). Groundwater flow patterns in a large peatland. *Journal of Hydrology, 246*, 142-154. doi:10.1016/S0022-1694(01)00362-6

Freeman, C., Ostle, N., & Kang, H. (2001). An enzymic 'latch' on a global carbon store. *Nature, 409*, 149. doi:10.1038/35051650

Frolking, S., & Roulet, N. T. (2007). Holocene radiative forcing impact of northern peatland carbon accumulation and methane emissions. *Global Change Biology, 13*(5), 1079-1088. doi:10.1111/j.1365-2486.2007.01339.x

Frolking, S., Talbot, J., Jones, M. C., Treat, C. C., Kauffman, J. B., Tuittila, E.-S., & Roulet, N. (2011). Peatlands in the Earth's 21st century climate system. *Environmental Reviews, 19*(NA), 371-396. doi:10.1139/a11-014

Gažovič, M., Forbrich, I., Jager, D. F., Kutzbach, L., Wille, C., & Wilmking, M. (2013). Hydrology-driven ecosystem respiration determines the carbon balance of a boreal peatland. *Sci Total Environ, 463-464*, 675-682. doi:10.1016/j.scitotenv.2013.06.077

Genxu, W., Guangsheng, L., & Chunjie, L. (2012). Effects of changes in alpine grassland vegetation cover on hillslope hydrological processes in a permafrost watershed. *Journal of Hydrology, 444-445*, 22-33. doi:10.1016/j.jhydrol.2012.03.033

Goodrich, J. P., Campbell, D. I., Clearwater, M. J., Rutledge, S., & Schipper, L. A. (2015). High vapor pressure deficit constrains GPP and the light response of NEE at a Southern Hemisphere bog. *Agricultural and Forest Meteorology, 203*, 54-63. doi:10.1016/j.agrformet.2015.01.001

Goodrich, J. P., Campbell, D. I., & Schipper, L. A. (2017). Southern Hemisphere bog persists as a strong carbon sink during droughts. *Biogeosciences, 14*(20), 4563-4576. doi:10.5194/bg-14-4563-2017

Goulden, M. L., Litvak, M., & Miller, S. D. (2007). Factors that control Typha marsh evapotranspiration. *Aquatic Botany, 86*(2), 97-106. doi:10.1016/j.aquabot.2006.09.005

Granger, R. J. (1989). An examination of the concept of potential evaporation. *Journal of Hydrology, 111*, 9-19. doi:10.1016/0022-1694(89)90248-5

Guevara-Escobar, A., González-Sosa, E., Véliz-Chávez, C., Ventura-Ramos, E., & Ramos-Salinas, M. (2007). Rainfall interception and distribution patterns of gross precipitation around an isolated *Ficus benjamina* tree in an urban area. *Journal of Hydrology, 333*(2-4), 532-541. doi:10.1016/j.jhydrol.2006.09.017

Harris, L. I., Richardson, K., Bona, K. A., Davidson, S. J., Finkelstein, S. A., Garneau, M., . . . Ray, J. C. (2021). The essential carbon service provided by northern peatlands. *Frontiers in Ecology and the Environment, 20*(4), 222-230. doi:10.1002/fee.2437

He, H., Moore, T., Humphreys, E. R., Lafleur, P. M., & Roulet, N. T. (2023). Water level variation at a beaver pond significantly impacts net CO_2 uptake of a continental bog. *Hydrology and Earth System Sciences, 27*(1), 213-227. doi:10.5194/hess-27-213-2023

Helbig, M., Waddington, J. M., Alekseychik, P., Amiro, B. D., Aurela, M., Barr, A. G., . . . Zyrianov, V. (2020). Increasing contribution of peatlands to boreal evapotranspiration in a warming climate. *Nature Climate Change, 10*(6), 555-560. doi:10.1038/s41558-020-0763-7

Helfter, C., Campbell, C., Dinsmore, K. J., Drewer, J., Coyle, M., Anderson, M., . . . Sutton, M. A. (2015). Drivers of long-term variability in CO_2 net ecosystem exchange in a temperate peatland. *Biogeosciences, 12*(6), 1799-1811. doi:10.5194/bg-12-1799-2015

Hember, R. A., Lafleur, P. M., & Cogley, J. G. (2005). Synoptic controls on summer evapotranspiration from a bog peatland in southern Canada. *International Journal of Climatology, 25*(6), 793-809. doi:10.1002/joc.1154

Herbst, M., Rosier, P. T. W., McNeil, D. D., Harding, R. J., & Gowing, D. J. (2008). Seasonal variability of interception evaporation from the canopy of a mixed deciduous forest. *Agricultural and Forest Meteorology, 148*(11), 1655-1667. doi:10.1016/j.agrformet.2008.05.011

Hodges, T. A., & Rapson, G. L. (2010). Is *Empodisma minus* the ecosystem engineer of the FBT (fen–bog transition zone) in New Zealand? *Journal of the Royal Society of New Zealand, 40*(3-4), 181-207. doi:10.1080/03036758.2010.503564

Holden, J. (2005). Peatland hydrology and carbon release: why small-scale process matters. *Philosophical Transactions of the Royal Society A: Mathematical Physical and Engineering Sciences, 363*(1837), 2891-2913. doi:10.1098/rsta.2005.1671

Humphreys, E. R., Lafleur, P. M., Flanagan, L. B., Hedstrom, N., Syed, K. H., Glenn, A. J., & Granger, R. (2006). Summer carbon dioxide and water vapor fluxes across a range of northern peatlands. *Journal of Geophysical Research: Biogeosciences, 111*(G4). doi:10.1029/2005jg000111

Jeanguenin, L., Mir, A. P., & Chaumont, F. (2017). Uptake, Loss and Control. In *Encyclopedia of Applied Plant Sciences* (pp. 135-140).

Joosten, H., & Clarke, D. (2002). *Wise use of mires and peatlands*. Retrieved from Totnes: https://citeseerx.ist.psu.edu/document?repid=rep1&type=pdf&doi=3fa5336900382d4bf46805bcaadc7a07741af3f6

Kelliher, F. M., Whitehead, D., & Pollock, D. S. (1992). Rainfall interception by trees and slash in *Pinus radiata* D. Don stand. *Journal of Hydrology, 131*, 187-204. doi:10.1016/0022-1694(92)90217-J

Keyte Beattie, A. M. (2014). *The role of Empodisma robustum litter in CO_2 exchange at Kopuatai bog.* (M.S.). University of Waikato, Hamilton, New Zealand. Retrieved from https://hdl.handle.net/10289/8695

Kim, J., Rochefort, L., Hogue-Hugron, S., Alqulaiti, Z., Dunn, C., Pouliot, R., . . . Kang, H. (2021). Water Table Fluctuation in Peatlands Facilitates Fungal Proliferation, Impedes *Sphagnum* Growth and Accelerates Decomposition. *Frontiers in Earth Science, 8*. doi:10.3389/feart.2020.579329

Kim, J., & Verma, S. B. (1996). Surface exchange of water vapour between an open *Sphagnum* fen and the atmosphere. *Boundary-Layer Meteorology, 79*, 243–264. doi:10.1007/BF00119440

Klaassen, W. (2001). Evaporation From rain-wetted forest in relation to canopy wetness, canopy cover, and net radiation. *Water Resources Research, 37*(12), 3227-3236. doi:10.1029/2001wr000480

Komatsu, H., Shinohara, Y., Kume, T., & Otsuki, K. (2008). Relationship between annual rainfall and interception ratio for forests across Japan. *Forest Ecology and Management, 256*(5), 1189-1197. doi:10.1016/j.foreco.2008.06.036

Kuder, T., Kruge, M. A., Shearer, J. C., & Miller, S. L. (1998). Environmental and botanical controls on peatification—a comparative study of two New Zealand restiad bogs using Py-GCrMS, petrography and fungal analysis. *International Journal of Coal Geology, 37*, 3–27. doi:10.1016/S0166-5162(98)00022-6

Kurbatova, J., Arneth, A., Vygodskaya, N. N., Kolle, O., Varlargin, A. V., Milyukova, I. M., . . . Lloyd, J. (2002). Comparative ecosystem–atmosphere exchange of energy and mass in a European Russian and a central Siberian bog I. Interseasonal and interannual variability of energy and latent heat fluxes during the snowfree period. *Tellus Series B: Chemical and Physical Meteorology, 54*(5). doi:10.3402/tellusb.v54i5.16683

Kwon, M. J., Ballantyne, A., Ciais, P., Qiu, C., Salmon, E., Raoult, N., . . . Zona, D. (2022). Lowering water table reduces carbon sink strength and carbon stocks in northern peatlands. *Global Change Biology, 28*(22), 6752-6770. doi:10.1111/gcb.16394

Lafleur, P. M. (2008). Connecting Atmosphere and Wetland: Energy and Water Vapour Exchange. *Geography Compass, 2*(4), 1027–1057. doi:10.1111/j.1749-8198.2007.00132.x

Lafleur, P. M. (2009). Connecting Atmosphere and Wetland: Trace Gas Exchange. *Geography Compass, 3*(2), 560–585. doi:10.1111/j.1749-8198.2008.00212.x

Lafleur, P. M., Hember, R. A., Admiral, S. W., & Roulet, N. T. (2005). Annual and seasonal variability in evapotranspiration and water table at a shrub-covered bog in southern Ontario, Canada. *Hydrological Processes, 19*(18), 3533-3550. doi:10.1002/hyp.5842

Lafleur, P. M., & Roulet, N. T. (1992). A comparison of evaporation rates from two fens of the Hudson Bay Lowland. *Aquatic Botany, 44*, 59-69. doi:10.1016/0304-3770(92)90081-S

Lafleur, P. M., Roulet, N. T., & Admiral, S. W. (2001). Annual cycle of CO_2 exchange at a bog peatland. *Journal of Geophysical Research: Atmospheres, 106*(D3), 3071-3081. doi:10.1029/2000jd900588

Lawrence, J., Mackey, B., Chiew, F., Costello, M. J., Hennessy, K., Lansbury, N., . . . A.Wreford. (2022). Contribution of Working Group II to the Sixth Assessment Report of the Intergovernmental Panel on Climate Change. In H.-O. Pörtner, D. C. Roberts, M. Tignor, E. S. Poloczanska, K. Mintenbeck, A. Alegría, M. Craig, S. Langsdorf, S. Löschke, V. Möller, A. Okem, & B. Rama (Eds.), *Climate Change 2022: Impacts, Adaptation and Vulnerability*. Cambridge, UK and New York, NY, USA: Cambridge University Press.

Leuning, R., van Gorsel, E., Massman, W. J., & Isaac, P. R. (2012). Reflections on the surface energy imbalance problem. *Agricultural and Forest Meteorology, 156*, 65-74. doi:10.1016/j.agrformet.2011.12.002

Li, Y., Cai, T., Man, X., Sheng, H., & Ju, C. (2015). Canopy interception loss in a *Pinus sylvestris* var. mongolica forest of Northeast China. *Journal of Arid Land, 7*(6), 831-840. doi:10.1007/s40333-015-0013-4

Lian, X., Zhao, W., & Gentine, P. (2022). Recent global decline in rainfall interception loss due to altered rainfall regimes. *Nat Commun, 13*(1), 7642. doi:10.1038/s41467-022-35414-y

Liljedahl, A. K., Hinzman, L. D., Harazono, Y., Zona, D., Tweedie, C. E., Hollister, R. D., . . . Oechel, W. C. (2011). Nonlinear controls on evapotranspiration in arctic coastal wetlands. *Biogeosciences, 8*(11), 3375-3389. doi:10.5194/bg-8-3375-2011

Lindsay, R. (2018). Peatland Classification. In *The Wetland Book* (pp. 1515-1528).

Llorens, P., & Domingo, F. (2007). Rainfall partitioning by vegetation under Mediterranean conditions. A review of studies in Europe. *Journal of Hydrology, 335*(1-2), 37-54. doi:10.1016/j.jhydrol.2006.10.032

Lund, M., Christensen, T. R., Lindroth, A., & Schubert, P. (2012). Effects of drought conditions on the carbon dioxide dynamics in a temperate peatland. *Environmental Research Letters, 7*(4). doi:10.1088/1748-9326/7/4/045704

Ma, C., Luo, Y., Shao, M., & Jia, X. (2022a). Estimation and testing of linkages between forest structure and rainfall interception characteristics of a *Robinia pseudoacacia* plantation on China's Loess Plateau. *Journal of Forestry Research, 33*(2), 529-542. doi:10.1007/s11676-021-01324-w

Ma, L., Zhu, G., Chen, B., Zhang, K., Niu, S., Wang, J., . . . Zuo, H. (2022b). A globally robust relationship between water table decline, subsidence rate, and carbon release from peatlands. *Communications Earth & Environment, 3*(1). doi:10.1038/s43247-022-00590-8

Magliano, P. N., Whitworth-Hulse, J. I., & Baldi, G. (2019a). Interception, throughfall and stemflow partition in drylands: Global synthesis and meta-analysis. *Journal of Hydrology, 568*, 638-645. doi:10.1016/j.jhydrol.2018.10.042

Magliano, P. N., Whitworth-Hulse, J. I., Florio, E. L., Aguirre, E. C., & Blanco, L. J. (2019b). Interception loss, throughfall and stemflow by *Larrea divaricata*: The role of rainfall characteristics and plant morphological attributes. *Ecological Research, 34*(6), 753-764. doi:10.1111/1440-1703.12036

Marin, C. T., Bouten, W., & Sevink, J. (2000). Gross rainfall and its partitioning into throughfall, stemflow and evaporation of intercepted water in four forest ecosystems in western Amazonia. *Journal of Hydrology, 237*, 40–57. doi:10.1016/S0022-1694(00)00301-2

Massmann, A., Gentine, P., & Lin, C. (2019). When Does Vapor Pressure Deficit Drive or Reduce Evapotranspiration? *Journal of Advances in Modeling Earth Systems, 11*(10), 3305-3320. doi:10.1029/2019MS001790

McCarter, C. P. R., & Price, J. S. (2014). Ecohydrology of *Sphagnum* moss hummocks: mechanisms of capitula water supply and simulated effects of evaporation. *Ecohydrology, 7*(1), 33-44. doi:10.1002/eco.1313

McGlone, M. S. (2009). Postglacial history of New Zealand wetlands and implications for their conservation. *New Zealand Journal of Ecology, 33*(1), 1-23.

Miralles, D. G., Brutsaert, W., Dolman, A. J., & Gash, J. H. (2020). On the Use of the Term "Evapotranspiration". *Water Resources Research, 56*(11), e2020WR028055. doi:10.1029/2020WR028055

Miralles, D. G., De Jeu, R. A. M., Gash, J. H., Holmes, T. R. H., & Dolman, A. J. (2011). Magnitude and variability of land evaporation and its components at the global scale. *Hydrology and Earth System Sciences, 15*(3), 967-981. doi:10.5194/hess-15-967-2011

Mizutani, K., Yamanoi, K., Ikeda, T., & Watanabe, T. (1997). Applicability of the eddy correlation method to meas,ure sensible heat transfer to forest under rainfall conditions. *Agricultural and Forest Meteorology, 86*, 193-203. doi:10.1016/S0168-1923(97)00012-9

Moore, T. R., Bubier, J. L., Frolking, S. E., Lafleur, P. M., & Roulet, N. T. (2002). Plant biomass and production and CO_2 exchange in an ombrotrophic bog. *Journal of Ecology, 90*(1), 25-36. doi:10.1046/j.0022-0477.2001.00633.x

New, M., Todd, M., Hulme, M., & Jones, P. (2001). Precipitation measurements and trends in the twentieth century. *International Journal of Climatology, 21*(15), 1889-1922. doi:10.1002/joc.680

Newnham, R. N., de Lange, P. J., & Lowe, D. J. (1995). Holocene vegetation, climate and history of a raised bog complex, northern New Zealand based on palynology, plant macrofossils and tephrochronology. *The Holocene, 5*(3), 267-282.

Nimmo, D. G., Mac Nally, R., Cunningham, S. C., Haslem, A., & Bennett, A. F. (2015). Vive la resistance: reviving resistance for 21st century conservation. *Trends Ecol Evol, 30*(9), 516-523. doi:10.1016/j.tree.2015.07.008

Novick, K. A., Ficklin, D. L., Stoy, P. C., Williams, C. A., Bohrer, G., Oishi, A. C., . . . Phillips, R. P. (2016). The increasing importance of atmospheric demand for ecosystem water and carbon fluxes. *Nature Climate Change, 6*(11), 1023-1027. doi:10.1038/nclimate3114

Ochoa-Sánchez, A., Crespo, P., & Célleri, R. (2018). Quantification of rainfall interception in the high Andean tussock grasslands. *Ecohydrology, 11*(3). doi:10.1002/eco.1946

Oke, T. R. (1987). *Boundary Layer Climates* (2nd ed.). London: Methuen Co.

Page, S. E., & Baird, A. J. (2016). Peatlands and Global Change: Response and Resilience. *Annual Review of Environment and Resources, 41*(1), 35-57. doi:10.1146/annurev-environ-110615-085520

Page, S. E., Rieley, J. O., & Wüst, R. (2006). Lowland tropical peatlands of Southeast Asia. In *Peatlands - Evolution and Records of Environmental and Climate Changes* (pp. 145-172).

Parmentier, F. J. W., van der Molen, M. K., de Jeu, R. A. M., Hendriks, D. M. D., & Dolman, A. J. (2009). CO_2 fluxes and evaporation on a peatland in the Netherlands appear not affected by water table fluctuations. *Agricultural and Forest Meteorology, 149*(6-7), 1201-1208. doi:10.1016/j.agrformet.2008.11.007

Peichl, M., Sagerfors, J., Lindroth, A., Buffam, I., Grelle, A., Klemedtsson, L., . . . Nilsson, M. B. (2013). Energy exchange and water budget partitioning in a boreal minerogenic mire. *Journal of Geophysical Research: Biogeosciences, 118*(1), 1-13. doi:10.1029/2012jg002073

Price, J. S. (1991). Evaporation from a blanket bog in a foggy coastal environment. *Boundary-Layer Meteorology, 57*, 391-406. doi:10.1007/BF00120056

Ratcliffe, J. L., Campbell, D. I., Clarkson, B. R., Wall, A. M., & Schipper, L. A. (2019). Water table fluctuations control CO_2 exchange in wet and dry bogs through different mechanisms. *Sci Total Environ, 655*, 1037-1046. doi:10.1016/j.scitotenv.2018.11.151

Roehm, C. L., & Roulet, N. T. (2003). Seasonal contribution of CO_2 fluxes in the annual C budget of a northern bog. *Global Biogeochemical Cycles, 17*(1). doi:10.1029/2002gb001889

Roulet, N. T., Lafleur, P. M., Richard, P. J. H., Moore, T. R., Humphreys, E. R., & Bubier, J. (2007). Contemporary carbon balance and late Holocene carbon accumulation in a northern peatland. *Global Change Biology, 13*(2), 397-411. doi:10.1111/j.1365-2486.2006.01292.x

Runkle, B. R. K., Wille, C., Gažovič, M., Wilmking, M., & Kutzbach, L. (2014). The surface energy balance and its drivers in a boreal peatland fen of northwestern Russia. *Journal of Hydrology, 511*, 359-373. doi:10.1016/j.jhydrol.2014.01.056

Rutter, A. J., Kershaw, K. A., Robins, P. C., & Morton, A. J. (1971). A predictive model of rainfall interception in forests, 1. Derivation of the model from observations in a plantation of Corsican pine. *Agricultural Meteorology, 9*, 367-384. doi:10.1016/0002-1571(71)90034-3

Rutter, A. J., Morton, A. J., & Robins, P. C. (1975). A Predictive Model of Rainfall Interception in Forests. II. Generalization of the Model and Comparison with Observations in Some Coniferous and Hardwood Stands. *Journal of Applied Ecology, 12*(1), 367-380. doi:10.2307/2401739

Rydin, H., Gunnarsson, U., & Sundberg, S. (2006). The Role of *Sphagnum* in Peatland Development and Persistence. In R. K. Wieder & D. H. Vitt (Eds.), *Boreal Peatland Ecosystems* (Vol. 188). Berlin: Springer-Verlag.

Rydin, H., & Jeglum, J. K. (2013a). Diversity of life in peatlands. In *The Biology of Peatlands* (2 ed., pp. 21-47). Oxford: Oxford University Press.

Rydin, H., & Jeglum, J. K. (2013b). Peatland hydrology. In *The Biology of Peatlands* (2 ed., pp. 148-174). Oxford: Oxford University Press.

Scharlemann, J. P. W., Tanner, E. V. J., Hiederer, R., & Kapos, V. (2014). Global soil carbon: understanding and managing the largest terrestrial carbon pool. *Carbon Management, 5*(1), 81-91. doi:10.4155/cmt.13.77

Serrato, F. B., & Diaz, A. R. (1998). A simple technique for measuring rainfall interception by small shrub: "interception flow collection box". *Hydrological Processes, 12*, 471-481. doi:10.1002/(SICI)1099-1085(19980315)12:3<471::AID-HYP586>3.0.CO;2-E

Shearer, J. C. (1997). Natural and anthropogenic influences on peat development in Waikato/Hauraki Plains restiad bogs. *Journal of the Royal Society of New Zealand, 27*(3), 295-313. doi:10.1080/03014223.1997.9517540

Shimoyama, K. (2003). Seasonal and interannual variation in water vapor and heat fluxes in a West Siberian continental bog. *Journal of Geophysical Research, 108*(D20). doi:10.1029/2003jd003485

Shimoyama, K. (2004). Controls on evapotranspiration in a west Siberian bog. *Journal of Geophysical Research, 109*(D8). doi:10.1029/2003jd004114

Shuttleworth, W. J. (1976). Experimental evidence for the failure of the Penman-Monteith equation in partially wet conditions. *Boundary-Layer Meteorology, 10*, 91-94. doi:10.1007/BF00218726

Smith, J. (2003). *Fluxes of Carbon Dioxide and Water Vapour at a Waikato Peat Bog.* (PhD). The University of Waikato, Hamilton, New Zealand. Retrieved from https://hdl.handle.net/10289/13975

Sonnentag, O., Van Der Kamp, G., Barr, A. G., & Chen, J. M. (2010). On the relationship between water table depth and water vapor and carbon dioxide fluxes in a minerotrophic fen. *Global Change Biology, 16*(6), 1762-1776. doi:10.1111/j.1365-2486.2009.02032.x

Staelens, J., De Schrijver, A., Verheyen, K., & Verhoest, N. E. C. (2008). Rainfall partitioning into throughfall, stemflow, and interception within a single beech (*Fagus sylvatica* L.) canopy:

influence of foliation, rain event characteristics, and meteorology. *Hydrological Processes, 22*(1), 33-45. doi:10.1002/hyp.6610

Strack, M., & Price, J. S. (2009). Moisture controls on carbon dioxide dynamics of peat-*Sphagnum* monoliths. *Ecohydrology, 2*(1), 34-41. doi:10.1002/eco.36

Strack, M., Waddington, J. M., Lucchese, M. C., & Cagampan, J. P. (2009). Moisture controls on CO_2 exchange in a *Sphagnum*-dominated peatland: results from an extreme drought field experiment. *Ecohydrology, 2*(4), 454-461. doi:10.1002/eco.68

Strilesky, S. L., & Humphreys, E. R. (2012). A comparison of the net ecosystem exchange of carbon dioxide and evapotranspiration for treed and open portions of a temperate peatland. *Agricultural and Forest Meteorology, 153*, 45-53. doi:10.1016/j.agrformet.2011.06.006

Su, L., Zhao, C., Xu, W., & Xie, Z. (2016). Modelling interception loss using the revised Gash model: a case study in a mixed evergreen and deciduous broadleaved forest in China. *Ecohydrology, 9*(8), 1580-1589. doi:10.1002/eco.1749

Takagi, K., Tsuboya, T., Takahashi, H., & Inoue, T. (1999). Effect of the invasion of vascular plants on heat and water balance in the Sarobetsu mire, northern Japan. *Wetlands, 19*, 246-254. doi:10.1007/BF03161754

Temmink, R. J. M., Lamers, L. P. M., Angelini, C., Bouma, T. J., Fritz, C., van de Koppel, J., . . . van der Heide, T. (2022). Recovering wetland biogeomorphic feedbacks to restore the world's biotic carbon hotspots. *Science, 376*(6593), eabn1479. doi:10.1126/science.abn1479

Thompson, M. A., Campbell, D. I., & Spronken-Smith, R. A. (1999). Evaporation from natural and modified raised peat bogs in New Zealand. *Agricultural and Forest Meteorology, 95*, 85-98. doi:10.1016/S0168-1923(99)00027-1

Toba, T., & Ohta, T. (2005). An observational study of the factors that influence interception loss in boreal and temperate forests. *Journal of Hydrology, 313*(3-4), 208-220. doi:10.1016/j.jhydrol.2005.03.003

Toba, T., & Ohta, T. (2008). Factors affecting rainfall interception determined by a forest simulator and numerical model. *Hydrological Processes, 22*(14), 2634-2643. doi:10.1002/hyp.6859

Tong, B., Guo, J., Xu, H., Wang, Y., Li, H., Bian, L., . . . Zhou, S. (2022). Effects of soil moisture, net radiation, and atmospheric vapor pressure deficit on surface evaporation fraction at a semi-arid grass site. *Sci Total Environ, 849*, 157890. doi:10.1016/j.scitotenv.2022.157890

Valente, F., David, J. S., & Gash, J. H. C. (1997). Modelling interception loss for two sparse eucalypt and pine forests in central Portugal using reformulated Rutter and Gash analytical models. *190*, 141-162. doi:10.1016/S0022-1694(96)03066-1

van Dijk, A. I. J. M., Gash, J. H., van Gorsel, E., Blanken, P. D., Cescatti, A., Emmel, C., . . . Wohlfahrt, G. (2015). Rainfall interception and the coupled surface water and energy balance. *Agricultural and Forest Meteorology, 214-215*, 402-415. doi:10.1016/j.agrformet.2015.09.006

Villegas, J. C., Breshears, D. D., Zou, C. B., & Law, D. J. (2010). Ecohydrological controls of soil evaporation in deciduous drylands: How the hierarchical effects of litter, patch and vegetation mosaic cover interact with phenology and season. *Journal of Arid Environments, 74*(5), 595-602. doi:10.1016/j.jaridenv.2009.09.028

Vitt, D. H. (2006). Functional Characteristics and Indicators of Boreal Peatlands. In R. K. Wieder & D. H. Vitt (Eds.), *Boreal Peatland Ecosystems*. Berlin: Springer-Verlag.

Waddington, J. M., Morris, P. J., Kettridge, N., Granath, G., Thompson, D. K., & Moore, P. A. (2015). Hydrological feedbacks in northern peatlands. *Ecohydrology, 8*(1), 113-127. doi:10.1002/eco.1493

Wagstaff, S. J., & Clarkson, B. R. (2012). Systematics and ecology of the Australasian genus *Empodisma* (Restionaceae) and description of a new species from peatlands in northern New Zealand. *PhytoKeys*(13), 39-79. doi:10.3897/phytokeys.13.3259

Wang, M., Wu, J., & Lafleur, P. (2020). Comparison of energy fluxes between an undisturbed bog and an adjacent abandoned peatland pasture. *Agricultural and Forest Meteorology, 291*. doi:10.1016/j.agrformet.2020.108086

Williams, T. G., & Flanagan, L. B. (1996). Effect of changes in water content on photosynthesis, transpiration and discrimination against $^{13}CO_2$ and $C^{18}O^{16}O$ in *Pleurozium* and *Sphagnum*. *Oecologia, 108*, 38-46. doi:10.1007/BF00333212

Wilson, C. R. (2020). *The influence of fire on vegetation dynamics of a New Zealand restiad bog.* (MSc). The University of Waikato, Hamilton, New Zealand. Retrieved from https://hdl.handle.net/10289/13808

Woods, R., & Rowe, L. (1996). The changing spatial variability of subsurface flow across a hillside. *Journal of Hydrology, 35*(1), 49-84.

Wu, J., Kutzbach, L., Jager, D., Wille, C., & Wilmking, M. (2010). Evapotranspiration dynamics in a boreal peatland and its impact on the water and energy balance. *Journal of Geophysical Research, 115*(G4). doi:10.1029/2009jg001075

Xu, J., Morris, P. J., Liu, J., & Holden, J. (2018). PEATMAP: Refining estimates of global peatland distribution based on a meta-analysis. *Catena, 160*, 134-140. doi:10.1016/j.catena.2017.09.010

Yimam, Y. T., Ochsner, T. E., & Kakani, V. G. (2015). Evapotranspiration partitioning and water use efficiency of switchgrass and biomass sorghum managed for biofuel. *Agricultural Water Management, 155*, 40-47. doi:10.1016/j.agwat.2015.03.018

Yu, Z., Loisel, J., Brosseau, D. P., Beilman, D. W., & Hunt, S. J. (2010). Global peatland dynamics since the Last Glacial Maximum. *Geophysical Research Letters, 37*(13), n/a-n/a. doi:10.1029/2010gl043584

Zhang, Y.-f., Wang, X.-p., Hu, R., Pan, Y.-x., & Paradeloc, M. (2015). Rainfall partitioning into throughfall, stemflow and interception loss by two xerophytic shrubs within a rain-fed re-vegetated desert ecosystem, northwestern China. *Journal of Hydrology, 527*, 1084-1095. doi:10.1016/j.jhydrol.2015.05.060

Zhong, Y., Jiang, M., & Middleton, B. A. (2020). Effects of water level alteration on carbon cycling in peatlands. *Ecosystem Health and Sustainability, 6*(1). doi:10.1080/20964129.2020.1806113

Zou, C. B., Caterina, G. L., Will, R. E., Stebler, E., & Turton, D. (2015). Canopy Interception for a Tallgrass Prairie under Juniper Encroachment. *PLoS One, 10*(11), e0141422. doi:10.1371/journal.pone.0141422

Appendices

Appendix A

Table A1. Methods and instruments used for data collection at Kopuatai and Mer Bleue.

Variable	Kopuatai	Mer Bleue
Latent heat flux (*LE*)	4.25 m CSAT3 & CSAT3B (CSI); LI-7500 (LI-COR)	3.0 m 1012R3 & R3-50 (Gill); LI-6262 & LI7000 (LI-COR)
Sensible heat flux (*H*)	4.25 m CSAT3 & CSAT3B (CSI)	1012R3 & R3-50 (Gill)
Soil (peat) heat flux (*G*)	HFP01 (Hukseflux); TCAV (CSI)	N/A
Net radiation flux density (R_n)	2 m NR01 (Hukseflux)	CNR1 (Kipp & Zonen)
Air temperature (T_{air}) and vapour pressure deficit (VPD)	4.2 m HMP155 (Vaisala)	2 m HMP various models (Vaisala)
Precipitation (*P*)	0.6 m TB03 (Hydrological Services)	0.3 m TM525 tipping bucket gauge (Texas Instruments) Winter snowfall from Environment Canada weather station at Ottawa Airport
Water table depth (WTD)	Dipwell, WL1000 (Hydrological Services)	Float & potentiometer, and OTT PLS

Appendix B

Antecedent Precipitation Index (API)

The antecedent precipitation index (API) is an exponential function used to predict the duration of canopy wetness after a rainfall event, with inputs of rainfall depth and time since rainfall (Keyte Beattie, 2014). Initially conceived by Woods & Rowe (1996) for predicting catchment moisture conditions prior to a rain event, the API function was then modified by Smith (2003) to estimate canopy wetness state:

$$API = \sum_{i=1}^{j} \frac{P_i}{1.104 \times 1.024^i} \quad \text{(B1)}$$

where P_i is precipitation (mm) measured during the i^{th} half-hour period before the current half hour, and j is the moving window size in half hours (48 in this study). An example of modelled canopy drying using the API function is shown in Figure B1. An API value of 0.2 units or less approximately represents a dry canopy, meaning that E is predominantly sourced from peat surface E and transpiration. When the API value is greater than or equal to 1, the vegetation canopy is deemed wet and interception loss is the dominant source of E.

Predictions of canopy wetness using the API have been shown to correspond reasonably well with leaf wetness sensor measurements at Kopuatai, using an API period of 18 hours for the upper canopy, 36 hours for the standing litter layer, and 60 hours for the lower canopy (Keyte Beattie, 2014). In this study, we defined wet canopy periods as times when the upper canopy was saturated, i.e., when interception loss likely made up the majority of E, so an 18-hour period would likely be appropriate for this study. However, in order to obtain a conservative identification of periods with a dry upper canopy, i.e., for greater certainty that the canopy is dry when API ≤ 0.2, a slightly longer period of 24 hours was used. While this approach has only been tested in the field at Kopuatai, for consistency we used the same function for separating wet and dry canopy measurements at Mer Bleue. Given the relatively sparse shrub canopy and absence of standing litter at Mer Bleue, API should provide conservative estimates

of canopy dryness. The use of MoD data in this study is beneficial as it would have reduced the impact of early morning wetting from dew, therefore reducing the number of instances where API predicted canopy wetness incorrectly.

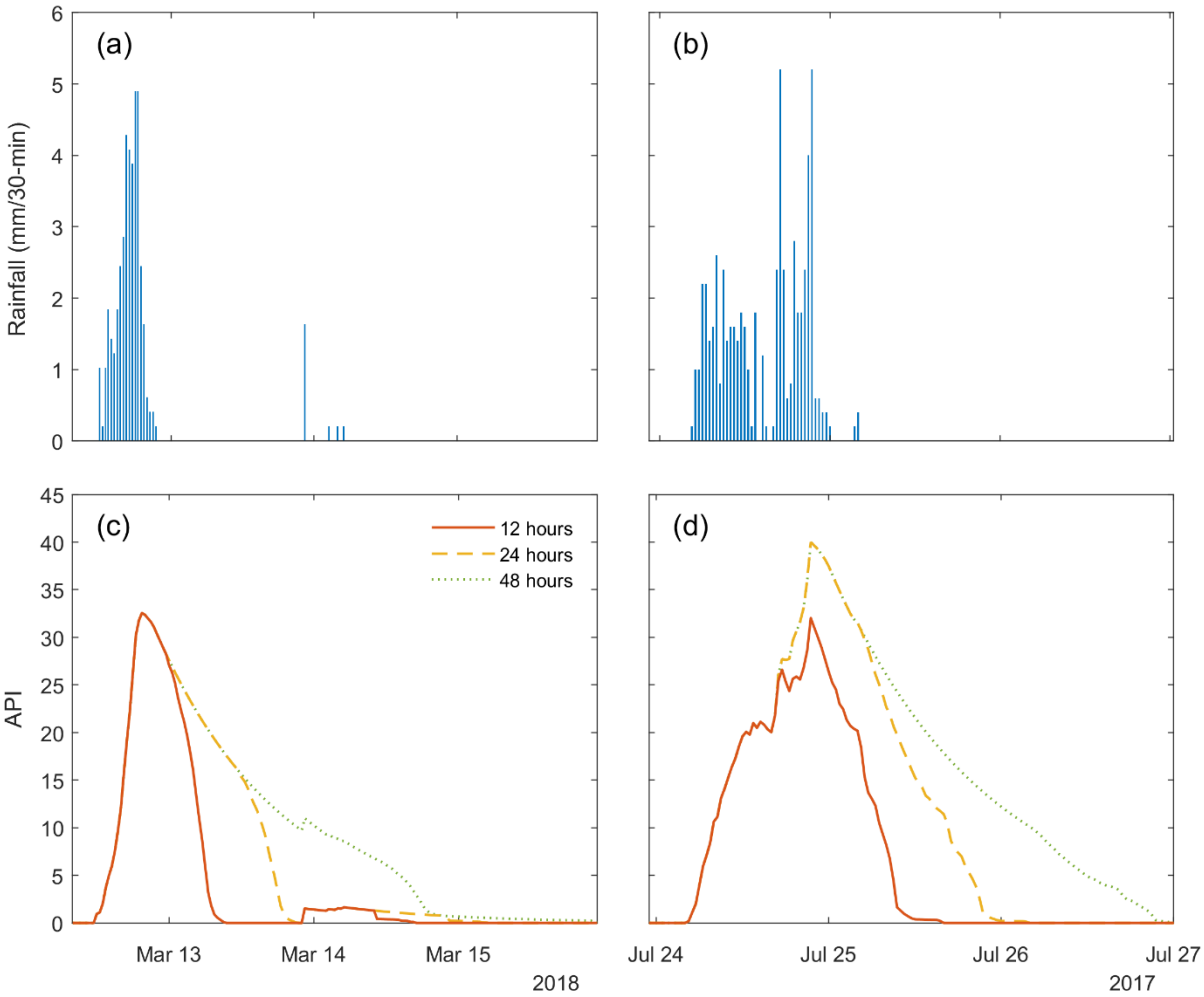

Figure B1. Examples of predicted canopy drying after rainfall using the antecedent precipitation index (API) with 24, 48, and 96 half hour time parameters. The rain event in (a) and (c) is from the Kopuatai dataset, while (b) and (d) consist of Mer Bleue data.

Appendix C

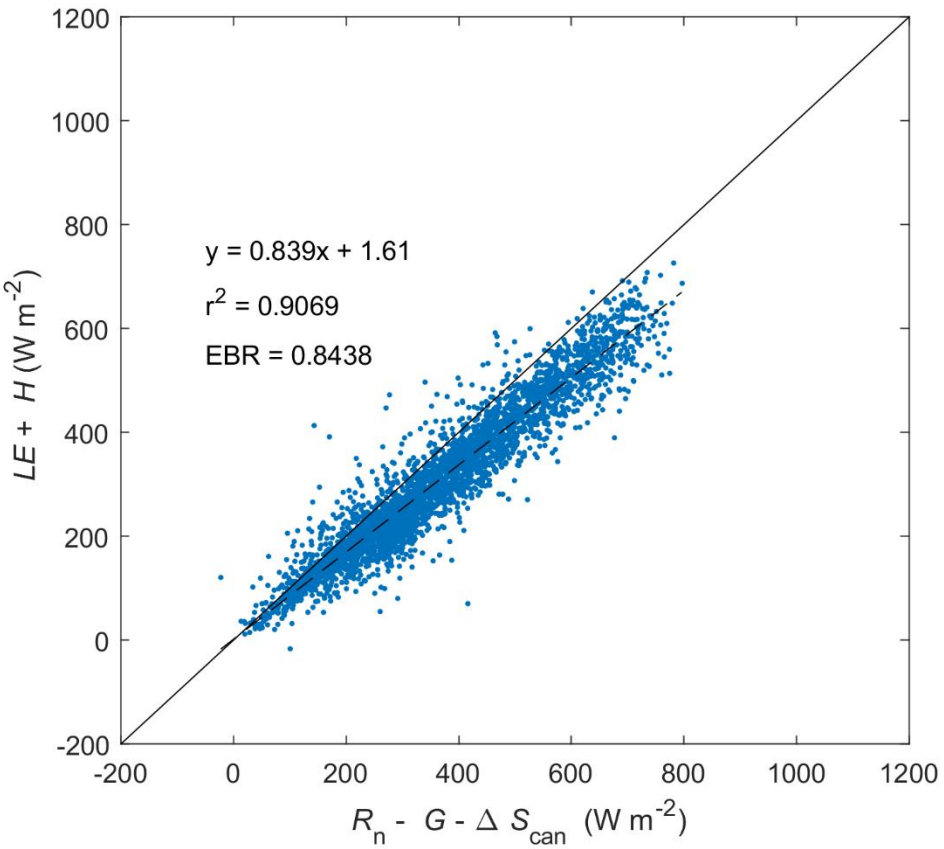

Figure C1. Energy balance closure at Kopuatai for 2012–2022 (inclusive), based on daily middle-of-day means of energy balance components. *LE*: latent heat flux; *H*: sensible heat flux; *G*: soil heat flux; R_n: net radiation; ΔS_{can}: canopy heat storage change. EBR is the energy balance ratio.

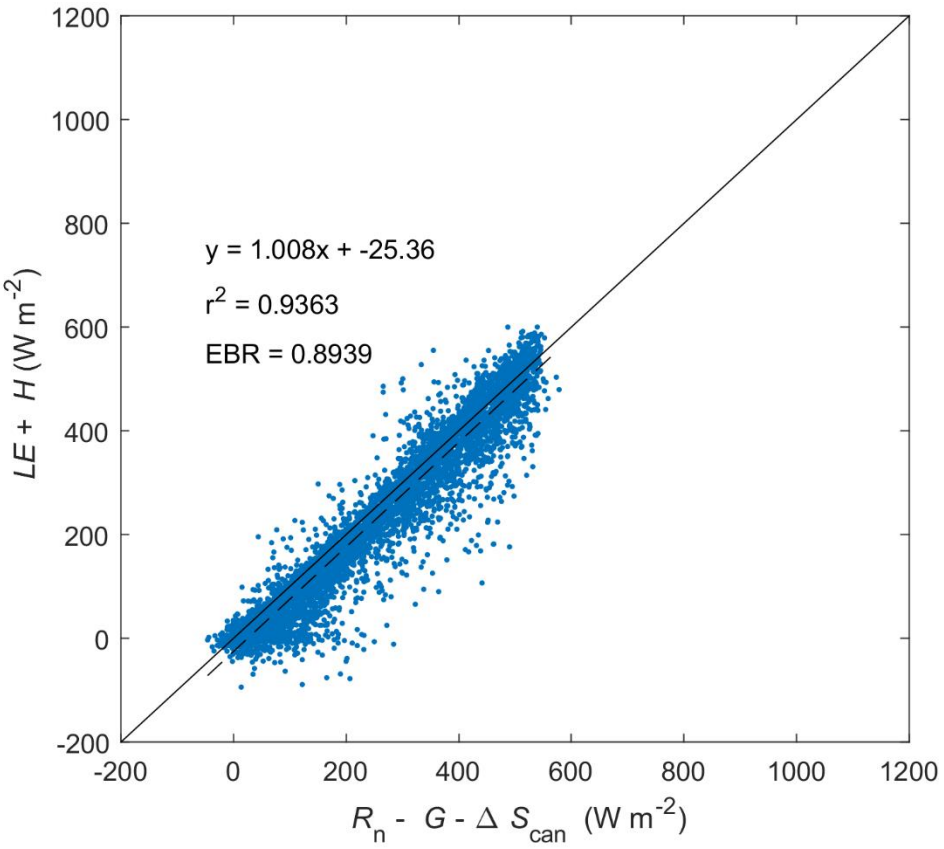

Figure C2. Energy balance closure at Mer Bleue for 1999–2018 (inclusive), based on daily middle-of-day means of energy balance components. For term definitions, see Figure C1. *G* is assumed to be 10% of R_n, while ΔS_{can} is assumed to be 3% of R_n.

Appendix D

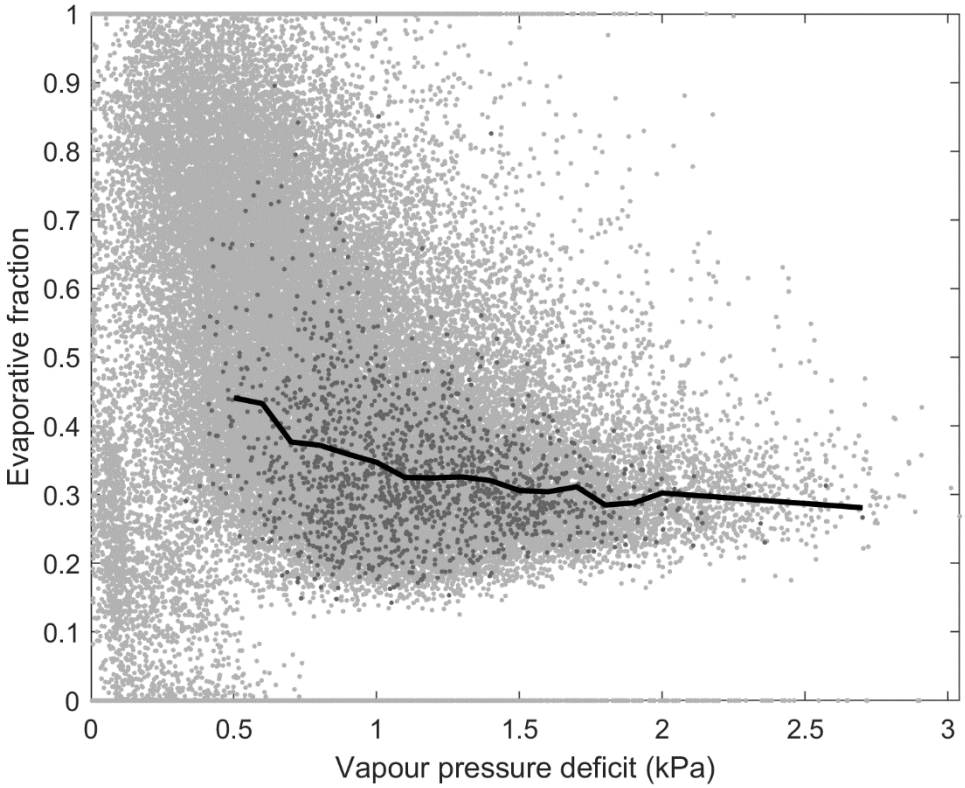

Figure D1. Relationship between evaporative fraction (EF) and vapour pressure deficit (VPD) at Kopuatai bog. Light grey data points represent raw, unfiltered 30-minute eddy covariance data, while dark grey data points show growing season (Sep–May), dry canopy, middle-of-day mean data used to calculate the binned means (black line).

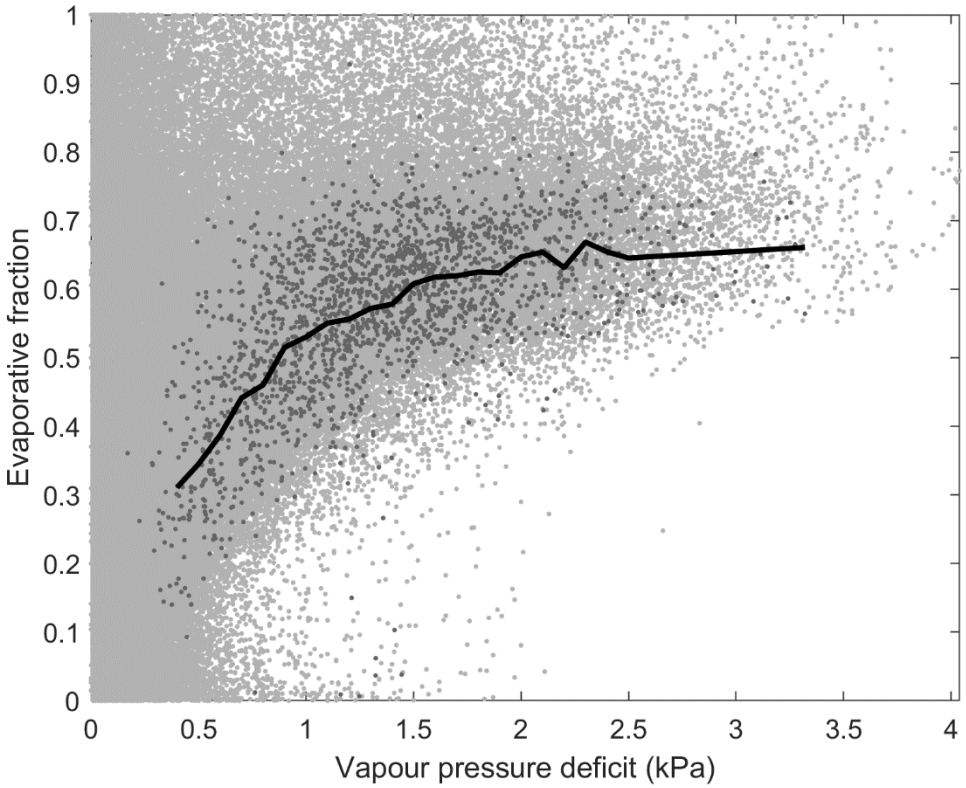

Figure D2. Relationship between evaporative fraction (EF) and vapour pressure deficit (VPD) at Mer Bleue bog. Light grey data points represent raw, unfiltered 30-minute eddy covariance data, while dark grey data points show growing season (May–Oct), dry canopy, middle-of-day mean data used to calculate the binned means (black line).

Appendix E

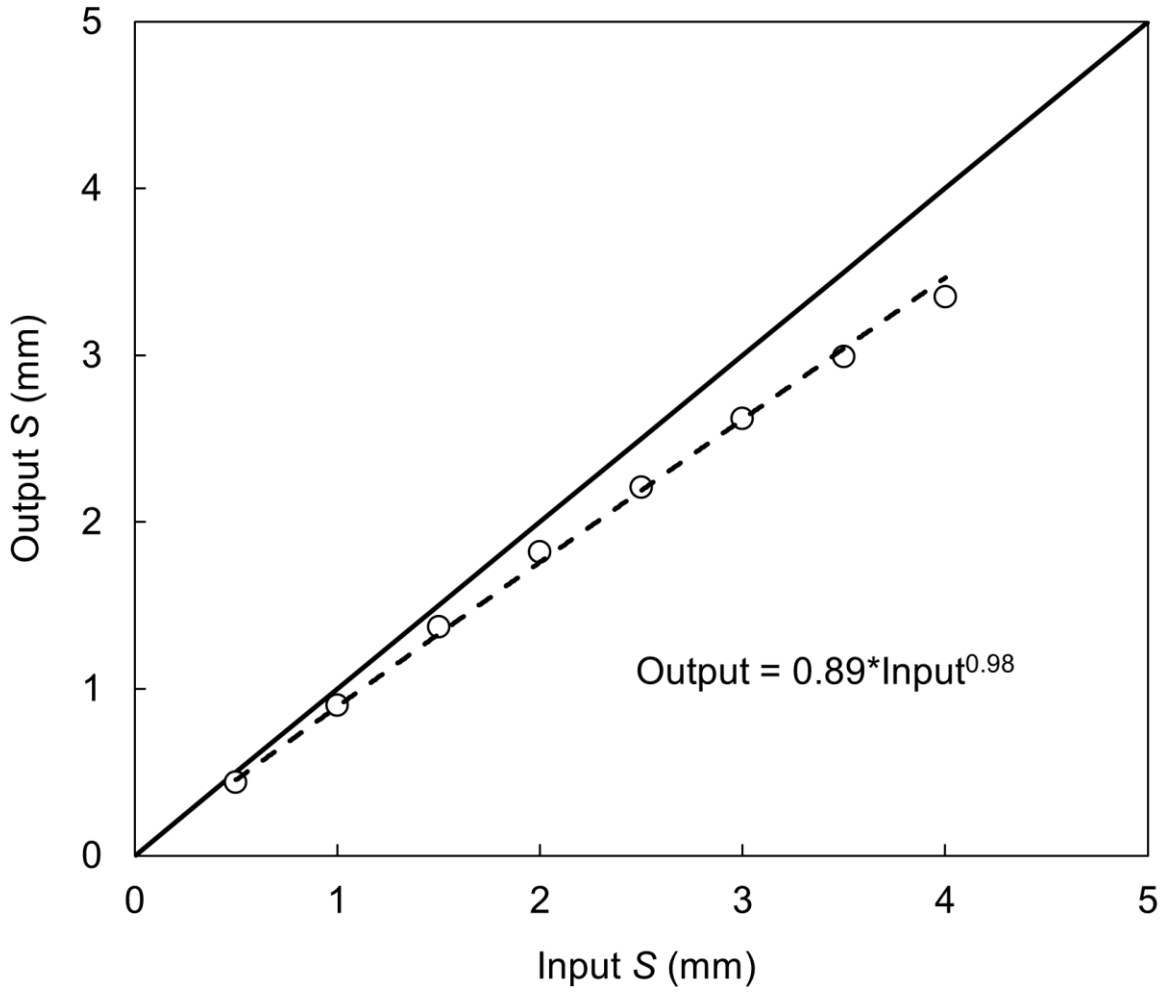

Figure E1. Relationship between input and output canopy storage capacity (*S*) in the Rutter model, produced using rain events extracted from the Kopuatai dataset (2012–2022).

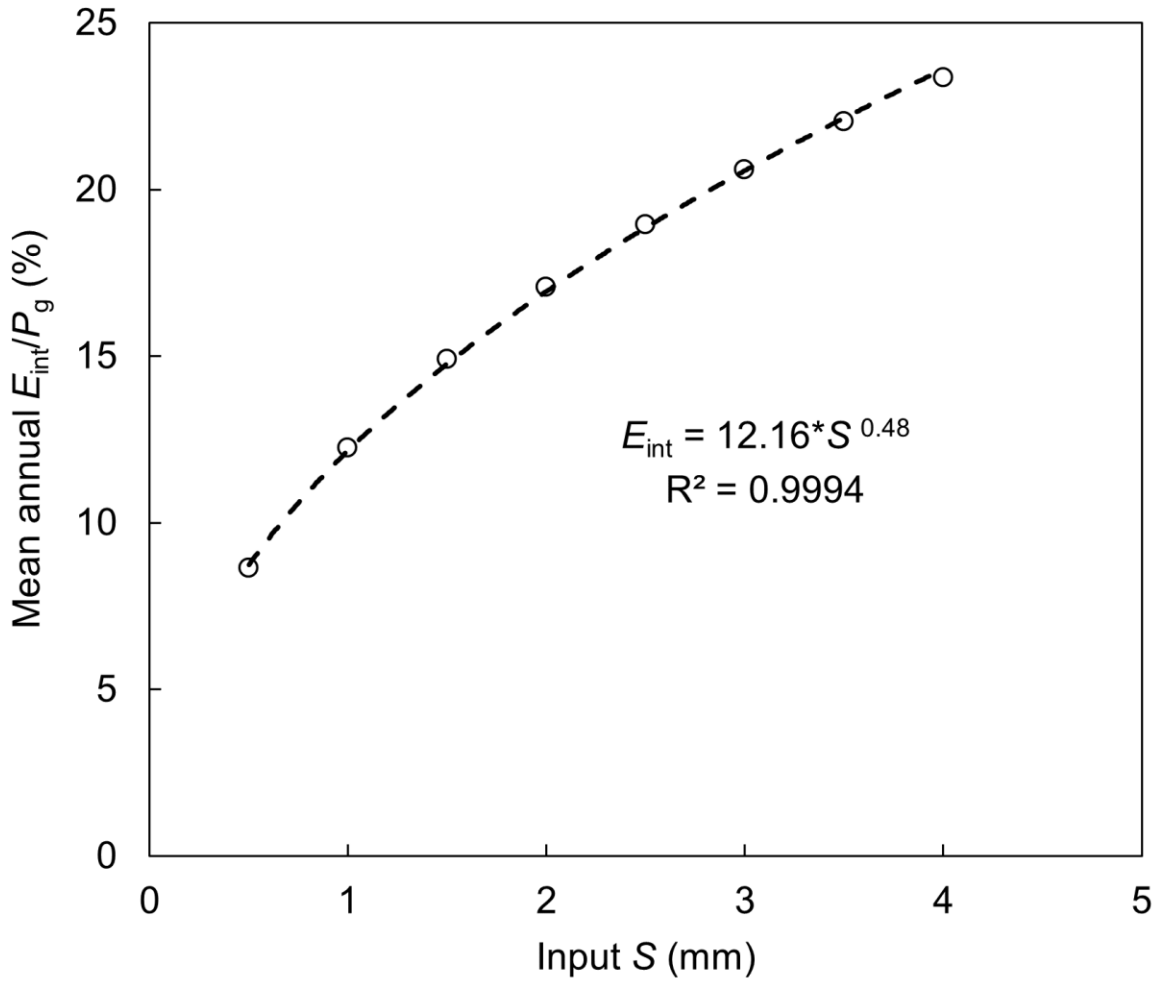

Figure E2. Relationship between input canopy storage capacity (S) and output mean annual interception loss fraction (E_{int}/P_g) for the Rutter model, produced using data from Kopuatai (2012–2022).

Appendix F

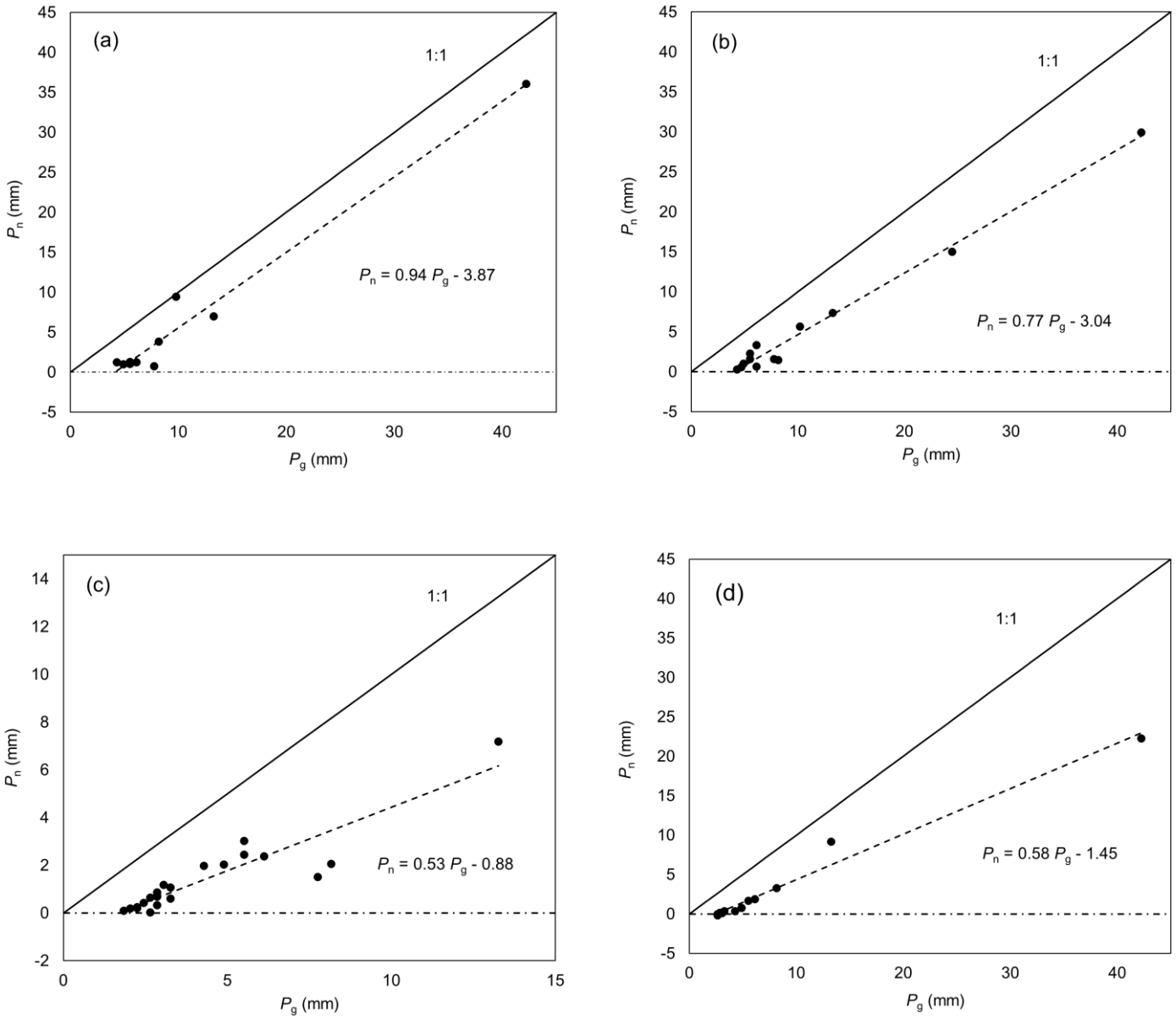

Figure F1. Relationship between sub-rain event gross and net precipitation (P_g and P_n, respectively) for Sites 1–4 (a–d), where P_n data was obtained through the collection tray method. The y-intercept represents the canopy storage capacity, S.